

# Renormalization Group Methods for Quantum Impurity Systems

Von der Mathematisch-Naturwissenschaftlichen Fakultät  
der Universität Augsburg  
zur Erlangung eines Doktorgrades der Naturwissenschaften  
genehmigte Dissertation

von  
Diplom-Physiker Walter Hofstetter  
aus  
München

Referent: Professor Dr. D. Vollhardt

Koreferenten: Professor Dr. Th. Kopp, Professor Dr. W. Zwerger

Tag der mündlichen Prüfung: 24. Juli 2000

---

# Contents

<b>Introduction</b>	<b>1</b>
<b>1 Models and methods</b>	<b>5</b>
1.1 Quantum impurity models . . . . .	5
1.2 Numerical renormalization group . . . . .	7
1.3 Flow equations . . . . .	13
<b>2 Narrow-band Anderson model</b>	<b>17</b>
2.1 Introduction . . . . .	17
2.2 Density of states . . . . .	18
2.3 Impurity susceptibility . . . . .	20
2.4 Spectral density and skeleton expansion . . . . .	22
2.5 Conclusion . . . . .	24
<b>3 Magnetic impurity in a correlated band</b>	<b>27</b>
3.1 Introduction . . . . .	27
3.2 Experimental motivation . . . . .	29
3.3 Model and dynamical mean-field theory . . . . .	30
3.4 NRG calculations . . . . .	34
3.5 Single-particle spectral functions . . . . .	35
3.6 Dynamical susceptibility . . . . .	39
3.7 Kondo scale . . . . .	44
3.8 Asymmetric impurity and band . . . . .	48
3.9 Wolff model . . . . .	51
3.10 Conclusion and experimental outlook . . . . .	53
<b>4 Generalized NRG for dynamical properties</b>	<b>55</b>
4.1 Introduction . . . . .	55
4.2 NRG at broken rotational symmetry . . . . .	56
4.3 Modified iterative diagonalization . . . . .	57
4.4 Generalized NRG . . . . .	59

---

4.5	Conclusion . . . . .	66
<b>5</b>	<b>Direct application of flow equations</b>	<b>69</b>
5.1	Luttinger model . . . . .	69
5.2	Wolff model . . . . .	79
5.3	Conclusion . . . . .	81
<b>6</b>	<b>Flow equation analysis of the Kondo model</b>	<b>83</b>
6.1	Introduction . . . . .	83
6.2	Bosonization . . . . .	84
6.3	Flow equations . . . . .	88
6.4	Approximate evaluation . . . . .	96
6.5	Kondo scale . . . . .	99
6.6	Calculation of observables . . . . .	100
6.7	Dynamical susceptibility . . . . .	102
6.8	Conclusion . . . . .	107
	<b>Summary</b>	<b>109</b>
	<b>A Details of the mapping on a linear chain</b>	<b>113</b>
	<b>B Iterative diagonalization with rotational symmetry</b>	<b>117</b>
	<b>C Calculation of <math>\rho(\omega)</math> and <math>\chi(\omega)</math></b>	<b>121</b>
	<b>D Details of the Wolff model flow</b>	<b>127</b>
	<b>Bibliography</b>	<b>133</b>
	<b>Publications</b>	<b>141</b>
	<b>Curriculum vitae</b>	<b>143</b>
	<b>Acknowledgements</b>	<b>145</b>

# Introduction

One of the fundamental problems in theoretical physics is the analysis of systems containing many degrees of freedom. In particular, the *solid state* of matter has been the subject of intensive study for many decades. Although the basic physical laws – provided by quantum mechanics – governing the behaviour of  $\mathcal{O}(10^{23})$  atoms are well established and can be formulated completely in terms of one- and two-body interactions, collective phenomena arise which may only be understood in a many-particle picture. Important examples are superconductivity and magnetic ordering.

Fortunately, not all degrees of freedom have to be taken into account to describe these effects. It turns out that many characteristics of crystalline solids (like the magnetic response and thermodynamics) are to a large extent determined by the electronic structure, which may be calculated in the adiabatic approximation of Born and Oppenheimer (1927) where the positions of the nuclei are taken to be fixed. Moreover, it is usually sufficient to focus on the dynamics of the *valence electrons* located in the outermost atomic shells. The theorem of Bloch (1928) then leads to the formation of *energy bands* which already contain the effect of the crystalline potential.

Within this effective model, one nontrivial complication remains: The finite Coulomb interaction between pairs of valence electrons usually renders an exact quantum mechanical treatment impossible. For weak interactions, these correlations may be successfully taken into account on a mean-field level, while in the case of *strongly correlated* systems – containing for example atoms with partially filled  $3d$  or  $4f$  shells – this approach fails. It is precisely the latter situation that is of interest in this work. In the *impurity* systems considered here, a small fraction of such strongly correlated atoms are distributed randomly in an otherwise pure crystalline host. With good accuracy they may be considered as independent and modelled by a single impurity Hamiltonian. Due to the internal degrees of freedom of these *magnetic impurities*, a new many-body phenomenon, the *Kondo effect*, arises: A large number of conduction electrons participate in forming a screening cloud that compensates for the otherwise free impurity moment. This screening causes characteristic experimental signals like the resistance minimum in dilute Kondo alloys. In recent years magnetic impurities have also been realized artificially in quantum dots, where parameters can be tuned

and theoretical predictions may be verified in detail.

Within the last decade quantum impurity models have received additional attention due to the dynamical mean-field theory (DMFT) of correlated lattice systems in high dimensions which is based on the work of Metzner and Vollhardt (1989*a*). In this approach, the local dynamics of the lattice fermions is described by an effective Anderson model with self-consistently determined parameters.

For these reasons it is of great interest to develop and improve nonperturbative methods which yield thermodynamic and spectral properties of impurity models in a controlled way. In this work, two such approaches will be discussed that are based on the idea of the renormalization group. The first one, Wilson's *numerical renormalization group* (NRG), has played a crucial role in the in the solution of the Kondo problem and is to some degree well established. We will, however, demonstrate that in the calculation of dynamical quantities an important aspect has so far been neglected and that in the presence of an external field the NRG procedure has to be generalized in order to lead to reliable results. The second technique, Wegner's *flow equation* approach, has been developed more recently. It can provide *analytic* insight into complex many-body phenomena like the Kondo effect. On the other hand, its range of applicability is so far limited by the necessary truncation of higher order interactions.

Besides the methodical objective of this thesis (illustration and further development of these two techniques) our goal will be to analyze several generalized impurity models in detail. In particular, extensions of the Anderson Hamiltonian will be studied where the conduction band is no more flat and noninteracting. Only few calculations for this more realistic situation exist so far, although it is of great experimental interest. Here we present the first nonperturbative treatment in  $d > 1$  using a combination of DMFT and NRG.

## Structure of this thesis

In chapter one we introduce the Kondo and Anderson Hamiltonians which will be the subject of study throughout this thesis. Furthermore the basic concepts of NRG and the flow equation method are outlined, including a brief discussion of previous applications.

In chapter two we analyze a modified version of the Anderson impurity model where the hybridization is much larger than the bandwidth. These calculations were initially motivated by one possible DMFT scenario of the Mott transition, which has lead to the question whether the self-consistent perturbation series converges or not. Later it was realized that such a narrow band may also be generated by interactions among the conduction electrons.

In chapter three we present the study of a magnetic impurity in a correlated

band. The single particle density of states and the dynamical susceptibility at zero temperature are calculated by NRG. Among the most important results, we find characteristic spectral features (side peaks) as a consequence of the small effective bandwidth. A strong enhancement of the Kondo temperature due to correlations is observed. In addition, we discuss the effects of doping and particle–hole asymmetry of the impurity. Future ESR measurements are proposed where the enhanced Kondo scale and its dependence on the band filling could be observed.

In chapter four, an external magnetic field is applied to the Anderson impurity. No NRG simulations for this situation exist so far. On the one hand this is due to the reduced symmetry of the Hamiltonian, which requires modifications of iterative diagonalization. In the course of our study, however, more fundamental difficulties appeared. It became clear that the procedure used so far to calculate dynamical properties within NRG is not rigorous and fails explicitly in the presence of an external field. To solve the problem, we introduce a new algorithm based on the concept of the *reduced density matrix*, which correctly describes the subtle ground state dependency of spectral features at higher frequency. This method represents the true extension of Wilson’s original thermodynamic calculations.

The remaining two chapters of this thesis focus on Wegner’s flow equations and their applications. In chapter five, we consider the Luttinger and Wolff models: While the former serves as an exactly solvable test case where the validity of the method can be established, the Wolff study was motivated by a bosonization solution for the weak coupling limit. In both cases flow equations are formulated directly in the fermionic language, which makes truncations of higher many–particle terms inevitable.

A different approach is chosen in chapter six, where we first bosonize the anisotropic Kondo model and then diagonalize it using flow equations. In this framework, interaction terms can be parameterized efficiently by using *Vertex operators*, with a *scaling dimension* that describes the crossover from weak to strong coupling. The flow equations close exactly in the *Toulouse limit* which corresponds to a finite coupling strength and a nontrivial low temperature fixed point. For general initial couplings, the truncation is controlled by the *operator product expansion* of vertex operators. By determining the flow of an additional observable, the dynamical impurity susceptibility at zero temperature is also calculated.



# Chapter 1

## Models and methods

### 1.1 Quantum impurity models

In this work we will study the physical properties of metallic systems containing a small fraction of *magnetic* impurities with internal degrees of freedom. It is well known that effects caused by nonmagnetic impurities, like the residual resistance in metals, can be described in a single particle framework and have been understood for a long time. For magnetic alloys, the situation proved to be more complicated: In measurements by de Haas, de Boer and van den Berg (1934) on *Au* it was found that the resistivity – instead of dropping monotonically – exhibits a minimum at a finite temperature. It was only recognized later that this is an impurity effect associated with *3d* transition metal impurities such as *Fe*. Theoretical understanding of the resistance minimum was lacking until Zener (1951) introduced the fundamental *s-d Hamiltonian* (usually referred to as *Kondo model*, see below)

$$H_{sd} = \sum_{\mathbf{k}\sigma} \epsilon_{\mathbf{k}} c_{\mathbf{k}\sigma}^\dagger c_{\mathbf{k}\sigma} + J \sum_{\mathbf{k}\mathbf{k}'} \left( S^+ c_{\mathbf{k}\downarrow}^\dagger c_{\mathbf{k}'\uparrow} + S^- c_{\mathbf{k}\uparrow}^\dagger c_{\mathbf{k}'\downarrow} + S^z \left( c_{\mathbf{k}\uparrow}^\dagger c_{\mathbf{k}'\uparrow} - c_{\mathbf{k}\downarrow}^\dagger c_{\mathbf{k}'\downarrow} \right) \right) \quad (1.1)$$

describing the Heisenberg exchange interaction between a local moment of spin  $S$  and the conduction electrons. Note that throughout this work units will be chosen as  $\hbar = k_B = g = \mu_B = 1$ . Kondo (1964) discovered that in a perturbative calculation of the impurity resistivity all terms except the leading one are logarithmically divergent at low temperatures if the coupling is antiferromagnetic ( $J > 0$ )

$$R_{\text{imp}} = \alpha J^2 (1 - \beta J \ln T) + \mathcal{O}(J^4) \quad (1.2)$$

( $\alpha, \beta$  are constants). Together with the phonon contribution  $R_{\text{phonon}} \sim T^5$ , this leads to the minimum in the total resistivity. On the other hand, perturbation theory clearly breaks down once higher order terms are comparable to the leading one,

which is the case at the *Kondo temperature*  $T_K \sim \exp\{-1/(2\rho J)\}$  where  $\rho$  is the conduction electron density of states. Attempts by Abrikosov (1965) to sum the leading logarithmic contributions (parquet diagrams) up to infinite order could not restore convergence of the perturbation series. New nonperturbative methods had to be developed in order to access the low temperature regime  $T < T_K$ . In a first successful attempt in this direction, Anderson and Yuval (1969) demonstrated that the thermodynamics of a magnetic impurity can be reformulated in terms of a (classical) gas of alternately charged particles with a logarithmic interaction. In a subsequent renormalization group analysis of the Coulomb gas, Anderson, Yuval and Hamann (1970) showed that the effective coupling at low temperatures increases without bound in the antiferromagnetic case. The same behaviour was also obtained in a simple “poor man’s” scaling approach by Anderson (1970). Although perturbative scaling breaks down at a certain value of the coupling constant, it was nevertheless concluded that at zero temperature the effective exchange is infinite, thus leading to perfect screening of the local moment and a nonmagnetic singlet groundstate. This was later confirmed by the pioneering numerical renormalization group (NRG) calculation of Wilson (1975) which may be considered as the first exact solution of the Kondo problem. Details of this approach, which is based on a logarithmic discretization of the conduction band, are given in the next section. An analytic solution of the magnetic impurity problem was finally obtained with the *Bethe ansatz* by Andrei (1980) and Wiegmann (1980). This method is, however, restricted to integrable cases (excluding, for example, any energy dependence in the exchange coupling) and can furthermore only access static thermodynamic properties. More recently, conformal field theory and the *form factor approach* of Lesage, Saleur and Skorik (1996) have made the calculation of dynamic quantities possible.

In the Kondo Hamiltonian, the impurity is reduced to a spin degree of freedom. A more realistic model which takes charge fluctuations into account was introduced by Anderson (1961)

$$H_{\text{and}} = \sum_{\mathbf{k}\sigma} \epsilon_{\mathbf{k}} c_{\mathbf{k}\sigma}^{\dagger} c_{\mathbf{k}\sigma} + \sum_{\mathbf{k}\sigma} V_{\mathbf{k}} \left( f_{\sigma}^{\dagger} c_{\mathbf{k}\sigma} + h.c. \right) + U n_{f\uparrow} n_{f\downarrow} + \epsilon_f n_f \quad (1.3)$$

and also in a slightly different form by Wolff (1961). Here the *hybridization*  $V$  between the  $f$  impurity and the band is balanced by a local Coulomb repulsion  $U$  which suppresses double occupancy of the impurity. Besides the *local moment* regime, where (1.3) reduces to an effective Kondo Hamiltonian as demonstrated by Schrieffer and Wolff (1966), the Anderson model also displays *mixed valence*: If the impurity level  $\epsilon_d$  is sufficiently close to the Fermi energy, the impurity occupation number fluctuates between two different valence states. A complete description of the different physical regimes of (1.3) was obtained by Krishna-murthy, Wilkins and Wilson (1980) within the NRG where the authors focused on the situation with a flat band and noninteracting conduction electrons. Sakai, Shimizu and Kasuya (1989) and Costi,

Hewson and Zlatić (1994) later extended these calculations and obtained also spectral information.

In this thesis we will mainly focus on three different extensions of the impurity Hamiltonians discussed so far:

- The nontrivial strong coupling behaviour of the *anisotropic* Kondo model is studied by the flow equation method.
- Thermodynamic and spectral properties of the Anderson model with a *narrow* hybridization function are determined by NRG and exact diagonalization.
- The Anderson impurity problem with *correlated conduction electrons* is solved using a combination of NRG and the dynamical mean-field theory.

In the following, we give an introduction to the NRG and flow equation methods.

## 1.2 Numerical renormalization group

The essential difficulty in analyzing a (classical or quantum-mechanical) many-particle system arises from the large number of interacting degrees of freedom. A well-known example from statistical physics is the model introduced by Ising (1925) where classical spins are coupled by a short-range ferromagnetic interaction. In this model a transition to an ordered phase occurs if the spatial dimension is larger than one. Close to the associated *critical point* the spin-spin correlation length diverges: If one were to study this regime numerically, one would have to take into account an increasing number of spins that are strongly coupled to each other.

In the Kondo problem, a similar situation is encountered: At low temperatures, a large *screening cloud* compensating the impurity spin is formed in the conduction band. The number of electrons involved in the screening diverges exponentially at small exchange coupling  $J$ . A direct numerical treatment using, for example, exact diagonalization methods is therefore impossible.

It was precisely this situation that led to the development of the *renormalization group*. In fact, one is often interested only in physical properties at low energy (or equivalently long distances). As realized first by Kadanoff (1966) and later elaborated by Wilson (1971), short-wavelength degrees of freedom may be integrated out, leading to a coarse-grained system with renormalized effective interactions. Iterating the procedure, one finally arrives at a reduced system size where in principle other methods (like exact diagonalization) could be applied. Mostly, however, it is sufficient to know the flow of the renormalized interaction parameters (the *running couplings*) in the coarse-graining procedure in order to determine universal properties like critical exponents. Perturbative *scaling* of this kind was applied to the Kondo problem by Anderson (1970) (see fig. 1.1): In infinitesimal steps, conduction electrons close to

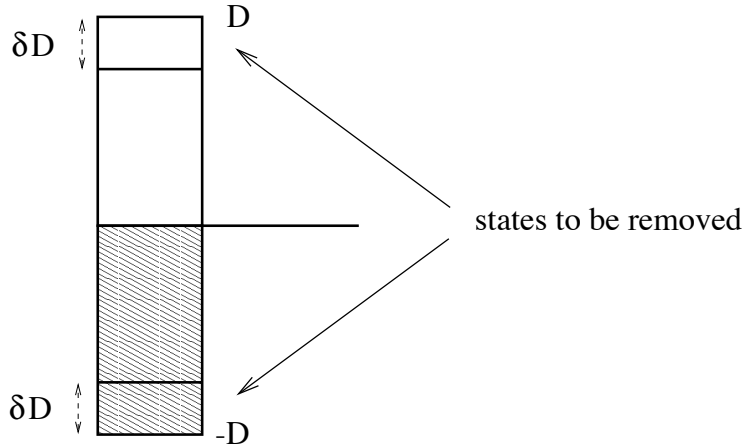


**Figure 1.1:** Poor man’s scaling for the Kondo problem. States far away from the Fermi edge are integrated out.

the band edges are integrated out and an effective Hamiltonian  $H_{\text{eff}}$  is derived that acts only on the low energy degrees of freedom. In the leading order of the exchange coupling,  $H_{\text{eff}}$  can again be parametrized by  $J(D)$  which now depends on the bandwidth  $D$ . For the antiferromagnetic Kondo problem, the effective coupling diverges at a finite  $D$ . This indicates the perturbative nature of the scaling equations which can therefore not access the zero temperature limit.

In order to remove the shortcomings of scaling, Wilson proposed to determine the effective Hamiltonian *numerically*, without any parametrization in terms of coupling constants. In the following we will outline the application of his method to the Anderson impurity model (1.3) following Krishna-murthy et al. (1980). In a first step, the model is mapped on a one-dimensional problem by considering only  $s$ -wave states in the conduction band. Introducing a continuous energy variable  $\epsilon$ , we write

$$H_{\text{and}} = \epsilon_f n_f + U n_{f\uparrow} n_{f\downarrow} + \sum_{\sigma} \int_{-1}^1 d\epsilon \epsilon c_{\epsilon\sigma}^{\dagger} c_{\epsilon\sigma} + \sum_{\sigma} \int_{-1}^1 d\epsilon \sqrt{\frac{\Delta(\epsilon)}{\pi}} (f_{\sigma}^{\dagger} c_{\epsilon\sigma} + h.c.) \quad (1.4)$$

where a hybridization function

$$\Delta(\epsilon) = \pi \sum_k \delta(\epsilon - \epsilon_k) V_k^2 \quad (1.5)$$

has been defined. Previous field theoretic results by Wilson (1965) motivated the introduction of a *logarithmic discretization* for the conduction electrons: After dividing the band into a series of intervals (“energy scales”) with exponentially decreasing width (fig. 1.2), a Fourier expansion is performed on each one of these intervals. One

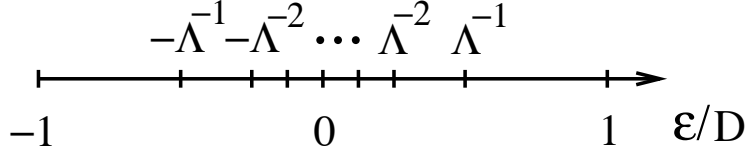


**Figure 1.2:** Logarithmic discretization of the conduction band.

defines a set of orthonormal functions according to

$$\Psi_{np}^{\pm}(\epsilon) = \begin{cases} \frac{1}{\sqrt{v_n}} e^{\pm i\omega_n p \epsilon} & \text{if } \Lambda^{-(n+1)} < \pm\epsilon < \Lambda^{-n} \\ 0 & \text{otherwise} \end{cases} \quad (1.6)$$

where  $v_n = \Lambda^{-n}(1 - \Lambda^{-1})$  is the width of the  $n$ -th interval and  $\omega_n = 2\pi/v_n$  is the corresponding fundamental Fourier frequency. The momentum space operators  $c_{\epsilon\sigma}$  can be expanded in this basis

$$c_{\epsilon\sigma} = \sum_{np} [a_{np\sigma} \Psi_{np}^{\dagger}(\epsilon) + b_{np\sigma} \Psi_{np}^{-}(\epsilon)] \quad (1.7)$$

where

$$a_{np\sigma} = \int_{-1}^1 d\epsilon [\Psi_{np}^{\dagger}(\epsilon)]^* c_{\epsilon\sigma} \quad , \quad b_{np\sigma} = \int_{-1}^1 d\epsilon [\Psi_{np}^{-}(\epsilon)]^* c_{\epsilon\sigma} \quad (1.8)$$

satisfy the usual fermionic anticommutation relations. Approximating the hybridization function  $\Delta(\epsilon)$  by a constant in each one of the intervals  $[\Lambda^{-(n+1)}, \Lambda^{-n}]$  (see fig. 1.3), it is easily shown that the impurity only couples to the  $p = 0$  states and the hybridization term takes the form

$$\sum_{\sigma} \int_{-1}^1 d\epsilon \sqrt{\frac{\Delta(\epsilon)}{\pi}} (f_{\sigma}^{\dagger} c_{\epsilon\sigma} + h.c.) = \sqrt{\frac{\xi_0}{\pi}} \sum_{\sigma} (f_{\sigma}^{\dagger} d_{0\sigma} + h.c.) \quad (1.9)$$

For the definition of the *maximally localized state*  $d_{0\sigma}$  and the coefficient  $\xi_0$ , see appendix A. In the special case of a constant hybridization function  $\Delta(\omega) = \Delta$  one obtains  $\xi_0 = 2\Delta$ . Regarding the conduction band, the coupling between terms with different  $p$  vanishes in the limit  $\Lambda \rightarrow 1$ . Wilson (1975) has demonstrated that even for a discretization parameter  $\Lambda = 2$  (used in this thesis), the  $p \neq 0$  contributions can be neglected in a very good approximation. The Hamiltonian then reads

$$\begin{aligned} H = & \epsilon_f n_f + U n_{f\uparrow} n_{f\downarrow} + \sqrt{\frac{\xi_0}{\pi}} \sum_{\sigma} (f_{\sigma}^{\dagger} d_{0\sigma} + h.c.) \\ & + \frac{1 + \Lambda^{-1}}{2} \sum_{\sigma} \sum_{n=0}^{\infty} \Lambda^{-n} (a_{n\sigma}^{\dagger} a_{n\sigma} - b_{n\sigma}^{\dagger} b_{n\sigma}) \end{aligned} \quad (1.10)$$

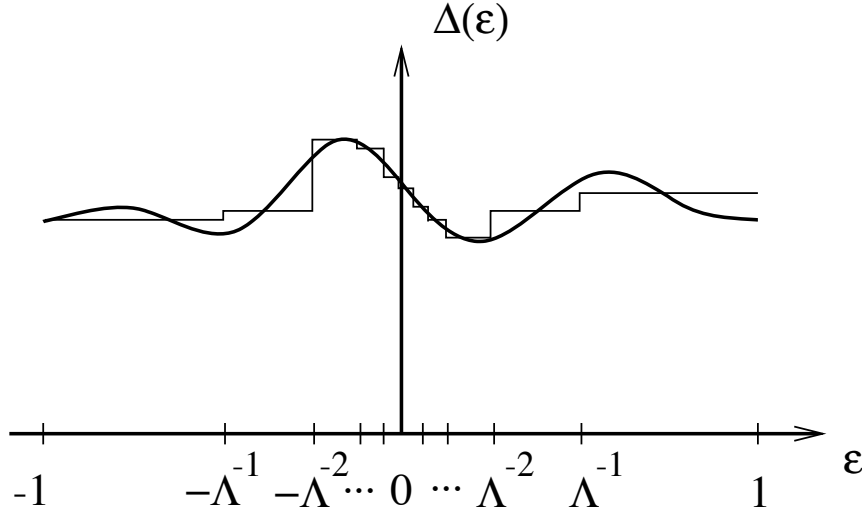


**Figure 1.3:** Approximation of the hybridization function.

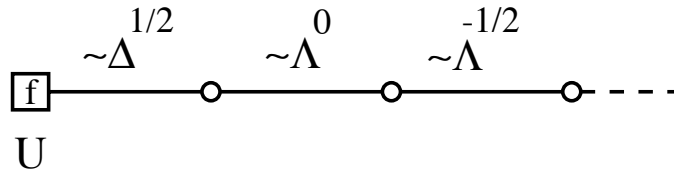


**Figure 1.4:** Representation of the Anderson model as a semi-infinite chain.

where the  $p$  index has been dropped. At this stage every energy scale is represented by two degrees of freedom; through the introduction of logarithmic discretization we have now achieved *energy scale separation*. Nevertheless, (1.10) still represents a nontrivial many-body problem. Wilson suggested solving it by iterative perturbation theory: Because the terms in the conduction band are now exponentially decreasing, they can be taken into account one after the other (see fig. 1.5). In order to do this, it is convenient to make a unitary transformation from the set of operators  $(a_{n\sigma}, b_{n\sigma})$  to a new orthonormal set  $(d_{n\sigma})$ . The new basis is chosen in such a way that the operators  $(d_{n\sigma})$  exhibit only nearest-neighbour coupling, i.e.  $d_{n\sigma}$  is coupled to  $d_{(n\pm 1)\sigma}$ . This can be achieved by Lanczos tridiagonalization of the conduction band, as described in appendix A. The resulting Hamiltonian has the form of a semi-infinite linear chain

$$\begin{aligned}
 H = & \epsilon_f n_f + U n_{f\uparrow} n_{f\downarrow} + \sqrt{\frac{\xi_0}{\pi}} \sum_{\sigma} \left( f_{\sigma}^{\dagger} d_{0\sigma} + h.c. \right) \\
 & + \sum_{\substack{n=0 \\ \sigma}}^{\infty} \epsilon_n \left( d_{n\sigma}^{\dagger} d_{(n+1)\sigma} + h.c. \right)
 \end{aligned} \tag{1.11}$$

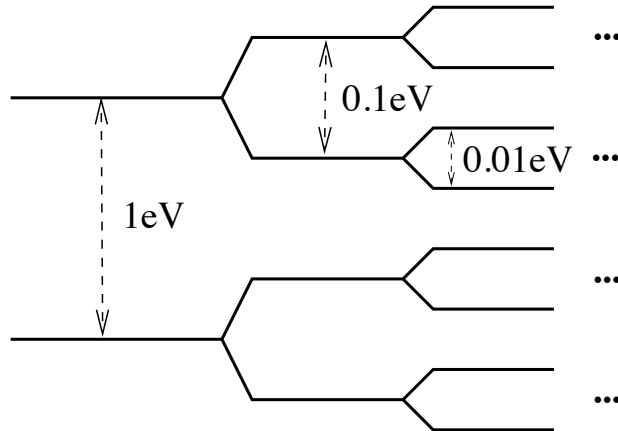


**Figure 1.5:** Concept of iterative perturbation theory.

as shown in fig. 1.4. For simplicity, we have focussed on a symmetric hybridization function at this point. The hopping terms decay asymptotically as  $\epsilon_n \sim \Lambda^{-n/2}$ . Following Wilson (1975), this Hamiltonian can be represented using a *shell model* (fig. 1.6) where the shells correspond to the states  $d_{n\sigma}$ . They are equivalent to wave packets centered at the impurity with an extent in position space that increases as  $\Lambda^{n/2}$ . In this basis, one neglects those states where the electron is far away from the impurity in real space *and* far away from the Fermi surface in momentum space.

Now the Hamiltonian (1.11) can be diagonalized iteratively. We truncate the chain after  $N$  sites and rescale

$$\begin{aligned}
 H_N = & \Lambda^{(N-1)/2} \left\{ \epsilon_f n_f + U n_{f\uparrow} n_{f\downarrow} + \sqrt{\frac{\xi_0}{\pi}} \sum_{\sigma} \left( f_{\sigma}^{\dagger} d_{0\sigma} + h.c. \right) \right. \\
 & \left. + \sum_{\substack{n=0 \\ \sigma}}^{N-1} \epsilon_n \left( d_{n\sigma}^{\dagger} d_{(n+1)\sigma} + h.c. \right) \right\}
 \end{aligned} \tag{1.12}$$

so that the low-lying excitations of  $H_N$  are always of the order  $\mathcal{O}(1)$ . The full system is then recovered in the limit

$$H = \lim_{N \rightarrow \infty} \Lambda^{-(N-1)/2} H_N \tag{1.13}$$

From (1.12) the following *renormalization group transformation* is easily derived:

$$\boxed{H_{N+1} = \Lambda^{1/2} H_N + \sum_{\sigma} \Lambda^{N/2} \epsilon_N \left( d_{N\sigma}^{\dagger} d_{(N+1)\sigma} + h.c. \right)} \tag{1.14}$$

Iterative diagonalization is based on this relation, which shows that knowledge of the eigenstates of  $H_N$  and of the matrix elements  $\langle |d_N^{\dagger}| \rangle_N$  is sufficient to solve the eigenvalue problem associated with  $H_{N+1}$ . Details are described in appendix B.

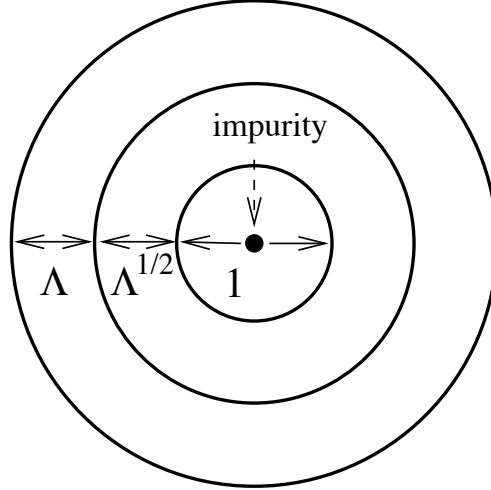


**Figure 1.6:** “Onion” shell model of the semi-infinite chain Hamiltonian (1.11).

In order to reduce the size of the remaining matrix problem, it is important to exploit symmetries which lead to a block-diagonal structure of the Hamiltonian. In the present case these are the total charge (relative to half filling)

$$Q_N = \sum_{\substack{n=0 \\ \sigma}}^N (d_{n\sigma}^\dagger d_{n\sigma} - 1) + \sum_{\sigma} (f_{\sigma}^\dagger f_{\sigma} - 1). \quad (1.15)$$

and the total spin

$$S_N^i = \frac{1}{2} \sum_{\substack{n=0 \\ \mu\nu}}^N d_{n\mu}^\dagger \sigma_{\mu\nu}^i d_{n\nu} + \sum_{\mu\nu} \frac{1}{2} f_{\mu}^\dagger \sigma_{\mu\nu}^i f_{\nu}. \quad (1.16)$$

In the absence of an external magnetic field, all three components  $i = x, y, z$  are conserved. In this case one can define simultaneous eigenstates of  $Q_N$ ,  $S_N^z$  and  $\mathbf{S}_N^2$  and label them as  $|Q, S, S^z, r\rangle$  where the quantum number  $r$  corresponds to the remaining degeneracy. Energy eigenvalues will be independent of  $S^z$  and one can take advantage of this fact by using Clebsch–Gordan coefficients and working entirely in terms of the *reduced matrix elements*  $\langle Q, S || f_N^\dagger || Q', S' \rangle$ . Details are given in appendix B. If a magnetic field is applied, however, diagonalization has to be performed at reduced symmetry. The necessary modifications are explained in chapter 4.

From a practical point of view, it is impossible to calculate all the eigenstates of  $H_N$  because the corresponding matrix size increases exponentially  $\sim 2^{2(N+2)}$ . As one is mainly interested in low-temperature properties of  $H$ , in each diagonalization step only a limited number  $M$  of low-lying eigenstates is retained. This leads to a

constraint on the possible values of the discretization parameter  $\Lambda$ : The error due to truncation rapidly increases as one approaches the continuum limit  $\Lambda = 1$ . Typical parameters used in our calculations are  $\Lambda = 2$  and  $M = 300$  (not counting the  $S_z$  degeneracy).

When diagonalization has been achieved, physical observables can be calculated from the eigenstates and matrix elements. For the narrow band Anderson model, we calculate the temperature-dependent impurity contribution  $\Delta\chi(T)$  to the magnetic susceptibility. Apart from this we will mainly be interested in zero temperature dynamical properties of the impurity, namely the single particle spectral function  $\rho(\omega)$  and the dynamical susceptibility  $\chi(\omega)$ . Details of the computation of  $\rho(\omega)$  were already given by Bulla (1994). In appendix C we also outline the calculation of  $\chi(\omega)$  in terms of reduced matrix elements of the local spin.

A completely new aspect of NRG is discussed in chapter 4 where we show that the technique of calculating spectral quantities used so far is only approximate and fails in the case of an external magnetic field. We introduce a new approach to dynamics – the DM–NRG – which solves the problem and represents the most general extension of the original thermodynamic calculations.

## 1.3 Flow equations

The flow equation method was originally introduced by Wegner (1994) as a new way of diagonalizing quantum many-particle Hamiltonians. Simultaneously Glazek and Wilson (1994) developed the closely related *similarity renormalization group* in the context of high energy physics. In the following, we will outline the basic ideas of Wegner’s approach.

While perturbative scaling aims at eliminating high energy degrees of freedom and thus reducing the size of the Hilbert space, flow equations are designed to leave the Hilbert space invariant and instead systematically reduce offdiagonal matrix elements of the Hamiltonian. This can be achieved by *Jacobi’s method*, well known from numerical mathematics (see Press, Teukolsky, Vetterling and Flannery (1995)): By applying discrete unitary transformations (“Jacobi rotation matrices”)

$$H \rightarrow U H U^\dagger \tag{1.17}$$

offdiagonal matrix elements connecting two different basis states are set to zero. Flow equations constitute, to some extent, a continuous version of this procedure. Here the rotation matrix is taken to be

$$U = 1 + \eta dl \tag{1.18}$$

where the generator  $\eta$  is antihermitean

$$\eta^\dagger = -\eta \tag{1.19}$$

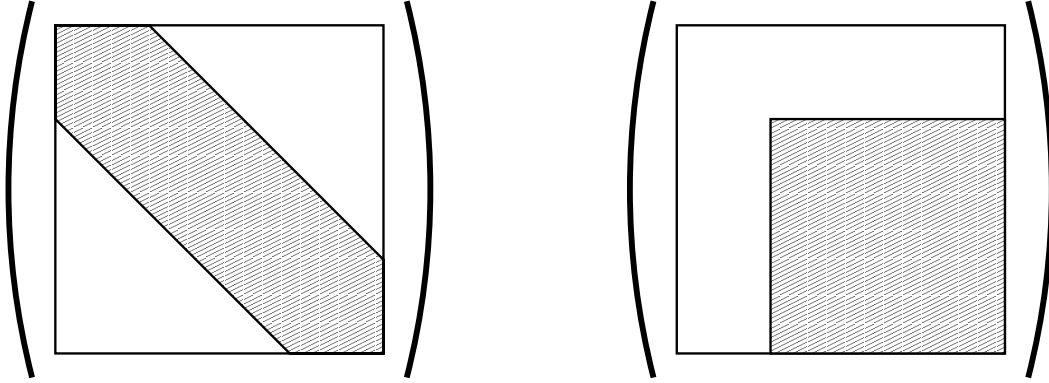


**Figure 1.7:** Left: Banded matrix resulting from flow equation diagonalization. Right: Block diagonal matrix obtained by usual scaling where high energy degrees of freedom are eliminated (upper left corner).

due to the unitarity condition. In addition, the *flow parameter*  $l$  has been introduced; a physical interpretation of this quantity will be given below. As a result, the basic flow equation reads

$$\partial_l H(l) = [\eta(l), H(l)]. \quad (1.20)$$

Whether the transformation (1.20) really leads to a simplification of the Hamiltonian depends on the choice of  $\eta$ . Wegner proposed the following ansatz:

$$\eta = [H_0, H] \quad (1.21)$$

where  $H_0$  denotes the diagonal part of the total Hamiltonian. For a general matrix problem this obviously requires the choice of an appropriate set of basis states, which is then considered “diagonal”. In the context of interacting fermions these are usually taken to be the Bloch states of an electron in a periodic potential.

With the choice (1.21), the Hamiltonian flow is given by

$$\partial_l H_{kn} = \sum_m (\epsilon_k + \epsilon_n - 2\epsilon_m) H_{km} H_{mn} \quad (1.22)$$

and it can be shown that the sum of the squared diagonal elements  $\epsilon_k$  is monotonously increasing:

$$\partial_l \left( \sum_k \epsilon_k^2 \right) = 2 \sum_{kk'} (\epsilon_k - \epsilon_{k'})^2 H_{kk'} H_{k'k}. \quad (1.23)$$

Due to conservation of the trace  $\partial_l \text{Tr} H^2 = 0$  this implies that the offdiagonal elements  $H_{kk'}$  are reduced and only resonant matrix elements survive.

Regarding the interaction part of  $H$  as a perturbation, the leading term of the flow is already obtained by replacing  $H \rightarrow H_0$  in (1.20). As a consequence, matrix

elements decay according to the difference in energy between the corresponding basis states:

$$H_{kk'}(l) \sim e^{-(\epsilon_k - \epsilon_{k'})^2 l}. \quad (1.24)$$

Flow equations therefore obey the principle of *energy scale separation*: States differing largely in energy are decoupled first, nearly resonant matrix elements later. The resulting matrix at intermediate stages of the flow has a banded structure (see fig. 1.7). Thus small energy denominators leading to divergences can be avoided, in contrast to perturbative scaling. The flow parameter  $l$  is a measure of the typical energy difference  $\Delta E$  being decoupled

$$l \sim \frac{1}{\Delta E^2} \quad (1.25)$$

Choices for the generator differing from (1.21) are possible (as an example see Kehrein and Mielke (1997)) and often motivated by the wish to keep the flow simple, that is to suppress the generation of certain additional interaction terms. In the Kondo model calculation (see chapter 6) we will employ a modification of this kind, too.

Apart from diagonalization of the Hamiltonian, flow equations also represent a useful tool for deriving *effective* low energy Hamiltonians which can then be analyzed by other methods. A well-known example for this approach is the Schrieffer–Wolff transformation mapping the low energy sector of the single impurity Anderson model onto an effective Kondo Hamiltonian. In the original calculation of Schrieffer and Wolff (1966) the transformation was achieved by a single unitary transformation. However, the appearance of small-energy denominators due to second-order perturbation theory leads to a singular behaviour of the  $k$ -dependent Kondo couplings close to the impurity energy. This drawback was removed by Kehrein and Mielke (1996) in a modified Schrieffer–Wolff transformation based on a sequence of *infinitesimal* unitary transformations. Due to energy scale separation no small-energy denominators appear in the modified approach.

The strong-coupling expansion of MacDonald, Girvin and Yoshioka (1988) for the Hubbard model has also been implemented via flow equations by Stein (1997). This calculation is an example where the “diagonal” part of the Hamiltonian is different from the kinetic energy: Here it is instead taken to be the local Coulomb repulsion (the *atomic limit* Hamiltonian). In this case, however, it is not possible to introduce the concept of normal ordering because the corresponding unperturbed ground state is highly degenerate. As a consequence, the flow equation results for the effective  $t - J$  model are strictly perturbative and therefore in principle equivalent to other ways of derivation like the degenerate perturbation theory of Takahashi (1977). Nevertheless, flow equations may provide a more efficient way of formulating perturbation theory. For a recent application to dimerized spin chains, see Knetter and Uhrig (2000).

In this thesis the focus will be on actual diagonalization of the Hamiltonian. In particular, it will be pointed out to what extent flow equations have a non-

perturbative character. In a preliminary attempt, we apply the method directly to fermionic Hamiltonians in second quantization (chapter 5.1). For a simple toy model, the *Luttinger model*, this turns out to be quite successful, at least on the Hamiltonian level. An analysis of the Wolff impurity model revealed, however, that the necessary truncations of higher interaction terms (which are inevitably generated by (1.20)) lead to an instability of the flow once the coupling becomes comparable to the bandwidth.

These problems motivated a different approach, where the Hamiltonian is first transformed by bosonization and then diagonalized by flow equations. It was originally developed for the Tomonaga–Luttinger model with backscattering by Kehrein (1999). In chapter 6 we apply this version of the flow equation method to the anisotropic Kondo model where the full crossover from weak to strong coupling can be described analytically.

# Chapter 2

## Narrow-band Anderson model

### 2.1 Introduction

As explained in the introduction, the model introduced by Anderson (1961) to describe magnetic impurities in a metallic band has usually been analyzed in the flat band limit, where the conduction electron bandwidth represents the largest energy scale. In this particular case an analytical solution for the thermodynamics of the model has been obtained with the Bethe ansatz (Wiegmann 1981).

In this chapter we solve the Anderson impurity model numerically in the extreme limit where the bandwidth is much smaller than the hybridization (*narrow band system*) as shown in fig. 2.1. This situation is of interest for two different reasons:

1) Narrow hybridization functions may be generated due to interactions among the conduction electrons. This is particularly relevant for the model introduced by Wolff (1961), extended to the case of a correlated conduction band, which will be studied in section 3.9.

2) Within the dynamical mean-field theory, based on the limit of a high coordination number (Metzner and Vollhardt 1989a), correlated lattice models like the Hubbard model can be described by a single Anderson impurity interacting with a bath of conduction electrons whose properties are determined in a self-consistent way (Georges, Kotliar, Krauth and Rozenberg 1996). The bath is characterized by a hybridization strength of the order of the bandwidth and a non-constant density of states. For this case no exact results exist and one has to rely either on analytical approximations (which are, however, not available in the whole parameter space) or on numerical methods. In the context of the Mott-Hubbard transition in high dimensions, models with a narrow hybridization band are self-consistently generated in the transition scenario of Moeller, Si, Kotliar, Rozenberg and Fisher (1995), which has recently been supported by NRG calculations (Bulla 1999). By analyzing the narrow-band limit (without the additional complications caused by the  $d \rightarrow \infty$  self-

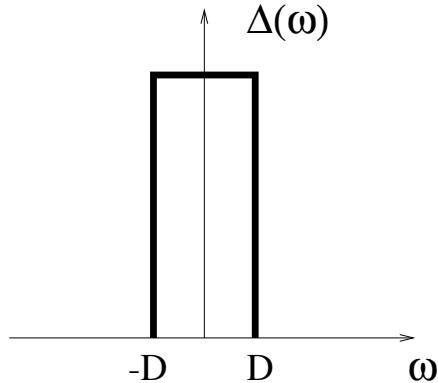


**Figure 2.1:** *Narrow hybridization function.*

consistency condition) we will establish two characteristic new features of Anderson impurity models that to some extent will also hold for intermediate situations:

i) The impurity density of states  $\rho_f(\omega)$  and the change in the density of states of the total system due to the impurity  $\Delta\rho(\omega)$  show a very different behaviour since the conduction electrons react to the presence of the impurity. This is in contrast to the flat band case where one always finds  $\rho_f(\omega) = \Delta\rho(\omega)$ . It leads to an interesting crossover in the thermodynamic impurity properties of the system when the interaction is turned on. ii) The skeleton expansion, which plays an important role in deriving properties of the interacting system, breaks down on intermediate energy scales. This has important implications for the Mott–Hubbard transition in  $d = \infty$ , as will be explained below.

## 2.2 Density of states

The Hamiltonian of the symmetric model is given by

$$H = \sum_{\mathbf{k},\sigma} \epsilon_{\mathbf{k}} c_{\mathbf{k}\sigma}^\dagger c_{\mathbf{k}\sigma} + \sum_{\mathbf{k},\sigma} (V_{\mathbf{k}} (c_{\mathbf{k}\sigma}^\dagger f_\sigma + h.c.) + U \left( f_\uparrow^\dagger f_\uparrow - \frac{1}{2} \right) \left( f_\downarrow^\dagger f_\downarrow - \frac{1}{2} \right)) \quad (2.1)$$

with the conduction electrons  $c_{\mathbf{k}}$  and the impurity orbital  $f$ . In the following, we will restrict ourselves to scalar  $k$ 's, implying – if necessary – a reduction to s–waves in the conduction band. The impurity density of states is defined by

$$\rho_f(\omega) = -\frac{1}{\pi} \text{Im} G_{ff}(\omega^+) , \quad (2.2)$$

where  $G_{ff}$  is the retarded zero temperature Green's function of the impurity orbital. On the other hand, the total change of the density of states due to the introduction

of the impurity into the conduction band is given by

$$\Delta\rho(\omega) = -\frac{1}{\pi}\text{Im} \left\{ \sum_k G_{kk}(\omega^+) + G_{ff}(\omega^+) \right\} + \frac{1}{\pi}\text{Im} \sum_k G_{kk}^{(0)}(\omega^+) \quad (2.3)$$

where  $G^{(0)}$  refers to the Green's function of the conduction electrons without the impurity. Using the equations of motion for  $G_{kk'}$  and  $G_{fk}$  one finds

$$\Delta\rho(\omega) = -\frac{1}{\pi}\text{Im} \left\{ G_{ff}(\omega^+) \left( 1 - \frac{\partial}{\partial\omega} \sum_k \frac{V_k^2}{\omega^+ - \epsilon_k} \right) \right\}. \quad (2.4)$$

Therefore the total change in the DOS can be expressed as a function of the impurity Green's function. We introduce the notation

$$\sum_k \frac{V_k^2}{\omega^+ - \epsilon_k} = \Lambda(\omega) - i\Delta(\omega), \quad (2.5)$$

where  $\Delta(\omega)$  is the hybridization function and the real part is given by the principal value integral  $\Lambda(\omega) = \mathcal{P} \int \frac{d\epsilon}{\pi} \frac{\Delta(\epsilon)}{\omega - \epsilon}$ . Now we can express  $\Delta\rho(\omega)$  in terms of the impurity density of states and write

$$\Delta\rho(\omega) = \rho_f(\omega) \left( 1 - \frac{\partial\Lambda}{\partial\omega} \right) - \frac{\partial\Delta}{\partial\omega} \mathcal{P} \int \frac{d\epsilon}{\pi} \frac{\rho_f(\epsilon)}{\omega - \epsilon}. \quad (2.6)$$

We define the *narrow band* limit by the property

$$\left. \frac{\partial\Lambda(\omega)}{\partial\omega} \right|_{\omega=\epsilon_F} \gg 1 \quad (2.7)$$

which leads to a negative coefficient multiplying the first term in (2.6) at the Fermi energy.

We will study one exemplary realization of a *narrow band* system with a constant hybridization function  $\Delta(\omega) = \Delta$  and conduction band energies extending from  $-D$  to  $D$  (we set  $\epsilon_F = 0$  in the sequel). In this case

$$\left. \frac{\partial\Lambda(\omega)}{\partial\omega} \right|_{\omega=0} = \frac{2\Delta}{\pi D} \quad (2.8)$$

and hence the *narrow band* limit is equivalent to  $\Delta \gg D$ . However, the main conclusions in the following analysis hold for other realizations of narrow band systems (2.7) as well, in particular even for systems without band edges at all.

We notice that for our model the second term of (2.6) vanishes inside the conduction band. Luttinger's theorem (Luttinger 1961, Langreth 1966) for the symmetric

Anderson model, which we will later verify numerically also for the narrow band case, ensures the “pinning” of the impurity spectral function at the Fermi energy at its noninteracting value

$$\rho_f(0) = \frac{1}{\pi\Delta} . \quad (2.9)$$

Therefore the first term in (2.6) gives a negative contribution

$$\Delta\rho(0) = \frac{1}{\pi\Delta} \left( 1 - \frac{2\Delta}{\pi D} \right) \quad (2.10)$$

at the Fermi energy. In the following we discuss the relation of  $\Delta\rho(\omega)$  to thermodynamic properties of the model.

### 2.3 Impurity susceptibility

In noninteracting fermionic models, the total density of states at the Fermi energy determines thermodynamic properties like the static susceptibility  $\chi$ . Introducing an impurity into the system induces a change in  $\chi$  proportional to  $\Delta\rho(0)$ . For the narrow-band Anderson systems analyzed here one therefore expects a negative impurity contribution to the susceptibility. This is obviously true for  $U = 0$  where one obtains the usual Pauli susceptibility in dimensionless units ( $\mu_B = \hbar = g = 1$ )

$$\chi_{\text{imp}} = \frac{\Delta\rho(0)}{2} = \frac{1}{2\pi\Delta} \left( 1 - \frac{2\Delta}{\pi D} \right) . \quad (2.11)$$

In order to determine whether this holds also for the interacting case, we have calculated  $\chi$  using the numerical renormalization group method with discretization parameter  $\Lambda = 2$  following Krishna-murthy et al. (1980). As outlined in section 1.2, the conduction band of (2.1) is logarithmically discretized and the eigenstates of the Hamiltonian are then calculated by iterative diagonalization. In each iteration step  $N$ , thermodynamic information can be obtained on a scale  $T_N = D(1 + \Lambda^{-1})\Lambda^{-(N-1)/2}/(2\bar{\beta})$  where  $\bar{\beta}$  is a dimensionless parameter of order one. Note that the prefactors arise due to the rescaling convention for the Hamiltonian  $H_N$  (see equation (1.12)). Now the impurity part of the susceptibility is written as

$$k_B T_N \chi_{\text{imp}}(T_N) = \frac{\text{Tr} S_{Nz}^2 \exp\{-\bar{\beta} H_N\}}{\text{Tr} \exp\{-\bar{\beta} H_N\}} - \frac{\text{Tr} S_{Nz}^{02} \exp\{-\bar{\beta} H_N^0\}}{\text{Tr} \exp\{-\bar{\beta} H_N^0\}} \quad (2.12)$$

where  $H_N^0$  denotes the conduction band without impurity and  $S_{Nz}^{02}$  is the corresponding total spin in  $z$  direction. At high temperatures, complete diagonalization of the logarithmically discretized 5-site model yields essentially exact results (continuous

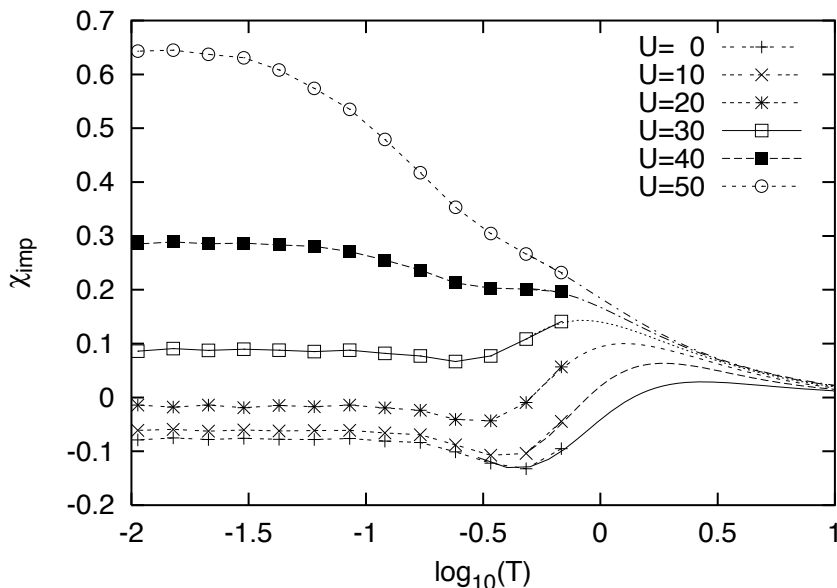


**Figure 2.2:** Impurity susceptibility vs. logarithmic temperature at hybridization  $\Delta = 10$  and half bandwidth  $D = 1$  for different interactions  $U$ .

lines), as no low-energy information is needed in that case. The results for fixed hybridization  $\Delta = 10$  and half bandwidth  $D = 1$  are shown in figure 2.2. At large  $T$ , the almost free orbital leads to  $\chi_{\text{imp}} = \frac{1}{8T}$ . Upon lowering the temperature, we find a characteristic dependence on the value of the interaction. For  $U \lesssim 2\Delta$  we see a crossover to a negative  $\chi_{\text{imp}}$ , which is due to the loss of spectral weight at low frequencies as a consequence of hybridization. After a characteristic minimum at finite temperature the susceptibility saturates at a negative value as  $T \rightarrow 0$ . For  $U \gtrsim 2\Delta$ , we recover the usual positive  $\chi_{\text{imp}}$  which is strongly enhanced at large  $U/\Delta$  by the Kondo effect defining a new exponentially small energy scale  $T_K$ . In spite of these different types of behaviour depending on the interaction, the impurity contribution to the density of states at the Fermi energy is negative (2.10) for *any*  $U$ . We therefore conclude that only in the weakly interacting case  $\Delta\rho(\epsilon_F)$  yields the thermodynamic properties of the model. In the strong coupling regime, the susceptibility enhancement is determined by the many-body resonance in  $\rho_f(\omega)$  which – similar to the wide band case – has to be interpreted as a quasiparticle peak with a large effective mass. The low-temperature behaviour of the system for strong correlations is governed by many-particle excitations which are not contained in  $\Delta\rho(\omega)$  and, in fact, completely dominate over the reduction in the single-particle DOS  $\Delta\rho(\epsilon_F) < 0$ .

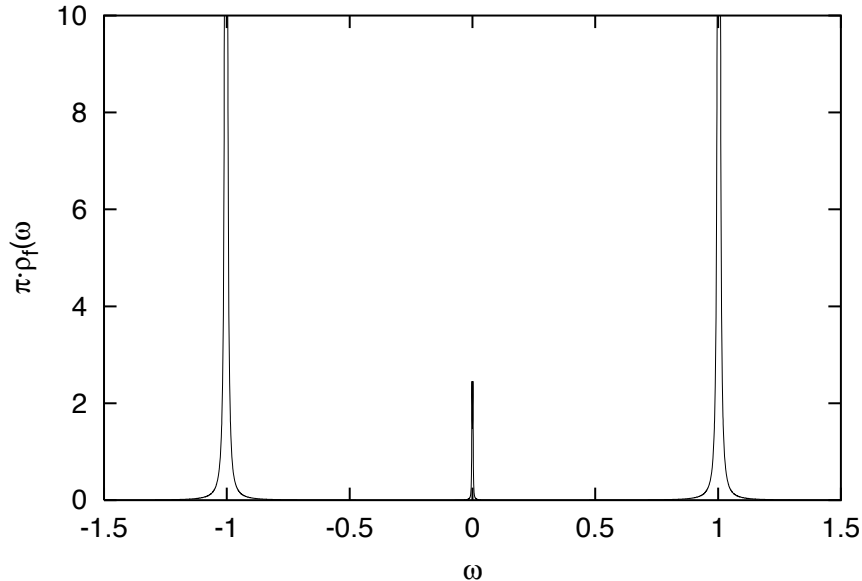


**Figure 2.3:** Spectral density of the narrow band Anderson model with the parameters  $U = 2.0$ ,  $\Delta = 1.0$  and  $D = 10^{-3}$ . Apart from the atomic levels, spectral weight is only found at frequencies  $\omega \sim D$ .

## 2.4 Spectral density and skeleton expansion

Next, we discuss the spectral density of narrow-band Anderson systems. The impurity orbital Green's function at zero temperature is determined using the Lanczos method as implemented by Krauth (see Georges et al. (1996)). We fix the values of the interaction  $U$  and the hybridization  $\Delta$  and then successively reduce the bandwidth, thus taking the limit  $D \rightarrow 0$ . For each set of parameters we calculate the spectral function  $\rho_f$ , using an Anderson star with  $11 + 1$  sites. For not too large  $U/\Delta$  the spectral density is found to be only weakly dependent on the number of sites. In the limit of small bandwidth at any finite value of the ratio  $U/\Delta$ , we find a three-peak structure (see fig. 2.3) consisting of the atomic levels at  $\omega = \pm U/2$  containing almost the full spectral weight and a central quasiparticle peak of width  $\sim D$ . Apart from numerical broadening effects there is no spectral weight between the peaks. This gives rise to resonances in the imaginary part of the self-energy, which can be seen in the following way (Zhang, Rozenberg and Kotliar 1993, Kehrein 1998): As a consequence of Dyson's equation, for values of  $\omega$  inside the gap (where spectral function and hybridization vanish) the self-energy  $\Sigma(\omega^+) = K(\omega) - iJ(\omega)$  is given by

$$\Sigma(\omega^+) = \omega - \Lambda(\omega) - \frac{1}{\Gamma(\omega) - i0^+}, \quad (2.13)$$

where we have defined  $\Gamma(\omega) \equiv \mathcal{P} \int d\epsilon \frac{\rho_f(\epsilon)}{\omega - \epsilon}$ . The imaginary part of the self-energy therefore has the form

$$J(\omega) = \pi \delta(\Gamma(\omega)) . \quad (2.14)$$

For the spectral density found here  $\Gamma(\omega)$  has zeros at energies  $\epsilon \sim \pm\sqrt{D}$  and this leads to  $\delta$ -functions in  $J(\omega)$  inside the gap as shown above.

As argued previously by Kehrein (1998), these resonances are incompatible with the skeleton expansion, i.e. the self-consistent perturbation theory in  $U$ . Within this expansion, the full propagator  $G_{ff}(\omega)$  is inserted into every diagram contributing to  $J(\omega)$ . As  $G_{ff}(\omega)$  possesses spectral weight only on the small energy scale  $D \ll \sqrt{D}$ , there is no possibility to generate the resonances at  $\pm\sqrt{D}$ . We therefore conclude that in our model already for small but finite bandwidth  $D$  the skeleton expansion breaks down at energies of the order  $\sqrt{D}$  (strictly speaking  $\sim \sqrt{\Delta D}$ , but note that here we have chosen  $\Delta = 1$  dimensionless).

As a measure of the convergence of the expansion at lower energies we take the Fermi liquid properties of the Anderson model, especially the “pinning” of the density of states at its noninteracting value (2.9). This is equivalent to the vanishing of the imaginary part of the self energy at the Fermi level. This property has been proved for a general class of systems (Luttinger 1961) by using the skeleton expansion to all orders. A proof for the (flat band) Anderson model within unrenormalized perturbation theory was given by Yamada (1975). In order to verify the pinning we focus on the central peak of  $\rho_f$  and compare different, not too strong interactions at constant broadening. The pinning of  $\rho_f(0)$  in the limit  $D \rightarrow 0$  is evident from fig. 2.4. At even larger interactions (not shown here), a narrow Kondo resonance develops inside the band, which cannot be resolved well on a small cluster. From the above, however, we do not expect deviations from Luttinger’s theorem for any interaction. As can also be seen in fig. 2.4, the “quasiparticle” resonance in  $\rho_f(\omega)$  has an internal structure itself (including bound states outside the band for small  $U/\Delta$ ). In the limit  $D \rightarrow 0$  this can be described by a scaling function

$$\rho_f(\omega) = f(\omega/D) , \quad (2.15)$$

where  $f$  is independent of  $D$ . The  $\delta$ -peaks in fig. 2.4, dominant at small  $U$ , can be understood by approximating the Hamiltonian as a “zero bandwidth” Anderson model (see Hewson (1993)) where the impurity couples to one single orbital and the hybridization is given by a  $\delta$ -function carrying the integrated weight  $\int d\epsilon \Delta(\epsilon)$ . The effect of the continuous hybridization band is to generate spectral density close to  $\omega = 0$  and to create sidebands also visible in fig. 2.4. For larger values of  $U$  the weight of the bound states decreases (from the zero bandwidth model we expect a decrease  $\sim 1/U^2$ ) and within the numerical resolution they merge with the continuum at small  $\omega$ .

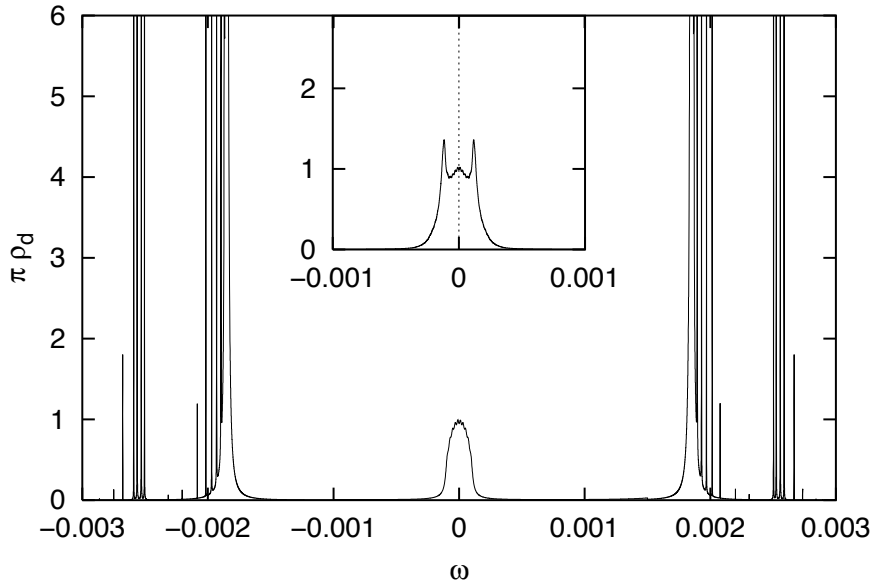


**Figure 2.4:** Central peak in the impurity density of states for different interactions  $U = 0.2$  and  $4.0$  (inset), hybridization  $\Delta = 1.0$  and bandwidth  $D = 10^{-4}$ . We have used a Lorentzian broadening of  $b = 1.5 \times 10^{-5}$  at the quasiparticle resonance and  $b = 5 \times 10^{-8}$  for the poles at higher frequencies. The atomic levels at  $\pm U/2$  carrying most of the spectral weight are not shown. At the Fermi edge,  $\pi \rho_f(0) = 1.00 \pm 0.02$  for both values of  $U$ .

For other hybridization functions in the narrow band limit (2.7) the main conclusions of the above analysis remain unaffected. A detailed numerical study is, however, difficult due to the limited number of orbitals that can be taken into account by using exact diagonalization. For example, in a “narrow” band with band tails extending to  $\pm\infty$  but  $\frac{\partial\Lambda}{\partial\omega}|_{\omega=0} \gg 1$ , the bound states for  $U = 0$  become sharp resonances. Likewise the imaginary part of the self-energy then contains sharp resonances at  $\pm O(\sqrt{D})$  instead of  $\delta$ -functions. Still the resonances contain the same spectral weight as these  $\delta$ -functions and the breakdown of the skeleton expansion occurs in the same manner (Kehrein 1998).

## 2.5 Conclusion

In this chapter we have studied the Anderson impurity model in the narrow band limit (2.7), using numerical methods. We have found two new features as compared to the usual wide band limit:

i) One observes a crossover in the impurity contribution to the susceptibility: For

small interactions the total susceptibility is reduced by the impurity, for large interactions it is enhanced. In fact, the same behaviour is also found for the specific heat, although this has not been discussed explicitly here. This crossover is in contrast to the observation that the impurity contribution to the total density of states at the Fermi level is *always* negative. This quantity does therefore not determine the thermodynamic properties of the system at large interactions.

ii) Holding  $U$  and  $\Delta$  fixed, the skeleton expansion breaks down for a sufficiently small (but still finite) bandwidth  $D$ . The breakdown occurs at energies of order  $\sqrt{D}$  and larger, while for smaller energies no problems can be found. This shows that the breakdown of the skeleton expansion is a generic feature of narrow band Anderson impurity systems<sup>1</sup>. On the other hand, the skeleton expansion is an essential tool for deriving the locality of the self-energy in the dynamical mean field theory in the Fermi liquid phase (Metzner and Vollhardt 1989*a*, Müller-Hartmann 1989). Its convergence provides a sufficient condition for the analytic continuation to the noninteracting Hubbard model. Notice also that recently Keiter and Leuders (2000) have discussed the relation between DMFT and finite-dimensional correlated systems in the context of the random-loop problem. At present, the question of the correct description of the Mott-Hubbard transition in large dimensions is under debate (Kehrein 1998, Logan and Nozières 1998, Georges and Kotliar 2000): NRG simulations by Bulla (1999) at  $T = 0$  indicate a preformed gap in the density of states and a corresponding coexistence between metallic and insulating solutions also at finite temperature. This has been confirmed by recent quantum Monte Carlo simulations, in contrast to the previously published data of Schlipf, Jarrell, van Dongen, Blümer, Kehrein, Pruschke and Vollhardt (1999). On the other hand, the *random dispersion approximation* introduced by Gebhard (1997) – an independent approach to the  $d = \infty$  limit – yields a second order transition at zero temperature without any coexistence regime as shown by Noack and Gebhard (1999). This discrepancy still needs to be solved. In any case, however, the analysis presented above shows that for the preformed gap scenario (which naturally leads to an effective action governed by a narrow band system in the sense of (2.7)) one has to address the question whether such systems can be related to the original Hubbard model in large dimensions.

---

<sup>1</sup>Lange (1998) has discussed convergence properties of the skeleton expansion for the zero bandwidth model. This model is characterized by two parameters  $U$  and  $V$ , where the limit  $V \sim \sqrt{D} \rightarrow 0$  corresponds to a two-site approximation of the narrow band system (2.1). It is shown that in this limit self-consistent perturbation theory fails. In contrast, we would like to point out the *frequency dependent* convergence properties of the skeleton expansion (at any  $U$ ), as explained above. The resulting distinction between the energy scales  $D$  and  $\sqrt{D}$  is only possible in a model with a finite bandwidth.



## Chapter 3

# Magnetic impurity in a correlated band

### 3.1 Introduction

In the preceding chapter we have analyzed a generalized version of the Anderson impurity model with a nontrivial hybridization function. While the detailed structure of the spectral density is strongly modified in this case, the impurity spin is still screened at low energies and the system remains a local Fermi liquid.

One very important characteristic of real materials is the interaction among the conduction electrons. This aspect is usually neglected, mostly for technical reasons. If taken into account, it should at least yield a renormalization of the conduction band Fermi liquid parameters which would then in turn affect the Kondo screening. The present study will focus on the question whether, in addition, qualitatively new physics is possible. An experimental realization frequently cited in this context is the cuprate compound  $Nd_{2-x}Ce_xCuO_4$  studied by Brugger, Schreiner, Roth, Adelman and Czjzek (1993), a concentrated impurity system where the  $Nd$  local moments are coupled to the strongly correlated  $Cu$  sites. At finite doping  $x > 0$  heavy fermion behaviour is observed; the measured coherence temperature is, however, incompatible with the standard Kondo picture. A more detailed discussion will be given in section 3.2. Experiments on *dilute* systems with strongly correlated conduction electrons (which are more accurately described by a single impurity model) can also be performed and will be discussed later.

Theoretical analysis of this problem has been fairly successful in one dimension. Here, the interacting host can be represented as a Luttinger liquid characterized by dimensionless Coulomb interaction strength parameters  $g_c$  and  $g_s$  for the charge and spin sector, respectively. While the effect of a potential scatterer in these systems is by now well understood due to Kane and Fisher (1992), the low temperature phase

diagram of a magnetic impurity in a Luttinger liquid is more difficult to access. For a Kondo impurity, Lee and Toner (1992) performed a perturbative RG analysis and found a power-law dependence of the Kondo scale  $T_K$  on the exchange coupling  $J$ . Furusaki and Nagaosa (1994) later extrapolated a similar scaling approach to the strong coupling regime where they found a stable strong-coupling fixed point for both antiferromagnetic and ferromagnetic exchange coupling. The low temperature critical properties of the impurity were shown to exhibit power-law type, non-Fermi-liquid (NFL) behaviour. On the other hand, an RG analysis by Schiller and Ingersent (1995) and numerical studies by Wang (1998) indicated a local Fermi liquid ground state. As shown by Fröjdh and Johannesson (1995), both of these possibilities are consistent with boundary conformal field theory, which allows a classification of possible fixed points but does not determine which one is actually realized. In a recent quantum Monte Carlo study by Egger and Komnik (1998) the NFL scenario is supported and the importance of additional potential scattering pointed out. Less is known about an Anderson impurity in a Luttinger liquid. Exact diagonalization studies of small systems by Hallberg and Balseiro (1995) yielded Friedel oscillations with interaction-dependent exponents. Renormalization group calculations by Phillips and Sandler (1996) and Schiller and Ingersent (1997) showed that the local moment may be enhanced due to the bulk correlations.

For the experimental realizations mentioned at the beginning, higher-dimensional representations of the conduction band are more relevant. Unlike the Luttinger case, an exact treatment of the correlated band electrons is then not possible anymore. Within a mean-field treatment, Tornow, Zevin and Zwicknagl (1996) took correlations into account by introducing antiferromagnetic long-range order in the host. Perturbative calculations in a slave boson representation by Khaliullin and Fulde (1995) yielded an increase<sup>1</sup> of the effective Kondo coupling. Very similar results were obtained by Schork (1996) in a  $1/N$  expansion and by Tornow, Zevin and Zwicknagl (1997) within the non-crossing approximation. The relation to the Kondo model was analyzed by Schork and Fulde (1994), who generalized the Schrieffer-Wolff transformation to the case of interacting conduction electrons. Furthermore, in the limit of high dimensions and using a variational treatment, Davidovich and Zevin (1998) found a qualitative change of the behaviour of the Kondo temperature  $T_K$ . According to these authors, above some intermediate value of the conduction band interaction,  $T_K$  is no longer exponentially small for a vanishing exchange coupling. We will discuss this issue in detail.

The studies listed above already indicate the competition of several effects:

- Correlations may change the density of states (DOS) of the conduction band.

---

<sup>1</sup>A different conclusion was reached by Itai and Fazekas (1996): Performing a Gutzwiller variational calculation for the periodic Anderson model, they found a *decrease* of the Kondo temperature due to band correlations. This result has to be considered as an artefact of the approximation used.

- A repulsive on-site interaction will suppress the hybridization of the impurity level.
- The conduction electrons will become increasingly polarized, thus enhancing the effective spin coupling of the impurity moment.

In order to determine which of the above is the main factor of influence, we choose the dynamical mean-field theory (DMFT) approach in combination with Wilson's nonperturbative numerical renormalization group.

## 3.2 Experimental motivation

Magnetic ions in metals may lead to a novel Fermi liquid state at low temperatures. This is for example the case in standard heavy fermion systems like  $CeAl_3$  or  $CeRu_2Si_2$ , where the rare earth spins are screened by the interaction with the conduction electrons.

Similar to these compounds, the doped cuprate  $Nd_{2-x}Ce_xCuO_4$  (see fig. 3.1) exhibits a large linear specific heat  $C \sim \gamma T$  and a strongly enhanced Pauli susceptibility  $\chi_0$  below a coherence temperature  $T^* \approx 2K$ . The corresponding Wilson ratio has the value  $R = \pi^2 k_B^2 \chi / (3\mu_{\text{eff}} \gamma) \approx 2$  consistent with a single impurity picture where the  $Nd$  ions are considered as independent Kondo spins. In the undoped compound  $Nd_2CuO_4$  the ground state is antiferromagnetically ordered. The specific heat displays a Schottky anomaly below  $10K$ , caused by an antiferromagnetic coupling between the  $Cu$  sites and their two next-nearest  $Nd$  neighbours (see Fulde, Zevin and Zwicknagl (1993)):

$$H_{\text{int}} = J \sum_i \sum_{\delta=1}^2 \mathbf{s}_i^{\text{Cu}} \cdot \mathbf{S}_{i+\delta}^{\text{Nd}} \quad (3.1)$$

The exchange coupling  $J$  is thus of the same order of magnitude as the coherence temperature itself. On the other hand, the standard Kondo picture would yield  $T^* \approx D \exp\{-1/(N(0)J)\}$  where the bandwidth  $D$  is of the order  $eV$  and  $N(0) \sim 1/D$  is the density of states. The resulting estimate for  $T^*$  is too small by

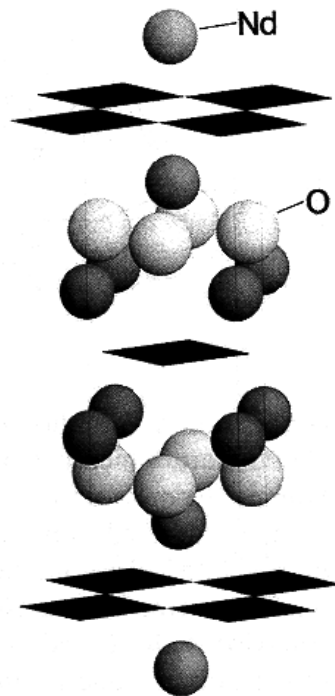


Figure 3.1: Structure of  $Nd_2CuO_4$ , see Fulde (1995).

many orders of magnitude. This discrepancy has been interpreted by Fulde et al. (1993) as an effect of the strong band correlations, which are expected to renormalize the Kondo scale. Additional complications may arise due to superconductivity which sets in below  $T_c \approx 20K$  for a doping strength  $x = 0.15$  as shown by Maiser, Mexner, Schäfer, Schreiner, Adelman, Czjzek, Peng and Greene (1997). It should also be mentioned that an alternative explanation of the measured heavy fermion behaviour, based on a competition between the  $Nd - Nd$  and  $Nd - Cu$  interactions, has been proposed by Henggeler, Chattopadhyay, Thalmeier, Vorderwisch and Furrer (1996).

### 3.3 Model and dynamical mean-field theory

In the following we will study a “minimal” theoretical model which consists of a spin 1/2 Anderson impurity (with both spin and charge degree of freedom) embedded into a correlated host. For the latter we employ the standard representation as a one-band *Hubbard* lattice (Gutzwiller 1963, Hubbard 1963, Kanamori 1963)

$$H_B = - \sum_{ij\sigma} (t_{ij} + \mu \delta_{ij}) c_{i\sigma}^\dagger c_{i\sigma} + U_B \sum_i n_{i\uparrow} n_{i\downarrow} \quad (3.2)$$

which is characterized by the competition between the hopping  $t$  and the on-site Coulomb energy  $U_B$ . We first give a brief survey of the phase diagram at half filling  $n = 1$  as obtained within DMFT and shown in fig. 3.2.

The ground state of a generic lattice is known to be antiferromagnetically (AFM) ordered for a sufficiently large value of the interaction (see for example Duffy and Moreo (1997), Hofstetter and Vollhardt (1998) and Schlipf (1998)). Increasing the temperature eventually destroys the long-range order. Depending on the interaction strength, the resulting paramagnetic phase has metallic or insulating properties. The transition between these two regimes – the *Mott* metal-insulator transition – is of great theoretical interest and still under intensive study. Note that, in general, this transition also occurs in the antiferromagnetic phase, as indicated in the phase diagram (fig. 3.2). Within DMFT, most studies have so far been performed for the paramagnetic region. One usually suppresses the AFM ordering by introducing frustration (including for example next-nearest neighbour hopping as done by Schlipf (1998)) or by simply ignoring symmetry breaking and constraining the calculation to the paramagnet.

The following results have emerged, outlined in parts already in the last chapter: At zero temperature the second order scenario of Georges et al. (1996) has finally been confirmed by Bulla (1999). Note that because of the “preformed” gap in the spectral density the validity of the DMFT equations is nontrivial, as discussed previously. For small but finite temperatures, exact diagonalization (Laloux, Georges and Krauth (1994)) and NRG indicate that the transition becomes first order due to coexistence

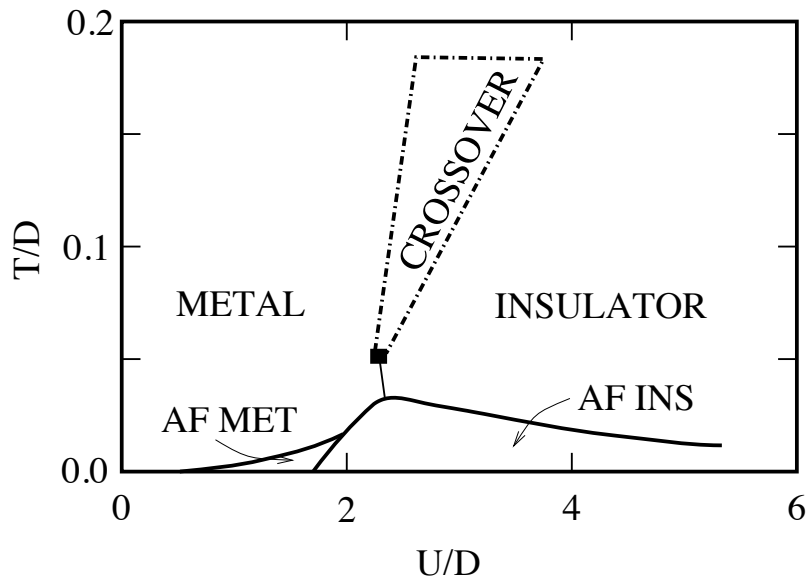


**Figure 3.2:** Phase diagram of the Hubbard model at half filling (see Georges et al. 1996).

of two different phases within dynamical mean–field theory. How far this coexistence region extends to higher temperatures and where the crossover region of fig. 3.2 starts is still subject of study (Schlipf et al. 1999, Bulla, Costi and Vollhardt 2000). Finally, it should be mentioned that calculations by Noack and Gebhard (1999) within an alternative approach to the  $d = \infty$  limit – the random dispersion approximation of Gebhard (1997) – yielded a zero temperature transition scenario that is not consistent with DMFT. The accuracy of these calculations may however be limited due to finite–size effects. In the following we will be mainly interested in the paramagnetic metallic phase where Kondo physics is expected. The additional impurity is assumed to hybridize with one single lattice site  $i = 0$ , with an amplitude  $V$ . In addition, it is correlated, i.e. double occupancy of the impurity gives rise to an on–site energy  $U$ . The total Hamiltonian including the impurity has the form

$$H = H_B + V \sum_{\sigma} \left( f_{\sigma}^{\dagger} c_{0\sigma} + h.c. \right) + U n_{f\uparrow} n_{f\downarrow} + \epsilon_f n_f \quad (3.3)$$

where at the moment we restrict ourselves to the particle–hole symmetric case for both the impurity ( $\epsilon_f = -U/2$ ) and the host lattice ( $\mu = U_B/2$ ). The latter is assumed to be bipartite. A graphical representation of this system is given on the left hand side of fig. 3.3.

About a decade ago, Metzner and Vollhardt (1989a) discovered that a controlled approach to the problem of correlated lattice fermions is possible in the limit of a high coordination number  $z$  or, equivalently, large space dimension  $d$  (for a review

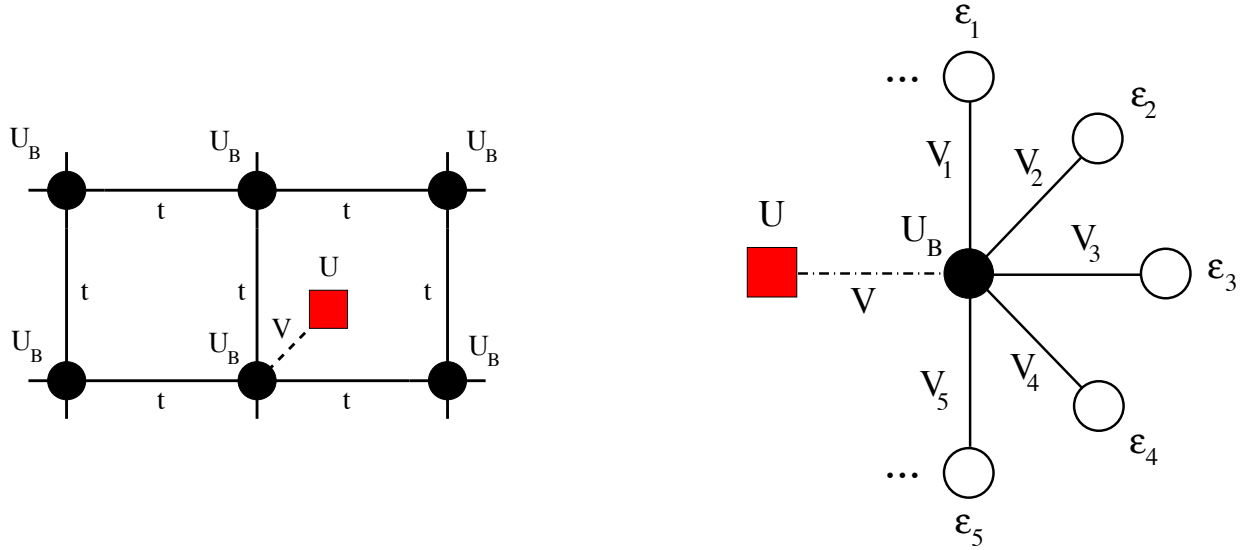


**Figure 3.3:** Left: Anderson impurity (square) coupled to one site of a correlated lattice (circles). The hybridization is taken to be purely local. Right: effective two-impurity model with noninteracting band orbitals (empty circles) of energy  $\epsilon_i$  and hybridization  $V_i$ .

see Vollhardt (1993)). In order to keep the kinetic energy of the model finite, the hopping matrix elements are scaled as

$$t = \frac{t^*}{\sqrt{z}} \quad (3.4)$$

where we have assumed next-neighbour hopping with a constant amplitude  $t$ . In our treatment we will use the Bethe lattice and take the noninteracting half-bandwidth  $D = 2t^* = 1$  as the unit of energy. Let us emphasize, however, that the choice of the lattice is merely motivated by calculational convenience and should have no qualitative effect on the results.

The  $z \rightarrow \infty$  limit leads to a local self-energy of the Hubbard model, thus permitting a mapping of the lattice model onto an effective single impurity problem. One way of deriving this equivalence is the *cavity method*, which we outline briefly, following Georges et al. (1996). Starting from the full partition function of the Hubbard model written in the path integral representation

$$Z = \int \prod_i Dc_{i\sigma}^\dagger Dc_{i\sigma} e^{-S} \quad (3.5)$$

with the action

$$S = \int_0^\beta d\tau \left( \sum_{i\sigma} c_{i\sigma}^\dagger \partial_\tau c_{i\sigma} - \sum_{ij,\sigma} t_{ij} c_{i\sigma}^\dagger c_{j\sigma} - \mu \sum_{i\sigma} c_{i\sigma}^\dagger c_{i\sigma} + U_B \sum_i n_{i\uparrow} n_{i\downarrow} \right) \quad (3.6)$$

we choose one Hubbard site (to be labelled by the index  $i = 0$ ) and derive an effective action for the local dynamics on this site by integrating out all the remaining fermionic degrees of freedom:

$$\frac{1}{Z_{\text{eff}}} e^{-\mathcal{S}_{\text{eff}}[c_{0\sigma}^\dagger, c_{0\sigma}]} \equiv \frac{1}{Z} \int \prod_{i \neq 0, \sigma} Dc_{i\sigma}^\dagger Dc_{i\sigma} e^{-S} \quad (3.7)$$

For infinite coordination number, the retarded part of the effective action is quadratic

$$\mathcal{S}_{\text{eff,ret}} = - \iint d\tau d\tau' c_{0\sigma}^\dagger \mathcal{G}_0^{-1}(\tau - \tau') c_{0\sigma}(\tau'). \quad (3.8)$$

The *Weiss function*  $\mathcal{G}_0$  is then determined by the DMFT self–consistency condition

$$G_0(\omega) = \sum_{\mathbf{k}} G_{\text{lattice}}(\mathbf{k}, \omega) \quad (3.9)$$

equating the effective impurity Green’s function to the local lattice  $G$ . Both  $\mathcal{G}$  and  $G$  are taken to be independent of the spin as we are interested in the paramagnetic phase. Recently it was pointed out by Davidovich and Zevin (1998) that the above line of reasoning is still valid if an additional fermionic impurity  $f^\dagger$  is coupled to the local Hubbard site. In particular, the retarded part of the effective action  $\mathcal{S}_{\text{eff}}[c_0^\dagger, c_0, f^\dagger, f]$  will be unchanged and  $\mathcal{G}_0$  is the same as in the Hubbard case. As a result, the system can be described as an effective two–impurity model (shown on the right–hand side of fig. 3.3)

$$\begin{aligned} H_{\text{eff}} = & \sum_{p\sigma} \epsilon_p a_{p\sigma}^\dagger a_{p\sigma} + \sum_{p\sigma} V_p \left( a_{p\sigma}^\dagger c_{0\sigma} + h.c. \right) - \mu c_{0\sigma}^\dagger c_{0\sigma} + U_B n_{0\uparrow} n_{0\downarrow} \\ & + \epsilon_f f_\sigma^\dagger f_\sigma + U n_{f\uparrow} n_{f\downarrow} + V \sum_{\sigma} \left( f_\sigma^\dagger c_{0\sigma} + h.c. \right) \end{aligned} \quad (3.10)$$

with an effective *noninteracting* bath defined by a hybridization function

$$\Delta_c(\omega) = \pi \sum_p |V_p|^2 \delta(\omega - \epsilon_p) \quad (3.11)$$

that is completely determined by the DMFT calculation *without* the impurity. In our analysis we will therefore follow a two–step procedure: First, we solve the Hubbard model in the limit  $d \rightarrow \infty$  for the paramagnetic phase. With the resulting  $\mathcal{G}_0$  as an input, we then analyze the two–impurity model. A simplified treatment without the DMFT step has recently been applied by Takayama and Sakai (1998).

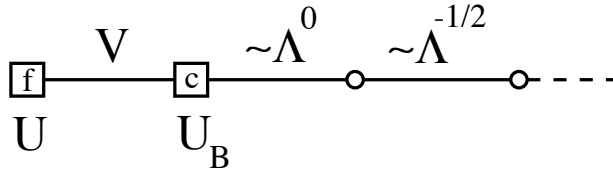


**Figure 3.4:** Semi-infinite chain representation of the effective two-impurity model.

### 3.4 NRG calculations

For the solution of the DMFT equations and the subsequent analysis of the two-impurity model (3.10) we use Wilson's numerical renormalization group described in section 1.2. After introducing a logarithmic discretization of the conduction band, the system is mapped on a semi-infinite chain (fig. 3.4) by using the Lanczos procedure outlined in appendix A. The resulting Hamiltonian then reads

$$\begin{aligned}
 H_{\text{chain}} = & \epsilon_f f_{\sigma}^{\dagger} f_{\sigma} + U n_{f\uparrow} n_{f\downarrow} + V \left( f_{\sigma}^{\dagger} c_{0\sigma} + h.c. \right) - \mu c_{0\sigma}^{\dagger} c_{0\sigma} + U_B n_{0\uparrow} n_{0\downarrow} \\
 & + \sum_{\substack{n=0 \\ \sigma}}^{\infty} \epsilon_n \left( c_{(n+1)\sigma}^{\dagger} c_{n\sigma} + h.c. \right). \quad (3.12)
 \end{aligned}$$

Here the  $c_n$  should *not* be identified with the original Hubbard fermions – this is only valid for  $c_0$  which corresponds to the local Hubbard site next to the impurity. The detailed shape of the hybridization function is now contained in the hopping amplitudes  $\epsilon_n$  according to a *continued fraction* representation of the spectral density. In our calculation, we choose the discretization parameter to be  $\Lambda = 2$ .

In this form, the system can be treated by iterative diagonalization, keeping in each step only a limited number of excited states and matrix elements. We focus on the dynamics at zero temperature, in particular on the one-particle spectral densities  $\rho_f(\omega)$  and  $\rho_c(\omega)$ , as well as the local susceptibility  $\chi(\omega)$ . At iteration  $n$ , the spectra are calculated close to the corresponding frequencies  $\omega_n \sim \pm\Lambda^{-n/2}$ . As discussed in the preceding chapter, the DMFT equations for the Hubbard model have to be solved first. For the Bethe lattice, the self-consistency condition (3.9) simplifies to

$$\Delta_c(\omega) = \pi (t^*)^2 \rho_c(\omega) \Big|_{V=0}. \quad (3.13)$$

In the paramagnetic phase this leads to the Mott transition scenario described by Bulla (1999). The corresponding spectral densities as a function of the band interaction  $U_B$  are displayed in fig. 3.5.

In our units, the metal-insulator transition takes place at a Hubbard interaction strength  $U_B \approx 2.92$ . Correlations strongly influence the structure of the DOS and,

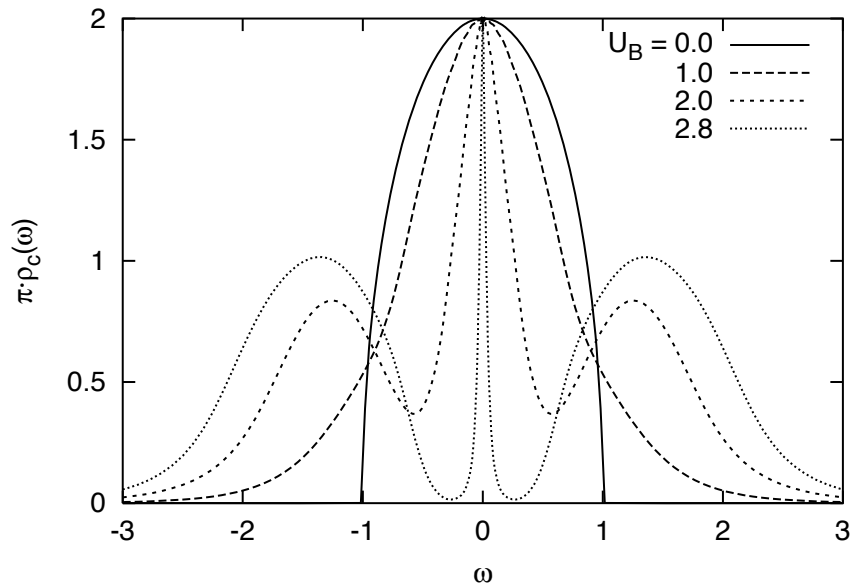


**Figure 3.5:** Local density of states of the Hubbard model.

close to the transition point, an effective narrow band is formed by the quasiparticle resonance. We define an effective bandwidth  $D_{\text{eff}}$  as the energy where  $\rho_c(\omega)$  has fallen to 4/5 of its  $\omega = 0$  value (see fig. 3.6, note that this definition is arbitrary).

In the next step, the  $f$ -impurity is added (see fig. 3.4) with an on-site interaction  $U_f$  and a hybridization matrix element  $V$  to the local Hubbard site. The combined system is then again treated using NRG, this time without the self-consistency loop. The band correlations enter via the previously determined DOS (fig. 3.5) and the  $c$ -site interaction  $U_B$ . In the present calculations we have confined ourselves to the metallic regime  $U_B < 2.92$ .

### 3.5 Single-particle spectral functions

Photoemission spectroscopy (PES or BIS) has provided the first direct verification of the “virtual bound state” concept, see for example Myers, Walldén and Karlsson (1968) and Drew and Doezema (1972). Measurements on dilute systems are usually difficult because of the weak signal. It was found, however, that single impurity properties persist even to fairly high concentrations (in thermodynamics and transport this was verified by Lin, Wallash, Crow, Mihalisin and Schlottmann (1987)). Single particle spectra may therefore be used to detect band correlation effects experimentally.

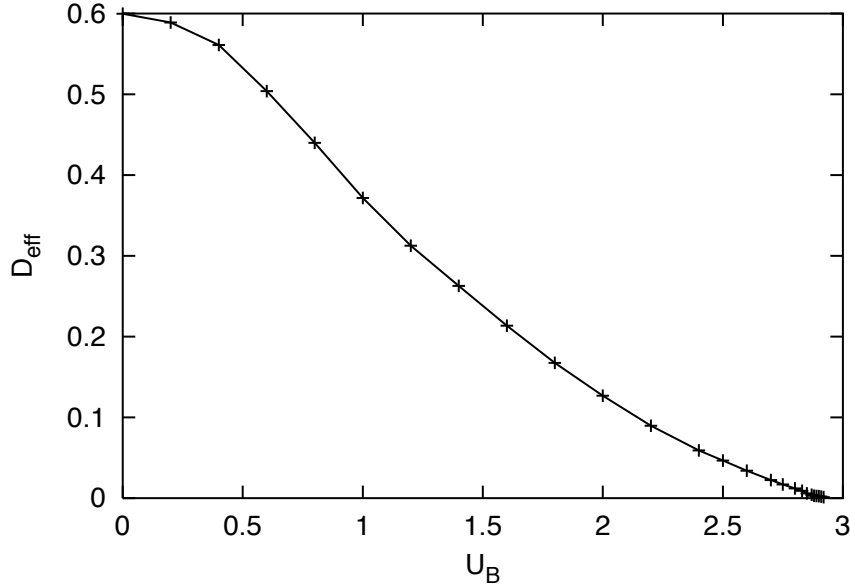


**Figure 3.6:** *Effective bandwidth of the Hubbard model.*

We consider the  $T = 0$  spectral functions of the impurity and the local Hubbard site:

$$\rho_{f(c)}(\omega) = -\frac{1}{\pi} \text{Im} G_{f(c)}^{\text{ret}}(\omega). \quad (3.14)$$

In the Lehmann representation (see Negele and Orland (1987)) one obtains

$$\begin{aligned} \rho_f(\omega) &= \sum_n |\langle n | f^\dagger | 0 \rangle|^2 \delta(\omega - (E_n - E_0)) \\ &+ \sum_n |\langle n | f | 0 \rangle|^2 \delta(\omega - (E_0 - E_n)) \end{aligned} \quad (3.15)$$

and a similar identity for  $\rho_c$ . Here  $|0\rangle$  is the ground state and  $|n\rangle$  denotes the excitations. Within the NRG procedure, the matrix elements of  $f$  and  $c$  are calculated recursively and the resulting spectral peaks are broadened by a logarithmic Gaussian (see appendix C).

First we show results for  $\rho_f$  close to the Mott transition in fig. 3.7. Already for  $U = 0$  and a “bare” hybridization

$$\boxed{\Delta = \frac{\pi V^2}{2D}} \quad (3.16)$$

significantly smaller than the noninteracting bandwidth, we obtain a three-peak structure in the spectrum. We attribute this to an effective bandwidth  $D_{\text{eff}} \approx 0.03$

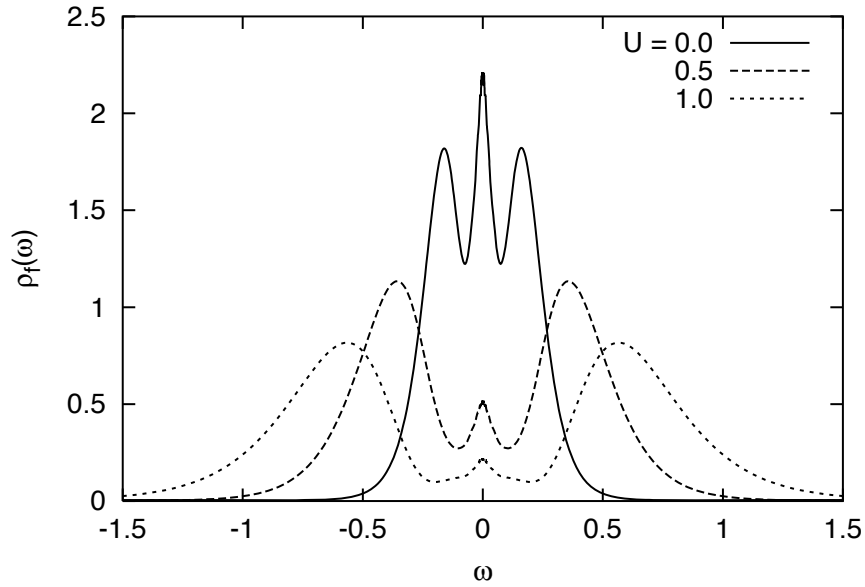


**Figure 3.7:** Spectral density of the impurity at zero temperature,  $\Delta = 0.1$  and  $U_B = 2.6$ .

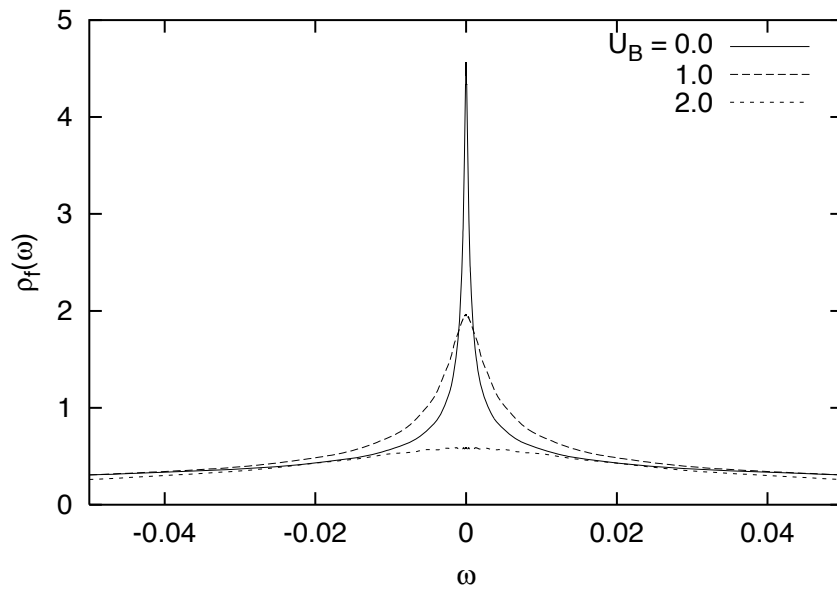


**Figure 3.8:** Broadening of the quasiparticle resonance due to band interactions. Impurity parameters are chosen as  $\Delta = 0.05$  and  $U = 1.0$ .

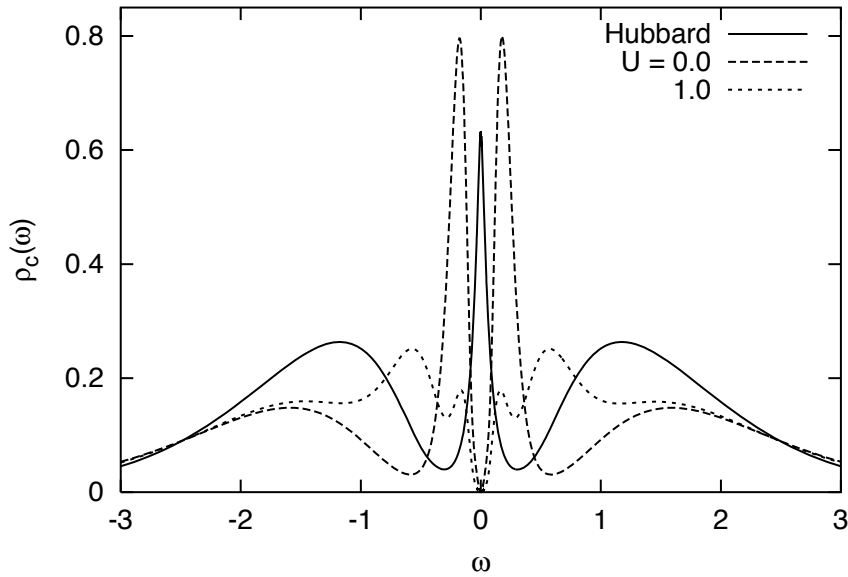


**Figure 3.9:** Spectral density of the local Hubbard site for the same parameters as in fig. 3.7. The Hubbard DOS calculated without the  $f$ -impurity is also shown for comparison.

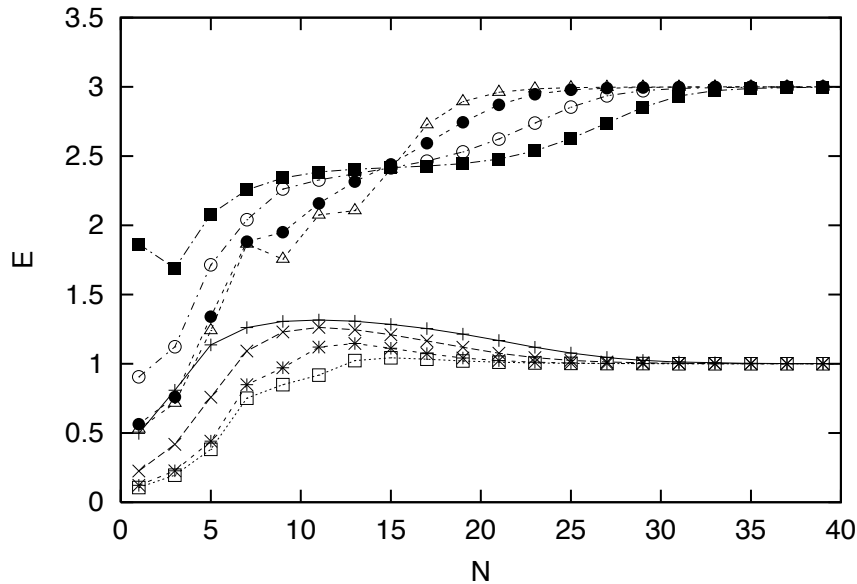


**Figure 3.10:** Flow of two selected levels in the  $Q = 1$ ,  $S = 0$  sector at odd iteration number  $N$  for different band interactions  $U = 0, 1, 2, 2.5$  (from right to left). The impurity parameters are chosen as  $\Delta = 0.05$  and  $U = 1$ . The lower level is normalized to unity in order to account for the change in the total bandwidth.

that is smaller than the hybridization, thus leading to resonances as demonstrated by Hofstetter and Kehrein (1999). Upon increasing  $U$ , these peaks are reduced and weight is shifted to the atomic levels which for large interaction can be found at  $\omega \approx \pm U/2$ . In addition, the height of the quasiparticle peak is significantly reduced. Luttinger's theorem (Luttinger 1961, Langreth 1966) which states that  $\rho_f(0)$  is pinned at its  $U = 0$  value is therefore not valid in the case of an interacting conduction band.

Furthermore, we notice that the width of the quasiparticle resonance is almost independent of  $U$ , in contrast to the situation at  $U_B = 0$ . This already indicates a strong enhancement of the Kondo scale due to band correlations, which can be seen more clearly in fig. 3.8.

The corresponding results for  $\rho_c$  are shown in fig. 3.9. For an impurity interaction strength  $U = 1.0$ , three different energy scales are visible: The Kondo temperature  $T_K$  is equivalent to the width of the hybridization gap,  $U$  and  $U_B$  define a resonance and a "shoulder" of the spectrum, respectively. Regarding the detailed structure at higher energies, however, one should keep in mind that in this region the resolution is limited due to the broadening procedure. The hybridization gap is formed at any finite  $\Delta$ . This is already the case at  $U = U_B = 0$  (not shown here) and persists for finite interactions, indicating that the system is a Fermi liquid (a nonvanishing self-energy at  $\omega = 0$  would smear out the gap). The Fermi liquid picture is independently supported by the fact that the fixed point of the NRG and its leading irrelevant eigenoperators are unchanged compared to the noninteracting case. This can be explicitly checked by plotting a set of NRG levels versus the iteration number  $N$  (see fig. 3.10): The behaviour at small  $N$  depends on the band interaction, but the  $N \rightarrow \infty$  fixed point and the asymptotic approach are universal.

## 3.6 Dynamical susceptibility

A quantity which is more easily accessible experimentally than the single particle spectrum is the (longitudinal) dynamical susceptibility, defined as the response of the impurity spin to a local magnetic field in the  $z$ -direction

$$\chi(\omega) = i \int_0^{\infty} dt e^{i\omega t} \langle [S_f^z(t), S_f^z(0)] \rangle. \quad (3.17)$$

It is related to the scattering function of neutron diffraction

$$S(\mathbf{q}, \omega) \sim F^2(\mathbf{q}) \text{Im}\chi(\omega) \quad (3.18)$$

where  $F(\mathbf{q})$  is the form factor of the impurity. Several classical Kondo systems have been investigated in this way like  $Mn$  in  $Cu$  (Murani and Tholence 1977) and

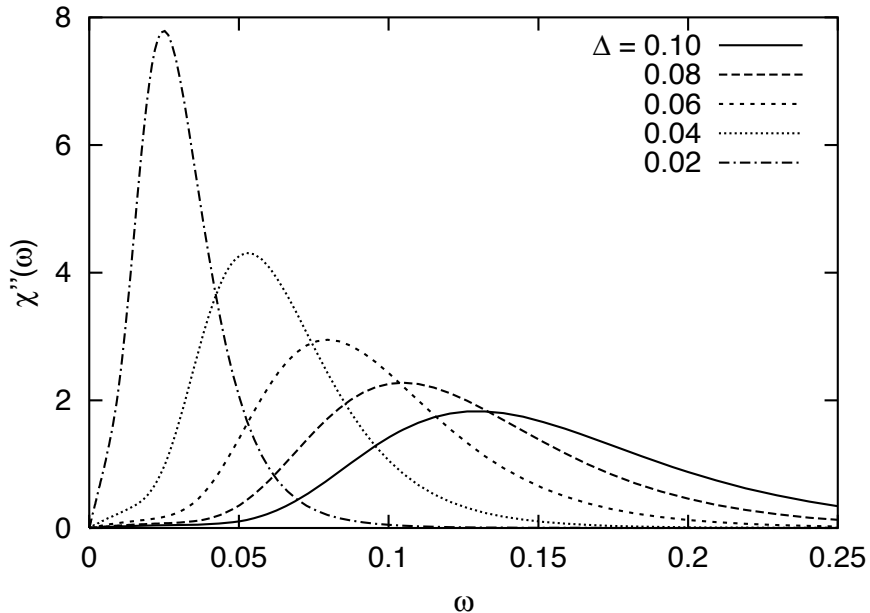


**Figure 3.11:** Dynamical impurity susceptibility for  $U = 1.0$  and  $U_B = 2.8$ .

*Fe* in *Au* (Scheuer, Loewenhaupt and Schmatz 1977). The local dynamical susceptibility is also directly obtained in electron spin resonance (ESR) measurements where it determines the microwave absorption (see for example Krug von Nidda (1997)). In this case a static magnetic field in the transverse direction is applied. In order to compare experiment and theory in detail one would have to perform susceptibility calculations in the absence of rotational symmetry, which we defer to a future publication. Let us note, however, that the magnitude of the applied field is usually small compared to the Kondo temperature of the ESR probe and can be neglected in a first approximation. We will therefore focus on the zero field susceptibility in the following.

Introducing a complete set of eigenstates, the Lehmann representation reads

$$\chi(\omega) = - \sum_{mn} |\langle m | \sigma^z | n \rangle|^2 \frac{\delta_{n,0} - \delta_{m,0}}{\omega - E_m + E_n + i0^+} \quad (3.19)$$

Within the NRG formalism it is convenient to calculate the imaginary part  $\chi''(\omega)$  directly from the reduced matrix elements of the impurity spin operator. Details of the iterative procedure are given in appendix C. The real part is then obtained by a

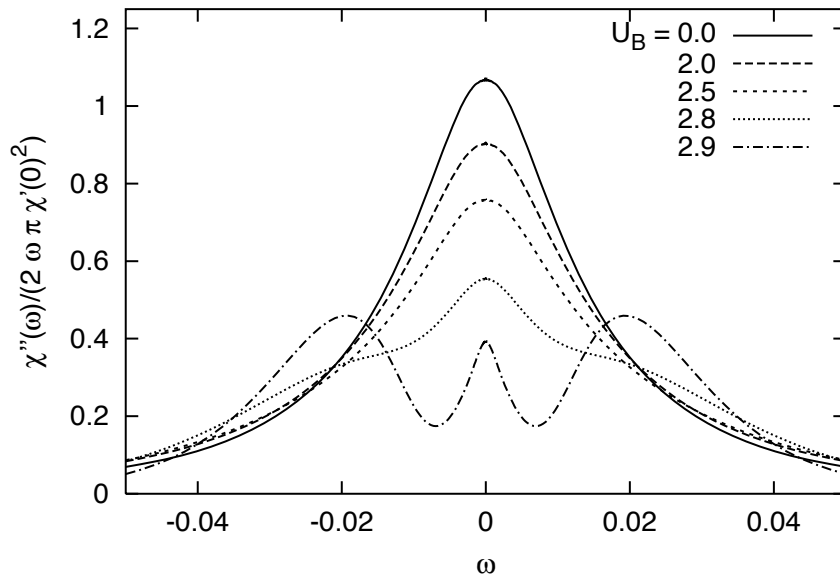


**Figure 3.12:** Normalized spin relaxation function for different strengths of the conduction band correlations. Here the impurity is taken to be noninteracting, with a hybridization  $\Delta = 0.01$ .

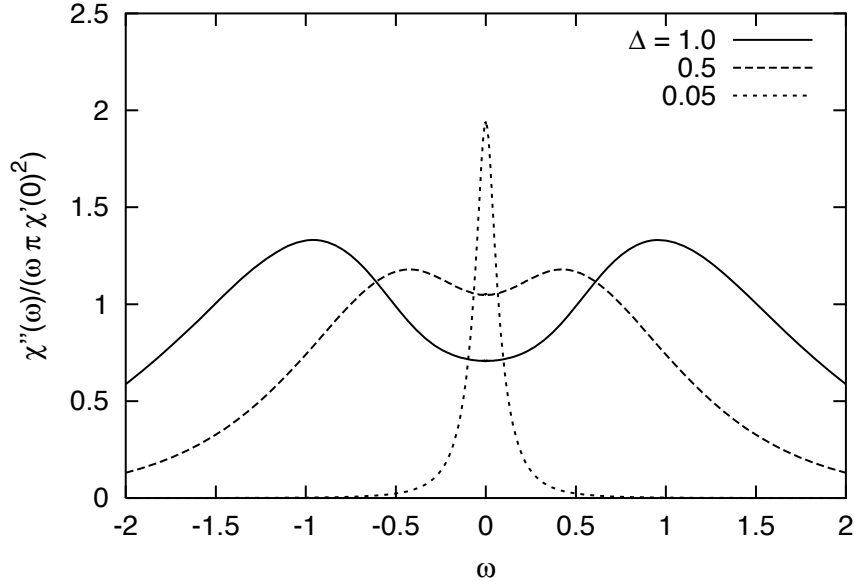


**Figure 3.13:** Normalized spin relaxation function for a noninteracting conduction band ( $U_B = 0, U = 0$ ) with different hybridization strengths. For large  $\Delta \gtrsim D$ , inelastic resonances arise.

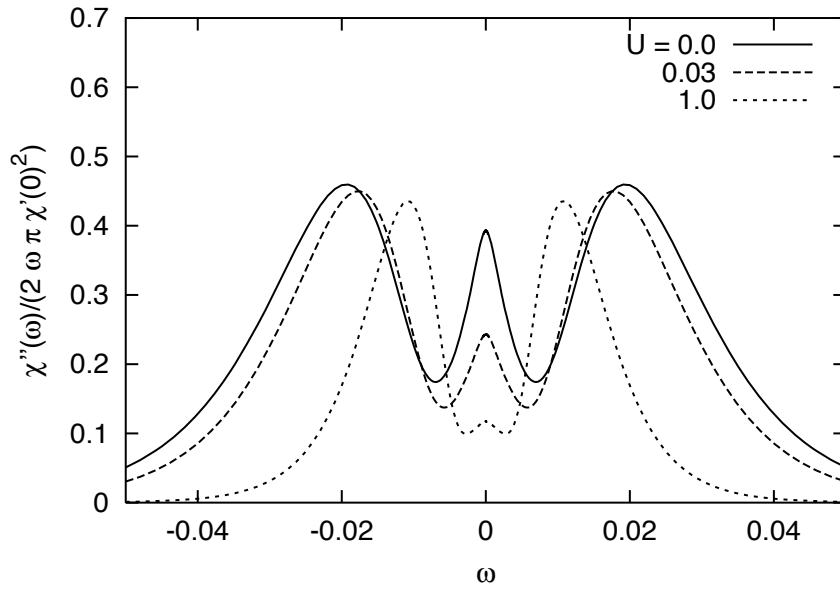


**Figure 3.14:** Normalized spin relaxation function for different impurity interactions. Here we have set  $\Delta = 0.01$  and  $U_B = 2.9$ .

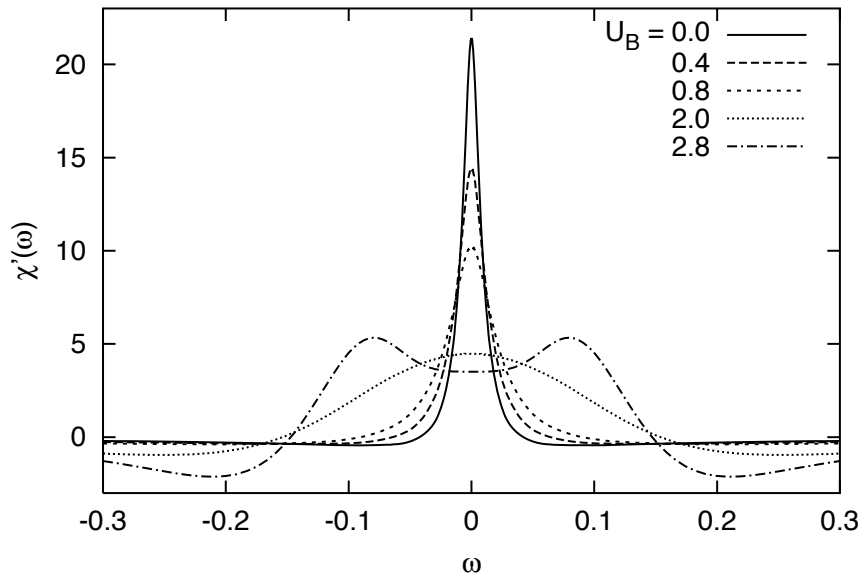


**Figure 3.15:** Real part of the dynamical susceptibility at  $\Delta = 0.1$  and  $U = 1.0$ .

Kramers–Kronig transformation

$$\chi'(\omega) = \mathcal{P} \int_{-\infty}^{\infty} \frac{d\omega'}{\pi} \frac{\chi''(\omega')}{\omega' - \omega} \quad (3.20)$$

In particular, the static susceptibility is given by  $\chi_0 = \chi'(0)$ .

Some examples for  $\chi''(\omega)$  are given in fig. 3.11: A broad peak defines the energy where the ground state singlet is formed; at lower frequencies the spectral weight decreases linearly. In the following we focus on the *spin relaxation function*

$$S(\omega) = \frac{\chi''(\omega)}{\pi\omega}. \quad (3.21)$$

In a first step, we consider its behaviour with increasing band correlations for fixed  $\Delta$  and  $U$  as shown in fig. 3.12. In this plot we have employed a normalization of  $\chi''$  suggested by the *Shiba relation*

$$\lim_{\omega \rightarrow 0} \frac{\chi''(\omega)}{\pi\omega} = 2\chi'(\omega)^2 \quad (3.22)$$

derived for  $U_B = 0$  by Shiba (1975). For the noninteracting band this relation is indeed satisfied, with an error of about 10% due to the NRG procedure. With increasing  $U_B$  systematic deviations arise, indicating that the general proof of Yoshimori and Zawadowski (1982) based on Ward identities breaks down for an interacting conduction band. The lineshape of  $\chi''(\omega)$  also depends on  $U_B$ . For a weakly correlated band, we obtain a single elastic peak with a width approximately corresponding to the Kondo temperature. Close to the metal–insulator transition at  $U_B^c = 2.92$ , two inelastic side peaks arise. They indicate that the Kondo singlet is formed at an energy scale which lies outside the effective band.

In order to demonstrate this more clearly, we compare our results with those for a noninteracting but *narrow* band (fig. 3.13). Clearly, for a weak hybridization smaller than the bandwidth, the Shiba relation is valid and we obtain the standard lineshape. With increasing  $\Delta$ , the singlet binding energy again exceeds the bandwidth, as expected. The results in fig. 3.12 are therefore at least partially due to an effective narrow band (note however that at small  $U_B$ , changes in the DOS can be neglected and the main effect is given by the interaction on the local Hubbard site).

In this context it is interesting to note that inelastic peaks have indeed been found for the compound  $CeSn_{3-x}In_x$  via neutron scattering by Murani (1987). Remarkably, the corresponding peak position scales as  $\omega_{\text{peak}} \sim \chi(0)^{-1} \sim T_K$  which is also the case for the side peaks in fig. 3.12. These inelastic lineshapes have been qualitatively explained by Bickers, Cox and Wilkins (1987) within the large degeneracy expansion. Still, the issue is not completely settled. The inelastic resonances are found to

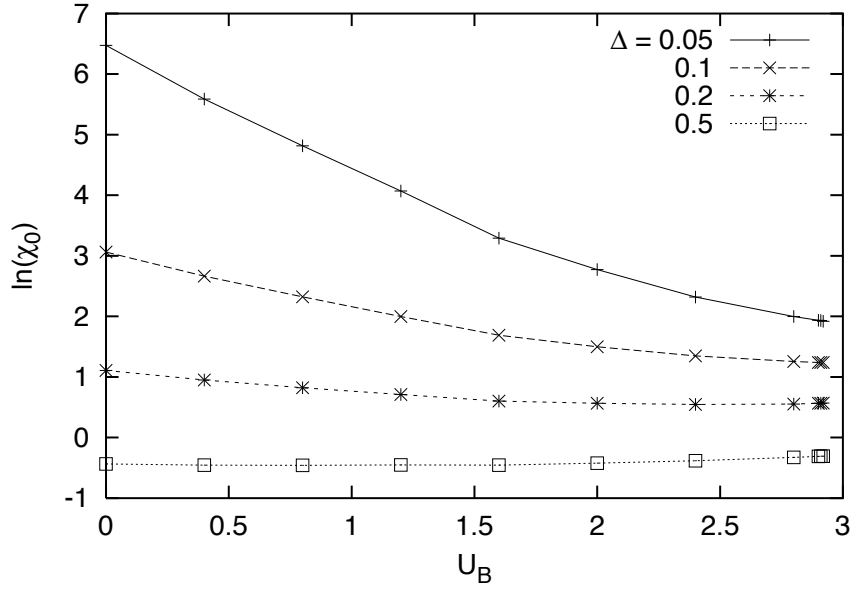


**Figure 3.16:** Static susceptibility as a function of the conduction band interaction strength ( $U = 1.0$ ).

disappear at higher temperatures, therefore a  $\chi''$  calculation at finite  $T$  would be of particular interest.

So far the impurity interaction has been considered as a fixed parameter. In fig. 3.14 we now increase  $U$  at a fixed band correlation strength close to the Mott transition. As can be clearly seen, this leads to a suppression of the elastic peak and a shift of the inelastic ones (corresponding to a slight reduction of the singlet binding energy). The  $U$ -independent width of the elastic peak is defined by the effective bandwidth, which in this case represents the smallest energy scale.

For the real part  $\chi'(\omega)$ , some typical results are shown in fig. 3.15: Already at a weak band interaction  $U_B$  (when the Hubbard DOS is well approximated by the noninteracting one) the static susceptibility  $\chi_0$  is strongly reduced. In a separate diagram (fig. 3.16) we display the dependence of  $\chi_0$  on the band interaction for different impurity parameters. Close to the Mott transition, the narrowing of the effective band may lead to a slight increase of  $\chi_0$ .

### 3.7 Kondo scale

Of particular interest is the hybridization dependence of the low-energy scale – the Kondo temperature  $T_K$  – at intermediate to strong band interaction. While there

is agreement on the fact that a small  $U_B$  enhances the effective Kondo coupling but still leads to an exponentially vanishing  $T_K$  at small hybridization  $\Delta$ , it was found by Davidovich and Zevin (1998) that above an intermediate  $U_B$  the Kondo temperature varies linearly in  $\Delta$ . We will now consider this issue in detail.

We define  $T_K$  to be equal to the binding energy of the local singlet, which is given by the position of the maximum in  $\chi''(\omega)$ . Only in the *universal* regime (flat band,  $T_K \ll D$ ) this definition is equivalent to others based on  $\chi_0^{-1}$  or the flow of the energy levels in the NRG iterations. The dependence of  $T_K$  on the hybridization is shown in fig. 3.17. With increasing  $\Delta$  we observe a crossover from an exponential to a linear behavior  $T_K \sim \Delta$ . The crossover point depends on  $U_B$  and is proportional to the effective bandwidth  $D_{\text{eff}}$ . For very small  $\Delta$ , the Kondo temperature always varies as  $\ln T_K \sim -U/\Delta$  (see fig. 3.18).

This is in agreement with the perturbative study of Khaliullin and Fulde (1995), where a renormalization of the effective exchange coupling was found

$$\tilde{J} = J(1 + \gamma(U_B)) \quad (3.23)$$

with  $\gamma$  depending linearly on the band interaction  $U_B$ . Here the low-energy sector of the Anderson model has been projected onto an effective Kondo Hamiltonian with dimensionless coupling  $\rho J = 8\Delta_f/\pi U$  by using the transformation of Schrieffer and Wolff (1966). The relative change in the Kondo temperature can then be written as

$$\frac{\tilde{T}_K}{T_K} = \exp \left\{ \frac{\pi U}{8\Delta_f} \frac{\gamma}{1 + \gamma} \right\} \quad (3.24)$$

where  $\Delta_f$  is the effective  $f$ -site hybridization. In our calculations we obtain a renormalization factor  $\gamma \sim U_B$  with a coefficient that is independent of the impurity parameters.

In contrast to Davidovich and Zevin (1998) we therefore find an exponentially small  $T_K$  at any  $U_B$ , as long as the host is metallic. The discrepancy may be due to the approximate variational method used by these authors. It should also be emphasized that their calculations were done at  $U = \infty$ , although no qualitative differences are expected in comparison with the symmetric model (Zevin 2000).

At a finite band interaction,  $U_B$  may lead to a non-monotonic behavior of  $T_K$ ; see fig. 3.19. The increase at small  $U_B$  can be attributed to the local interaction on the site  $i = 0$  while the decrease close to the MIT is due to band narrowing.

As  $U_B \rightarrow U_{\text{MIT}}$ , the Kondo scale approaches a finite limiting value, indicating that even in the paramagnetic insulator the local impurity is screened. We can understand this by considering the effective hybridization “seen” by the  $f$ -impurity

$$\Delta_f = \frac{V^2}{\omega + i0^+ - \Delta_c(\omega^+)}. \quad (3.25)$$

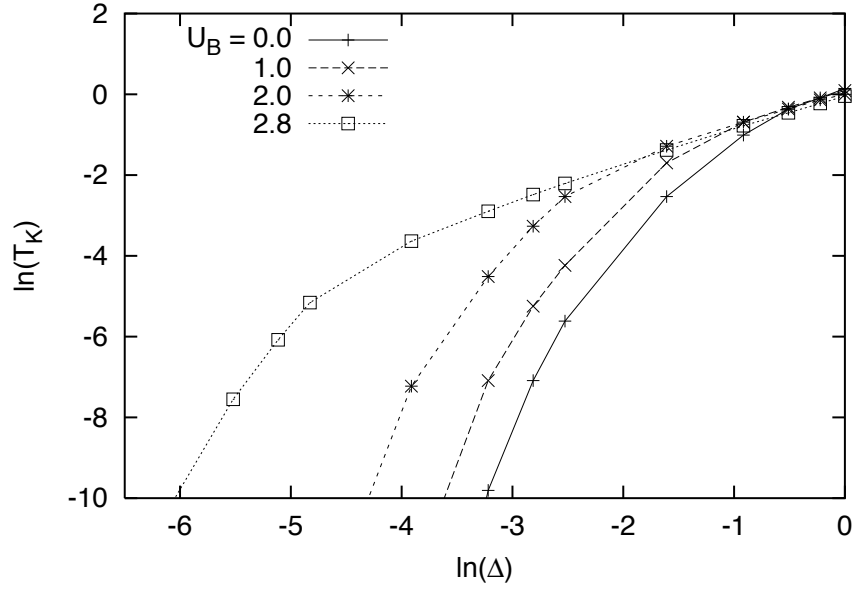


**Figure 3.17:** Kondo temperature as a function of hybridization for the impurity interaction strength  $U = 1.0$ . Note the crossover between a linear and an exponential dependence  $T_K(\Delta)$  at a hybridization  $\Delta \approx D_{\text{eff}}$ .

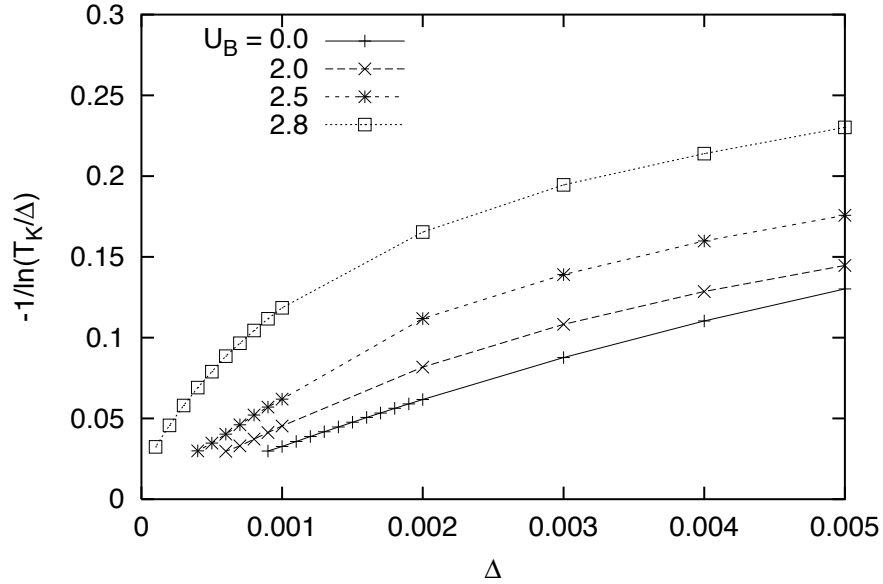


**Figure 3.18:** Kondo temperature in the limit of small hybridization (interaction strength  $U = 0.1$ ). The asymptotic linear behaviour is equivalent to an exponentially small Kondo scale. For  $U_B = 2.8$ , the subleading contribution  $\sim \Delta^2$  is still visible.

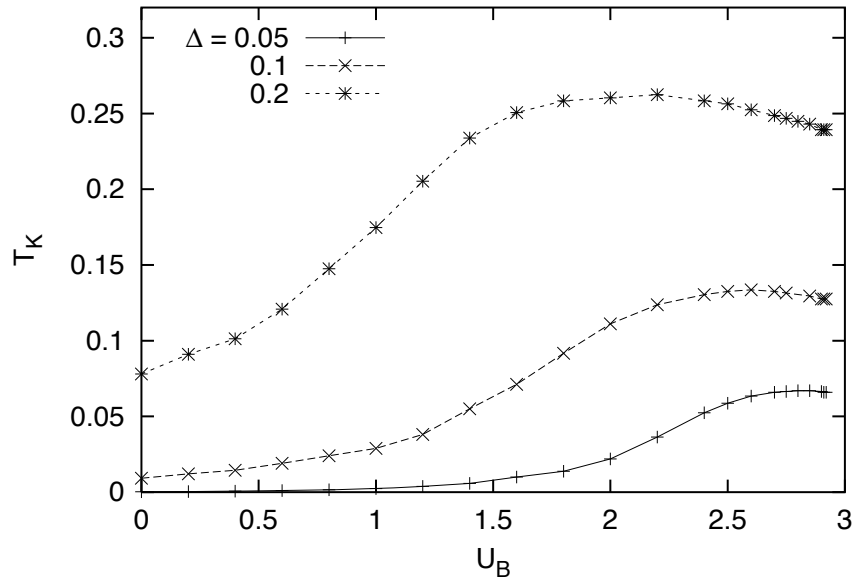


**Figure 3.19:** Kondo temperature as a function of the band interaction. The impurity correlation strength is taken as  $U = 1.0$ .

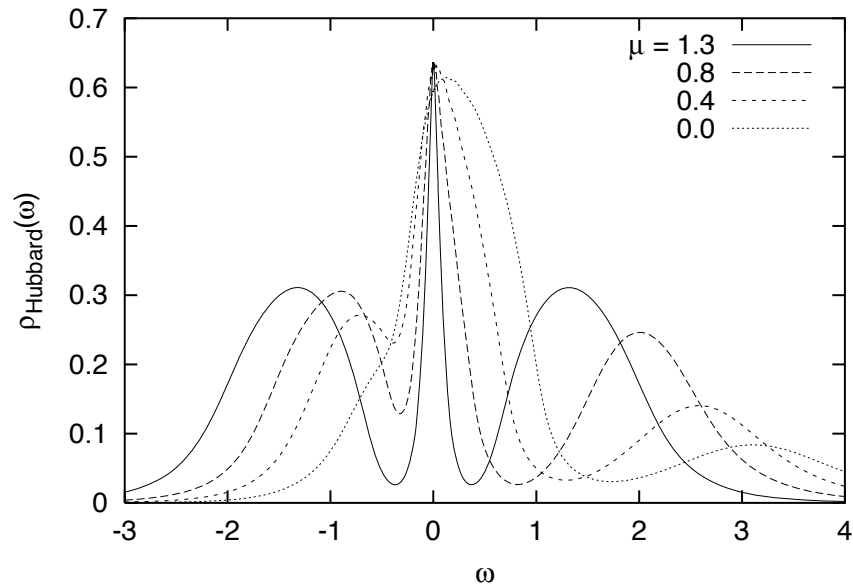


**Figure 3.20:** Effect of the chemical potential on the Hubbard DOS at  $U_B = 2.6$  (Bulla 2000). The corresponding filling degrees are  $n = 1.0, 0.93, 0.81, 0.57$ .

In the insulating host we have  $\Delta_c = 0$  and therefore

$$\Delta_f(\omega) \sim V^2 \delta(\omega). \quad (3.26)$$

In this case, the impurity couples exclusively to the  $i = 0$  site, the singlet is purely local and no Kondo many-particle physics is possible.

### 3.8 Asymmetric impurity and band

So far only the (most important) case of half-filling for both the impurity and the band has been considered. There the Mott transition and the associated vanishing energy scale at a finite interaction strength make a description in terms of the extreme narrow-band limit possible. The metal-insulator transition does not occur if the band is doped away from half-filling, and we expect the difference  $1 - n_{\text{Band}}$  to provide a cutoff in the effective bandwidth relevant for impurity properties (see fig. 3.20). An asymmetric impurity, on the other hand, will introduce mixed valence behaviour and mainly increase the Kondo scale. In the present section, both parameters will be varied and their impact on spectral properties will be discussed separately.

We begin by increasing the impurity energy from its value at particle-hole symmetry  $\epsilon_f = -U/2$ , retaining the symmetry of the strongly correlated band. The impurity spectral function is shown in fig. 3.21: As expected, the lower atomic level is shifted to higher frequencies and gaining weight while the upper one is flattened out. But in contrast to the well-known results for a noninteracting band, a resonance survives at the Fermi edge even up to the empty orbital regime where  $\epsilon_f > \Delta$ . This may be explained by the well-formed quasiparticle resonance in the Hubbard DOS (see fig. 3.5) at strong correlation. In the spectrum of the local band site  $c_0$  presented in fig. 3.22, the dominant  $\epsilon_f$  level is also visible. Furthermore, the pseudogap at the Fermi level is filled. This already occurs in the noninteracting case (not shown) and is thus unrelated to Fermi liquid properties of the model.

Next, we consider a variation of the chemical potential in the band, leading to a filling  $n \neq 1$  and an asymmetric Hubbard DOS, shown in fig. 3.20. The impurity DOS  $\rho_f$  (fig. 3.23) displays a marked increase in the spectral weight at the Fermi level and at the same time a narrowing of the quasiparticle peak corresponding to a *decrease* in the Kondo temperature. This is surprising, because the growing effective bandwidth of the Hubbard model would suggest the opposite trend. The reduced low energy scale is also clearly seen in the  $\rho_c$  spectrum where the hybridization gap narrows considerably (in fact there is no true gap any more, i.e.  $\rho_c(0)$  is nonvanishing for an asymmetric band).

These results indicate that for a fixed value of  $U_B$ , band correlations are strongest at half-filling. Doping the system to  $n < 1$  dilutes the conduction electrons which

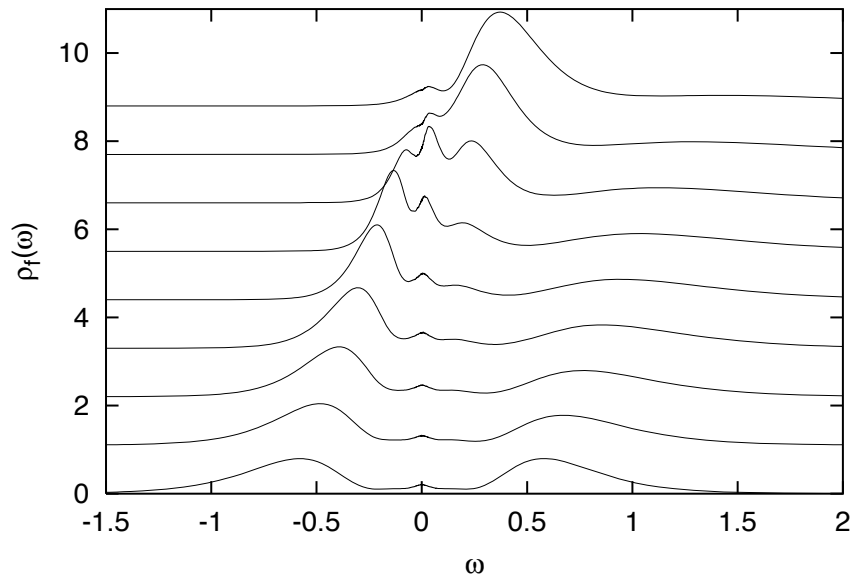


**Figure 3.21:** Variation of the impurity energy  $\epsilon_f = -0.5$  (bottom)  $\dots 0.3$  (top) for  $\Delta = 0.1$ ,  $U = 1.0$  and band correlation  $U_B = 2.6$ . In all cases a resonance remains visible at the Fermi energy.

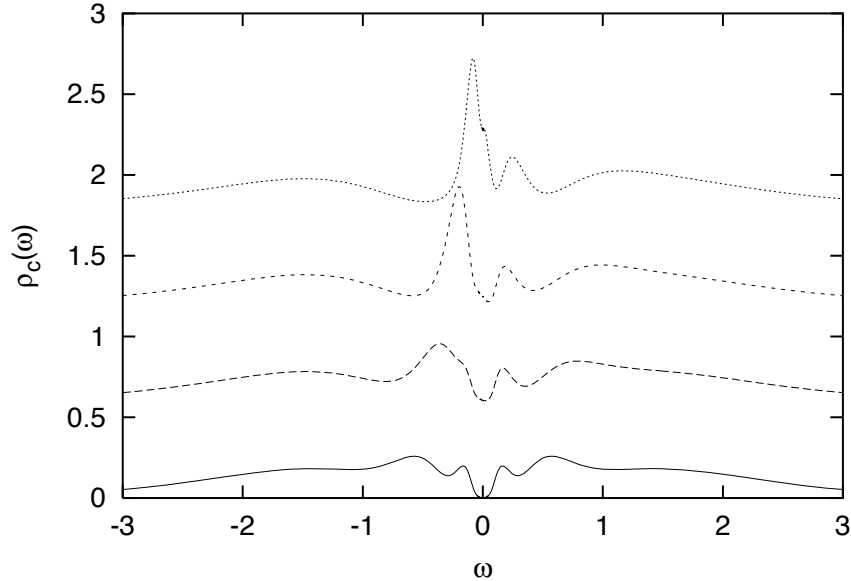


**Figure 3.22:** Local host site spectral density for the same parameters as in fig. 3.21 and impurity energies  $\epsilon_f = -0.5$  (bottom),  $-0.3$ ,  $-0.1$ ,  $0.1$  (top). Note that the hybridization gap at the Fermi edge disappears with increasing asymmetry.

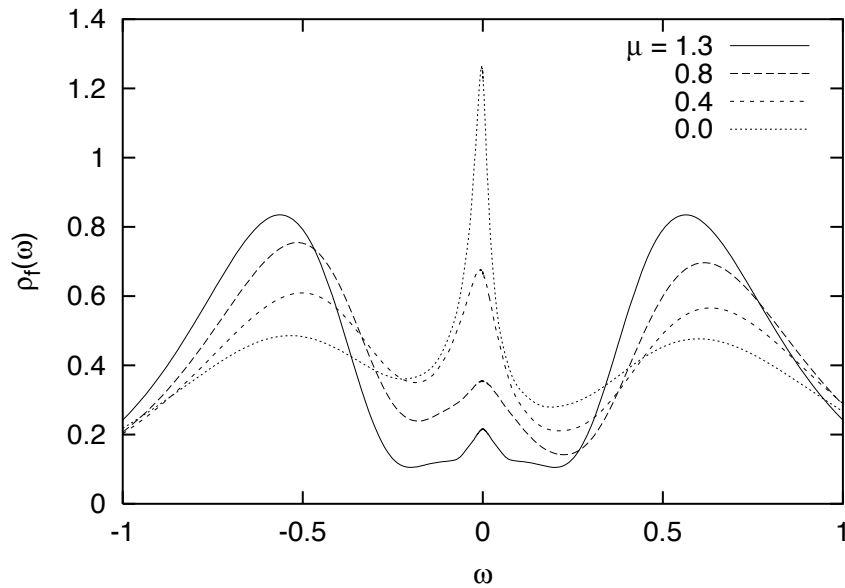


**Figure 3.23:** Impurity spectral function for an asymmetric band. Parameters are chosen as  $\Delta = 0.1$ ,  $U = 1.0$ ,  $\epsilon_f = -0.5$  and  $U_B = 2.6$ .

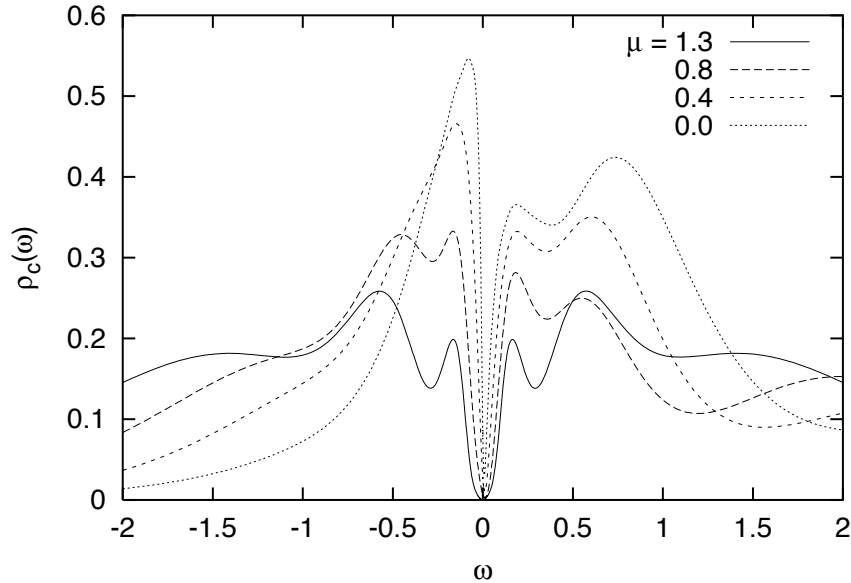


**Figure 3.24:** Single particle spectrum of the local Hubbard site in an asymmetric band for the same parameters as in fig. 3.23.

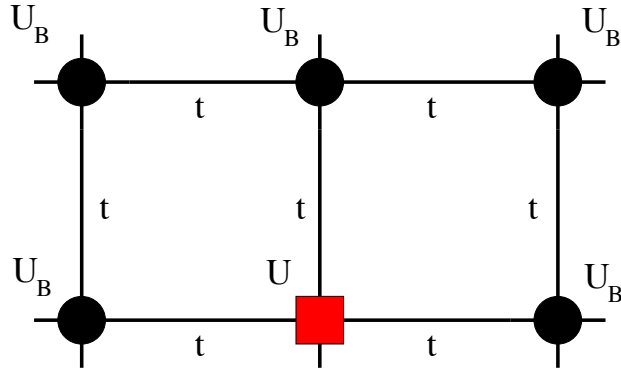


**Figure 3.25:** Wolff impurity in a correlated band.

then effectively behave more like free fermions. As a consequence, the strongest renormalization of the  $f$  spectral density occurs at  $n = 1$ , which can be seen most clearly by looking at the height of the quasiparticle peak.

### 3.9 Wolff model

So far our discussion of the interplay between band correlations and impurity physics has been in terms of the Anderson model. In this section we present some results for an alternative realization of a single magnetic impurity, the *Wolff model* (Wolff 1961). Here the impurity *replaces* one site of the correlated lattice, as shown in fig. 3.25. The hybridization is given by the hopping  $t$  and cannot be tuned independently any more. QMC studies of this model in one dimension have been performed by Yunoki, Mizuno and Maekawa (1996). We are again interested in the opposite limit of large coordination number. Tracing out the band degrees of freedom, one obtains the same quadratic effective action (3.8) as for the Anderson impurity, with a Weiss function  $\mathcal{G}_0$  again determined by the Hubbard host. The effective Hamiltonian, however, is now just a *single* impurity Anderson model

$$H_{\text{eff}} = \sum_{p\sigma} \epsilon_p a_{p\sigma}^\dagger a_{p\sigma} + \sum_{p\sigma} V_p (a_{p\sigma}^\dagger f_\sigma + h.c.) + \epsilon_f f_\sigma^\dagger f_\sigma + U n_{f\uparrow} n_{f\downarrow}. \quad (3.27)$$

where  $c_0$  has been replaced by  $f$ . In fact, after solving the effective DMFT impurity problem for the Hubbard host with interaction  $U_B$ , one simply has to “detune” the Coulomb interaction to the new value  $U$  and adjust the impurity level  $\epsilon_f$  accordingly. A second NRG calculation then directly yields the impurity spectrum.

Here we focus on the symmetric model ( $\epsilon_f = -U/2$ ) for which results are shown in fig. 3.26. A strongly correlated band with  $U_B = 2.6$  close to the Mott transition has

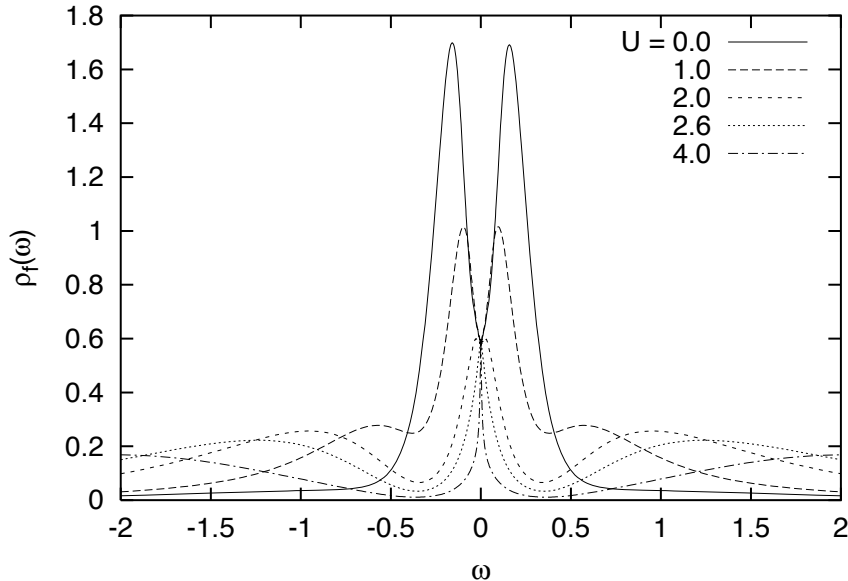


**Figure 3.26:** Single particle spectrum of the symmetric Wolff impurity in a strongly correlated band with interaction  $U_B = 2.6$ .

been assumed, where the density of states is similar to the largest interaction value shown in fig. 3.5. Remarkably, for a weak impurity interaction the quasiparticle resonance is split and one obtains side peaks at finite frequency. Only for interaction strengths  $U \geq U_B$  a single Kondo peak is found, with an exponentially small Kondo scale in the limit  $U \rightarrow \infty$ .

These findings can be explained by noting that here we have a realization of the *narrow band* Anderson model analyzed in the previous chapter. Indeed, the side peaks found here are similar to those in fig. 2.4, merging with the remaining quasiparticle peak for increasing  $U$ . In the present case, the transition to a single resonance takes place at  $U = U_B$  where – by definition – one is just looking at the Hubbard model.

In contrast to the Anderson model studied previously, no enhancement of the Kondo temperature is found upon increase of the band correlations. This qualitatively different behaviour is due to the specific form of the  $f$ -level hybridization function: For the Anderson impurity, it is given by (3.25), while in the Wolff case it is simply equal to  $\Delta_c(\omega)$ . Close to the Mott transition, both functions become increasingly narrow. But while in the first case the total hybridization weight is constant, it approaches zero in the second. In particular, the Wolff impurity is *not screened* in the paramagnetic insulator.

## 3.10 Conclusion and experimental outlook

In this chapter we have analyzed models describing a magnetic impurity in a correlated band. The limit of infinite dimensions has made a treatment by NRG within the dynamical mean-field theory possible. For the Anderson Hamiltonian, we have solved the corresponding effective two-impurity model and have obtained the one-particle spectra as well as the dynamical susceptibility. We have found that the system is always a local Fermi liquid as long as the host is metallic. Band correlations lead to a strongly enhanced Kondo scale, indicating that the dominant effect of  $U_B$  is to increase the spin polarization of the conduction electrons. Nevertheless,  $T_K$  remains exponentially small as a function of the hybridization. This is consistent with a Fermi liquid picture of the Hubbard host where the Kondo screening of the impurity is due to fermionic quasiparticles instead of bare electrons. In spectral quantities, a change of the lineshape and the formation of side peaks is observed close to the Mott transition. This is explained by a narrowing of the effective conduction band.

Different behaviour has been found for the Wolff model with correlated conduction electrons. Within DMFT, this system can be reduced to an effective narrow band Anderson model with the characteristic side peaks in the spectral density. Here we observe that the Kondo scale is always *reduced* by the band interaction, in contrast to studies on the one-dimensional case by Yunoki et al. (1996). For the Wolff model, the  $d \rightarrow \infty$  limit – which assumes a high coordination number also for the impurity – may therefore be less realistic than for the Anderson model.

At the beginning of this section the cuprate compound  $Nd_{2-x}Ce_xCuO_4$  – a concentrated impurity system – has been discussed as a possible experimental realization. Within the model analyzed here, the strong enhancement of the Kondo scale can be explained. A more realistic description of this material would, however, be given by the periodic Anderson model with correlated conduction electrons (Schork and Blawid 1997), which will be the subject of future studies.

Of course it would be desirable to compare our results with experiments on systems that can actually be considered as dilute. One promising line of research in this direction is provided by electron spin resonance (ESR). In this method, rare earth ions like  $Gd^{3+}$  or  $Eu^{2+}$  are introduced into the host metal as local probes which relax via an exchange interaction with the conduction electrons. The relevant Hamiltonian is given by (Krug von Nidda 1997)

$$H_{\text{probe}} = h S_{\text{probe}}^z + J \mathbf{S}_{\text{probe}} \cdot \mathbf{s}_{\text{cond}}. \quad (3.28)$$

In normal metals, the relaxation rate has a linear temperature dependence  $\tau^{-1} \sim N^2(\epsilon_F) T$ ; in this way the conduction electron density of states can be measured. It is known, however, that due to the exchange  $J$ , the ESR ion itself can be subject to the Kondo effect. This leads to logarithmic corrections both in the shift

of the  $g$ -factor and in the relaxation (Baberschke and Tsang 1980)

$$\Delta g \sim [\ln(T_K/T)]^{-1} \quad (3.29)$$

$$\tau^{-1}/T \sim [\ln(T_K/T)]^{-2} \quad (3.30)$$

and the Kondo temperature  $T_K$  can thus be determined from two independent quantities. For a conventional metal ( $Yb$  impurities in  $Au$ ) this has been done by Baberschke and Tsang (1980). It would be interesting to perform similar measurements – again with the ESR ion  $Yb^{3+}$  – on a strongly interacting host like  $CePd_3$ . The conduction electron correlations could then be tuned by doping with  $Ag$ , which is also suggested by our theoretical results on the interplay between band filling and Kondo physics (see section 3.8).

Another class of systems where bulk correlations lead to nontrivial impurity effects is given by cuprates ( $YBa_2Cu_3O_6$ ) doped with nonmagnetic defects ( $Zn^{2+}$ ). As demonstrated by the NMR measurements of Bobroff, MacFarlane, Alloul, Mendels, Blanchard, Collin and Marucco (1999) and Julien, Fehér, Horvatić, Berthier, Bakharev, Ségransan, Collin and Marucco (2000), the spinless  $Zn$  induces magnetic moments on its four neighbouring  $Cu$  sites. At low temperatures, these moments display a Curie–Weiss type susceptibility strongly reminiscent of the Kondo effect. Theoretical modelling of this system would probably require an extension of DMFT to include short range magnetic correlations.

Finally, an important new realization of single impurity effects is provided by scanning tunneling microscopy (STM). In this technique, the local surface density of states (LDOS) is probed by measuring the differential conductance  $dI/dV$  through the microscope tip (Hasegawa and Avouris 1993). Recent STM studies performed by Li, Schneider, Berndt and Delley (1998) on magnetic  $Ce$  atoms immersed in an  $Ag(111)$  electronic surface state have clearly shown a suppression of the LDOS characteristic for the Kondo effect. Substituting a correlated host, for example a cuprate compound, in the place of  $Ag$  might then be another way to realize the effects discussed in this chapter.

# Chapter 4

## Generalized NRG for dynamical properties

### 4.1 Introduction

In this chapter we present a new approach for calculating dynamics within the numerical renormalization group. Originally Wilson (1975) devised the method in order to obtain thermodynamic information at low energy scales. This was achieved by iterative diagonalization of the logarithmically discretized impurity model. Each iteration step was shown to correspond to a certain temperature where thermodynamic averages could be obtained with high precision. Later, the method was extended to zero temperature *dynamical* properties by several groups (Frota and Oliveira 1986, Sakai et al. 1989, Costi et al. 1994) and applied to a variety of problems including recent DMFT calculations by Bulla, Hewson and Pruschke (1998). In particular, we applied this technique to the magnetic impurity in a correlated band as discussed in the previous chapter (Hofstetter, Bulla and Vollhardt 2000).

In all these calculations the additional assumption had to be made that transitions from the *ground state* to higher excitations are already correctly described in the first iterations. It was realized only recently (Hofstetter 2000) that this way of proceeding is not rigorous and explicitly fails for the Anderson impurity model in an external magnetic field. To remedy the defect, we introduce a new approach based on the concept of the *reduced density matrix*. This procedure – henceforth referred to as DM–NRG – makes use of the full information contained in iterative diagonalization and represents the true extension of Wilson’s original work to dynamical quantities.

Before discussing the new method in detail, we present some technical modifications in iterative diagonalization which are necessary to treat models without rotational invariance. In particular, we demonstrate that even without using reduced matrix elements, one can still obtain spectral information with excellent accuracy.

Note that in this chapter the density matrix  $\hat{\rho}$  is introduced. In order to avoid confusion, we therefore write the spectral density as  $A(\omega)$ .

## 4.2 NRG at broken rotational symmetry

So far the numerical renormalization group has mostly been used to diagonalize impurity Hamiltonians with global spin rotation invariance where the total spin  $\mathbf{S}^2$  of impurity *and* conduction band is a good quantum number. In this situation one can introduce reduced matrix elements and formulate the recursive procedure completely without referring to  $S_z$ , thus eliminating the corresponding degeneracy. The main advantage of this approach is the reduced size of the matrices to be diagonalized, which was an important aspect at the time when Wilson developed the method. With the amount of computer power available today, it is possible to dispense with this restriction and consider more general problems with a reduced symmetry.

One important application of such a generalized procedure is the treatment of phases with long-range magnetic order in the Hubbard model within DMFT (see Georges et al. (1996)). In this case one obtains a spin-dependent hybridization function  $\Delta_\sigma(\omega)$  which needs to be determined self-consistently. To be specific, in the antiferromagnetic phase on the Bethe lattice the self-consistency condition has the form

$$\Delta(\omega)_\sigma = \pi (t^*)^2 A_{-\sigma}(\omega). \quad (4.1)$$

NRG calculations for this problem will be an important step towards a precise characterization of the AFM phase at weak and strong coupling. Properties of impurities in an antiferromagnetic host (see for example Nagaosa, Hatsugai and Imada (1989) and Sachdev, Buragohain and Vojta (1999)) can then be studied by extending the approach of the last chapter. This may be relevant for recent NMR experiments on High- $T_C$  cuprates performed by Bobroff et al. (1999).

Spin symmetry breaking also occurs if an external magnetic field  $h$  is applied to the local moment. Quantities which are of interest in such a situation include the average impurity magnetization  $\langle \sigma_f^z \rangle$  and in particular the spin resolved spectral density  $A_\sigma(\omega)$  which has been observed directly in measurements of the differential conductance through a quantum dot by Goldhaber-Gordon, Shtrikman, Mahalu, Abusch-Magder, Meirav and Kastner (1998). So far only the large degeneracy expansion (Kang and Min 1996), the modified perturbation theory (Takagi and Saso 1999*a*, Takagi and Saso 1999*b*) and the quantum Monte Carlo technique (Sakai, Suzuki, Izumida and Oguri 1999) have been applied to the Anderson impurity in a magnetic field. In the NRG calculations presented in the following we are able to overcome the limitations of these methods (small interaction, finite temperature) and explore the full parameter regime of the model.

### 4.3 Modified iterative diagonalization

The generalized Anderson Hamiltonian in a local magnetic field  $h$  is written as

$$H_{\text{and}} = \sum_{k\sigma} \epsilon_k c_{k\sigma}^\dagger c_{k\sigma} + \sum_{k\sigma} V_{k\sigma} \left( f_\sigma^\dagger c_{k\sigma} + h.c. \right) + U n_{f\uparrow} n_{f\downarrow} + \epsilon_f n_f - \frac{\hbar}{2} \sigma_f^z \quad (4.2)$$

where  $\sigma_f^z$  denotes the impurity spin and a flat conduction band extending in the range  $[-1, 1]$  is assumed. Let us emphasize again that we choose the units  $\hbar = k_B = g = \mu_B = 1$ . For notational simplicity, we focus on the case of a symmetric and spin independent hybridization function  $\Delta(\epsilon) = \pi \sum_k V_k^2 \delta(\epsilon - \epsilon_k)$ , the only spin dependence being introduced by the magnetic field. As in the rotationally invariant case (see introduction and appendix A) the conduction band is logarithmically discretized and mapped onto a linear chain:

$$\sum_{k\sigma} \epsilon_k c_{k\sigma}^\dagger c_{k\sigma} \longrightarrow \sum_{\substack{n=0 \\ \sigma}}^{\infty} \epsilon_n \left( d_{n\sigma}^\dagger d_{n+1\sigma} + h.c. \right). \quad (4.3)$$

These steps do not have to be modified. The main difference occurs in the iterative diagonalization: Without full rotational invariance of the system, the only remaining quantum numbers are the total charge  $Q$  and the total spin projection  $S^z$ . After adding a single site to the chain in iteration  $N$ , new basis states are defined as

$$\begin{aligned} |1, r, Q, S^z\rangle_{N+1} &\equiv |r, Q+1, S^z\rangle_N \\ |2, r, Q, S^z\rangle_{N+1} &\equiv d_{(N+1)\uparrow}^\dagger |r, Q, S^z - \frac{1}{2}\rangle_N \\ |3, r, Q, S^z\rangle_{N+1} &\equiv d_{(N+1)\downarrow}^\dagger |r, Q, S^z + \frac{1}{2}\rangle_N \\ |4, r, Q, S^z\rangle_{N+1} &\equiv d_{(N+1)\uparrow}^\dagger d_{(N+1)\downarrow}^\dagger |r, Q-1, S^z\rangle_N \end{aligned} \quad (4.4)$$

Again the new hopping term  $\overline{\Delta H} = \sum_\sigma \left( d_{N\sigma}^\dagger d_{(N+1)\sigma} + h.c. \right)$  needs to be expressed in terms of matrix elements defined in the previous step:

$$\begin{aligned} \langle 2, l', Q, S^z | \overline{\Delta H} | 1, l, Q, S^z \rangle_{N+1} &= \langle l, Q+1, S^z | d_{N\uparrow}^\dagger | l', Q, S^z - \frac{1}{2} \rangle_N \\ \langle 4, l', Q, S^z | \overline{\Delta H} | 3, l, Q, S^z \rangle_{N+1} &= -\langle l, Q, S^z + \frac{1}{2} | d_{N\uparrow}^\dagger | l', Q-1, S^z \rangle_N \\ \langle 3, l', Q, S^z | \overline{\Delta H} | 1, l, Q, S^z \rangle_{N+1} &= \langle l, Q+1, S^z | d_{N\downarrow}^\dagger | l', Q, S^z + \frac{1}{2} \rangle_N \\ \langle 4, l', Q, S^z | \overline{\Delta H} | 2, l, Q, S^z \rangle_{N+1} &= \langle l, Q, S^z - \frac{1}{2} | d_{N\downarrow}^\dagger | l', Q-1, S^z \rangle_N \end{aligned} \quad (4.5)$$

Keeping in mind that  $H_{N+1} = \Lambda^{1/2} H_N + \Lambda^{N/2} \epsilon_N \overline{\Delta H}$ , the Hamiltonian can now be diagonalized separately in each one of the  $(Q, S^z)$  sectors. One obtains the new eigenstates

$$|Q, S^z, \omega\rangle_{N+1} = \sum_{i,r} U_{QS^z}(\omega; i, r) |i, r, Q, S^z\rangle_{N+1}. \quad (4.6)$$

The matrix elements of  $d_{N+1}^\dagger$  in the new basis are then easily expressed as

$$\langle r', Q+1, S_z + \frac{1}{2} | d_{(N+1)\uparrow}^\dagger | r, Q, S_z \rangle_{N+1} = \quad (4.7)$$

$$\begin{aligned} &= \sum_{l \in (Q+1, S_z)_N} U_{Q+1, S_z + \frac{1}{2}}(r'; 2, l) U_{Q, S_z}(r; 1, l) \\ &+ \sum_{l \in (Q, S_z + \frac{1}{2})_N} U_{Q+1, S_z + \frac{1}{2}}(r'; 4, l) U_{Q, S_z}(r; 3, l) \end{aligned}$$

$$\langle r', Q+1, S_z - \frac{1}{2} | d_{(N+1)\downarrow}^\dagger | r, Q, S_z \rangle_{N+1} = \quad (4.8)$$

$$\begin{aligned} &= \sum_{l \in (Q+1, S_z)_N} U_{Q+1, S_z - \frac{1}{2}}(r'; 3, l) U_{Q, S_z}(r; 1, l) \\ &- \sum_{l \in (Q, S_z - \frac{1}{2})_N} U_{Q+1, S_z - \frac{1}{2}}(r'; 4, l) U_{Q, S_z}(r; 2, l) \end{aligned}$$

where each  $l$ -summation is performed in one sector of the previous iteration. With this recursion, the iterative diagonalization procedure for the Hamiltonian is complete. Comparing the lowest eigenstates calculated with and without the  $\mathbf{S}^2$  symmetry, one finds complete agreement to machine precision. As a rule of thumb, the number of levels has to be multiplied by a factor 2.25 to achieve the same accuracy without rotational invariance.

Next, we are interested in calculating the impurity single-particle spectrum at a temperature  $T = 1/\beta$ . Within the NRG, the following approximation has been used so far: Diagonalization of chains with increasing length  $N$  yields spectral information on a decreasing frequency scale  $\omega \sim \Lambda^{-N/2}$  according to

$$A_\sigma(\omega) \approx A_\sigma^N(\omega) = \sum_{nm} |\langle m | f_\sigma^\dagger | n \rangle_N|^2 \delta(\omega - E_m^N + E_n^N) \frac{e^{-\beta E_m^N} + e^{-\beta E_n^N}}{Z_N} \quad (4.9)$$

in the Lehmann representation where the  $|n\rangle_N$  are the many-particle eigenstates of  $H_N$  and  $Z_N$  is the partition function. It is therefore necessary to calculate the matrix elements of the impurity fermions in every iteration step by performing the basis transformation

$$\langle r', Q+1, S_z + \frac{1}{2} | f_\sigma^\dagger | r, Q, S_z \rangle_{N+1} = \quad (4.10)$$

$$\sum_{\substack{i' \\ i}} U_{Q+1, S_z + \frac{1}{2}}(r'; i', l) U_{Q, S_z}(r; i, l) \langle i, l', Q+1, S_z + \frac{1}{2} | f_\sigma^\dagger | i, l, Q, S_z \rangle_{N+1}$$

and keeping in mind the following recursion relations, which are just a consequence of the definitions (4.4):

$$\langle 1, l', Q+1, S_z + \frac{1}{2} | f_\sigma^\dagger | 1, l, Q, S_z \rangle_{N+1} = \langle l', Q+2, S_z + \frac{1}{2} | f_\sigma^\dagger | l, Q+1, S_z \rangle_N$$

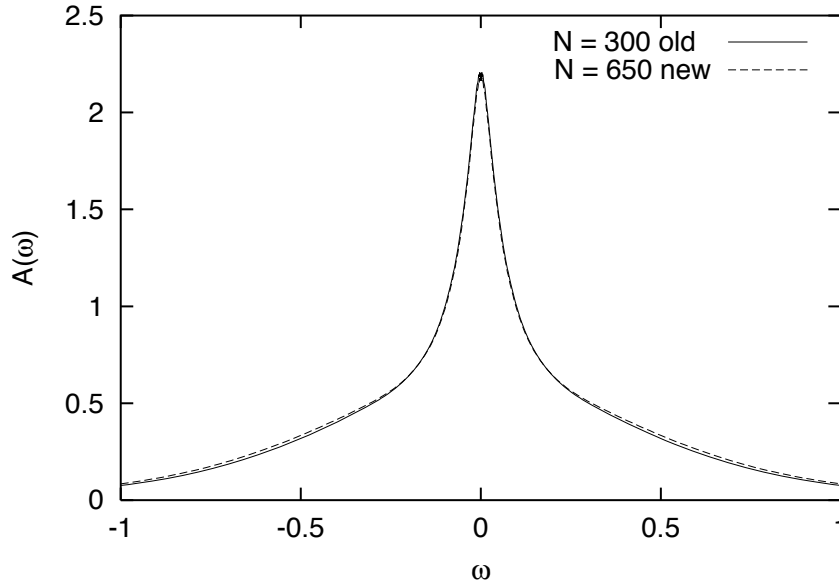


**Figure 4.1:** Comparison of NRG spectra at  $T = 0$  calculated with explicit rotational invariance (“old”) and without (“new”). In the first case, the  $S_z$  degeneracy is not taken into account in the level number. The impurity parameters are  $\Delta = 0.1$ ,  $U = 0.5$  and  $\epsilon_f = -U/2$ , no magnetic field is applied.

$$\begin{aligned}
 \langle 2, l', Q + 1, S_z + \frac{1}{2} | f_\sigma^\dagger | 2, l, Q, S_z \rangle_{N+1} &= -\langle l', Q + 1, S_z | f_\sigma^\dagger | l, Q, S_z - \frac{1}{2} \rangle_N \\
 \langle 3, l', Q + 1, S_z + \frac{1}{2} | f_\sigma^\dagger | 3, l, Q, S_z \rangle_{N+1} &= -\langle l', Q + 1, S_z + 1 | f_\sigma^\dagger | l, Q, S_z + \frac{1}{2} \rangle_N \\
 \langle 4, l', Q + 1, S_z + \frac{1}{2} | f_\sigma^\dagger | 4, l, Q, S_z \rangle_{N+1} &= \langle l', Q, S_z + \frac{1}{2} | f_\sigma^\dagger | l, Q - 1, S_z \rangle_N \quad (4.11)
 \end{aligned}$$

An example of the resulting spectral function is shown in fig. 4.1 and compared to the calculation based on reduced matrix elements (the effective level numbers have been chosen approximately equal, according to the rule of thumb mentioned previously). Note that at this point we are comparing two different ways of performing iterative diagonalization. The method of extracting spectral information – following equation (4.9) – is the same in both cases. We will now show that it fails in the presence of a magnetic field.

## 4.4 Generalized NRG

Let us once again outline how the model (4.2) is solved by iterative diagonalization: In each step only the lowest, most relevant levels are kept. The number of iterations then corresponds to the temperature one is interested in according to  $T_N = c \Lambda^{-(N-1)/2}$

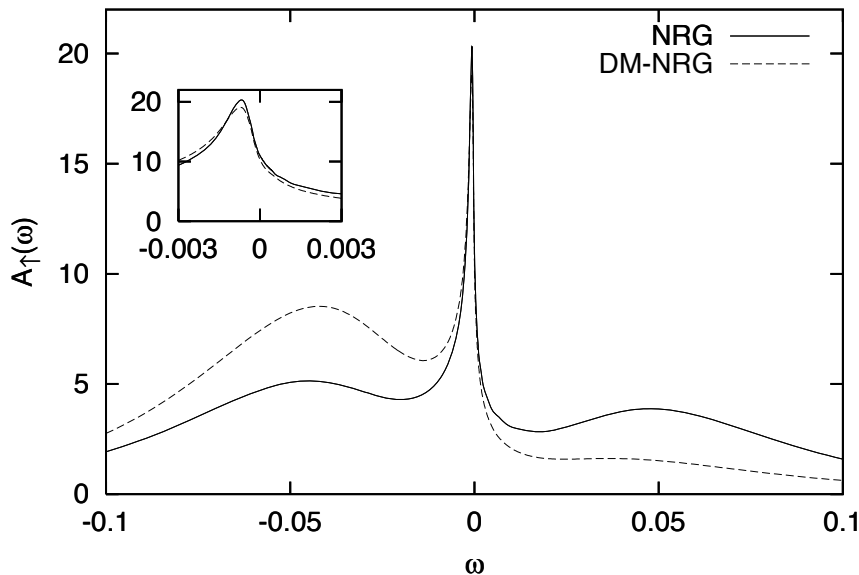


**Figure 4.2:** Comparison of single particle spectral functions for the symmetric model ( $\Delta = 0.01$ ,  $U = 0.1$ ,  $\epsilon_f = -0.05$ ) obtained by the method previously used (“NRG”) and the generalized procedure presented here (“DM-NRG”). The Kondo temperature is  $T_K = 6.8 \times 10^{-4}$  (determined from the width of the quasiparticle resonance). A small magnetic field  $h = 10^{-3}$  has been applied to the impurity.

where  $c$  is a constant of order one. For calculating thermodynamic expectation values, all necessary information is thus obtained because only excitations on the scale  $T_N$  are relevant. For dynamical properties, however, an additional energy scale is introduced by the frequency  $\omega$  which may be much larger than the temperature. This is easily seen by looking at the spin-resolved spectral density (4.9) with  $\beta = 1/T_N$ . Calculating spectral information at frequencies  $\omega \gg T_N$  obviously requires matrix elements between low-lying states and excitations which in iteration  $N$  are not available anymore (they have already been lost due to truncation). To circumvent this difficulty, the following procedure has been used so far (see previous section): In calculating  $A(\omega)$ , expression (4.9) was simply evaluated at an iteration step  $N' \gg N$  where  $T_{N'} \approx \omega$ , assuming that for this spectral regime the low energy levels were described “well enough”. There is no rigorous argument to justify this assumption, as for example the crossover to the strong-coupling fixed point and the corresponding change in the ground state may occur at a much lower temperature scale  $T_K \ll T_{N'}$ . Nevertheless, in the calculations performed so far (single particle spectra for the spin 1/2 Anderson impurity without symmetry breaking), this approximation seems to give reasonable results.

The situation changes in the presence of a magnetic field: In fig. 4.2 we present results for the Hamiltonian (4.2) at  $T = 0$  which have been calculated as described above. Without an external field, one obtains the well-known three-peak structure characteristic of a small Kondo temperature  $T_K$ . Switching on a small magnetic field  $h = \mathcal{O}(T_K)$  only affects the quasiparticle peak, while the high-energy spectrum is almost unchanged. This result is easily understood: At the iterations where the atomic levels are determined, the NRG procedure does not yet “know” about the tiny perturbation that eventually breaks the spin symmetry of the ground state. One can however easily verify that this result is incorrect: If we calculate the normalized ground state magnetization  $m$  (a static quantity) directly as a thermodynamic expectation value  $\langle (n_{f\uparrow} - n_{f\downarrow}) \rangle$  and compare it with the value derived from the spectrum

$$m = \int_{-\infty}^0 d\omega A_{\uparrow}(\omega) - \int_{-\infty}^0 d\omega A_{\downarrow}(\omega) \quad (4.12)$$

the results do not agree (see fig. 4.3). Physically, the strong polarization of the impurity due to a small magnetic perturbation should suppress the upper atomic level because no particle excitations are possible any more. This suppression is drastically underestimated by the method used so far (indeed, in the limit of vanishing Kondo temperature  $T_K$  it will not be seen at all). In order to capture this effect, it is clearly necessary to obtain the correct ground state *before* calculating the spectra. This is achieved by the following two-stage procedure:

1) NRG iterations are performed down to the temperature  $T_N$  of interest; in particular one chooses  $T_N \ll T_K$  to calculate ground state properties. For each iteration step, we keep the information on the transformation between one set of eigenstates and the next, i.e. we save the corresponding unitary matrix. After obtaining the relevant excitations at the temperature  $T_N$ , one can define the density matrix

$$\hat{\rho} = \sum_m e^{-E_m^N/T_N} |m\rangle_N \langle m| \quad (4.13)$$

which completely describes the physical state of the system. In particular, the equilibrium Green's function can be written as

$$G_{\sigma}(t) = i\theta(t)\text{Tr}(\hat{\rho} \{f_{\sigma}(t), f_{\sigma}^{\dagger}(0)\}) \quad (4.14)$$

2) Now we repeat the iterative diagonalization for the same parameters. Each iteration step  $N'$  yields the single particle excitations (and matrix elements of  $f^{\dagger}$ ) relevant at the frequency  $\omega \sim T_{N'}$ . But instead of using (4.9), we now employ (4.14) and evaluate the spectral function with respect to the correct *reduced density matrix* (see Feynman (1972)):

$$G_{\sigma}^{N'}(t) = i\theta(t)\text{Tr}(\hat{\rho}_{N'}^{\text{red}} \{f_{\sigma}(t), f_{\sigma}^{\dagger}(0)\}). \quad (4.15)$$

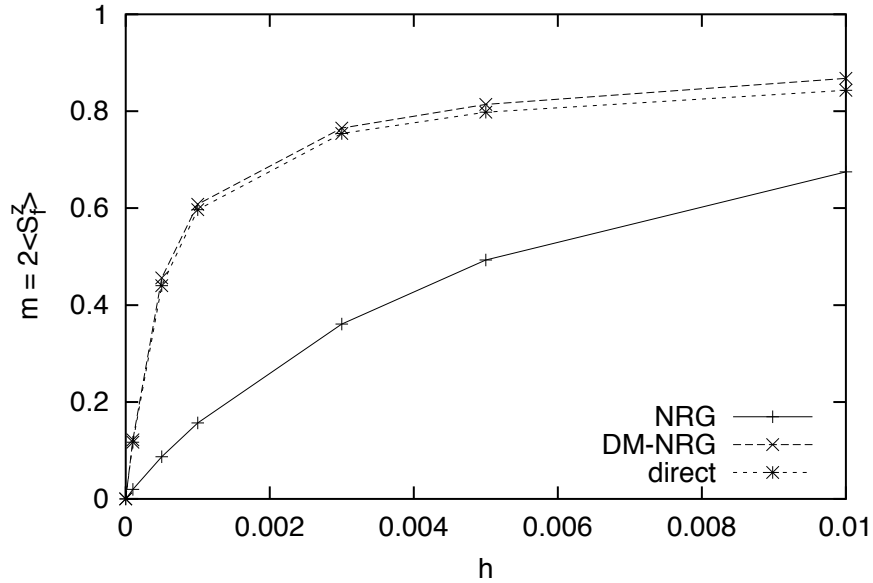


**Figure 4.3:** Normalized impurity magnetization obtained by different methods: from the spectrum (NRG vs. DM-NRG) and as a thermodynamic expectation value (direct). The impurity parameters are chosen as  $\Delta = 0.01$  and  $U = 0.1$ , the Kondo temperature is  $T_K = 6.8 \times 10^{-4}$ .

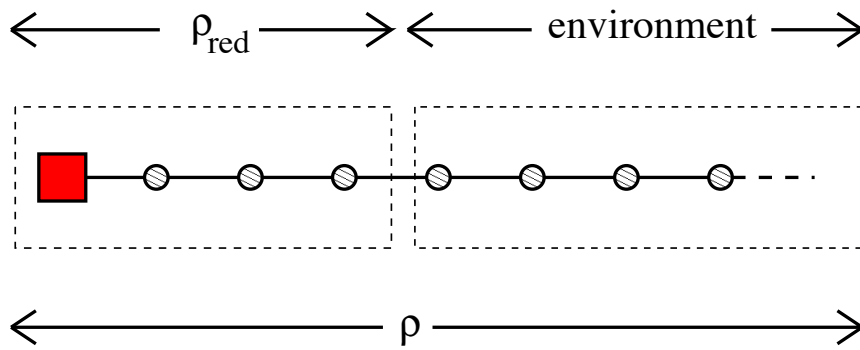


**Figure 4.4:** Reduced density matrix obtained by tracing out “environment” degrees of freedom of the chain.

As depicted in fig. 4.4, the complete chain is split into a smaller cluster of length  $N'$  and an *environment* containing the remaining degrees of freedom. In the product basis of these two subsystems, the full density matrix has the form

$$\hat{\rho} = \sum_{\substack{m_1 m_2 \\ n_1 n_2}} \rho_{m_1 n_1, m_2 n_2} |m_1\rangle_{\text{env}} |n_1\rangle_{\text{sys}} \langle n_2| \langle m_2| \quad (4.16)$$

which is in general not diagonal any more. Performing a partial trace on the environment then yields the density submatrix

$$\hat{\rho}^{\text{red}} = \sum_{n_1 n_2} \rho_{n_1 n_2}^{\text{red}} |n_1\rangle_{\text{sys}} \langle n_2| \quad (4.17)$$

with

$$\rho_{n_1 n_2}^{\text{red}} = \sum_m \rho_{m n_1, m n_2}. \quad (4.18)$$

This projection is easily done by using the previously stored unitary transformation matrices. Note that  $\hat{\rho}^{\text{red}}$  – defined only on the shorter chain – contains all the relevant information about the quantum mechanical state of the *full* system<sup>1</sup>. This concept has been applied very successfully in the density matrix renormalization group (DMRG) developed by White (1992), where the projection on a smaller subsystem is essential for obtaining eigenstates of the model. In NRG, on the other hand, diagonalization can be performed directly due to the logarithmic discretization, but to describe the effect of the chain degrees of freedom on the impurity (or a small cluster) one has to determine  $\hat{\rho}^{\text{red}}$ . In the following, we therefore refer to the calculational scheme presented here as DM–NRG.

In fig. 4.2 we compare the spectrum obtained in this way to the “old” result (the same number of levels has been used in both calculations). The strong shift of spectral weight due to the polarized impurity is now clearly seen, as well as a slight change in the height and shape of the quasiparticle peak. The magnetization has been calculated from (4.12) for different values of  $h$  and is in good agreement with the static calculation (see fig. 4.3). The remaining deviation of less than three percent is due to an error in the total spectral weight. The resulting field dependence of the spectrum is displayed in fig. 4.5. With increasing  $h$ , the Kondo resonance is suppressed and eventually merges with the lower atomic level. Regarding the total density of states  $A_{\text{tot}}(\omega) = \sum_{\sigma} A_{\sigma}(\omega)$ , the Kondo peak is split by the field and the DOS at the Fermi level is strongly reduced. This effect has been observed directly in measurements of the differential conductance through a quantum dot by Goldhaber-Gordon et al. (1998).

---

<sup>1</sup>Approximation (4.9), on the other hand, is equivalent to replacing  $\hat{\rho}_{N'}^{\text{red}}$  by the *diagonal* density matrix  $\hat{\rho}_{N'}$  of the short chain.

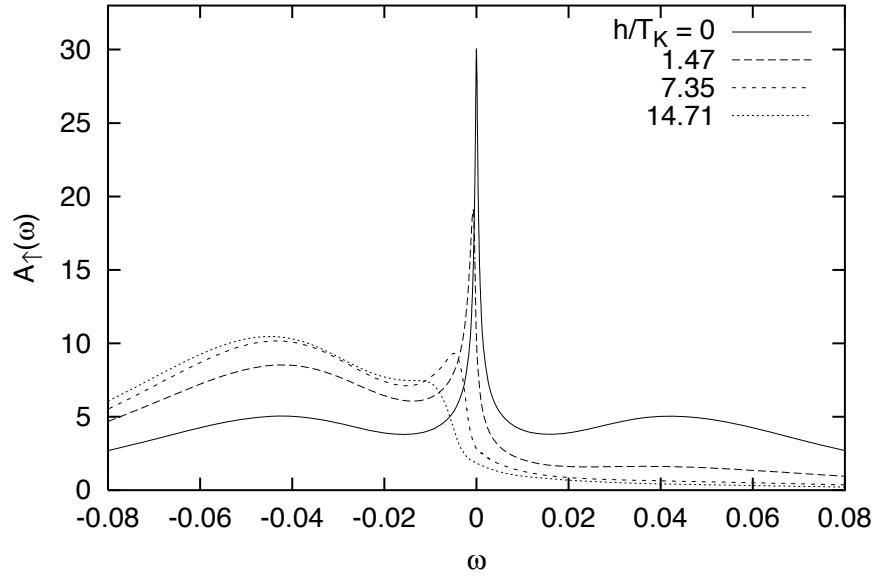


**Figure 4.5:** Shift of the spectral function with increasing magnetic field at zero temperature. The impurity parameters are chosen as  $\Delta = 0.01$  and  $U = 0.1$ , the Kondo temperature is  $T_K = 6.8 \times 10^{-4}$ .

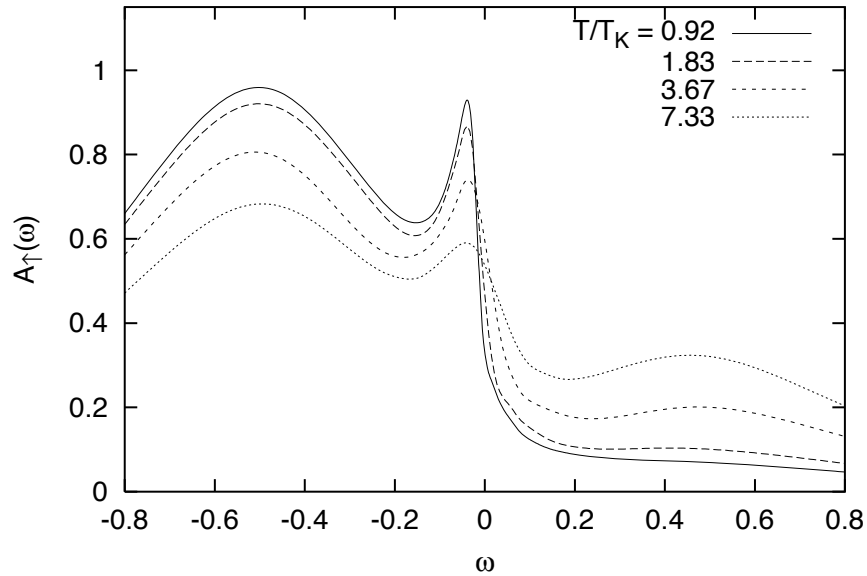


**Figure 4.6:** Temperature dependence of the spectrum for  $\Delta = 0.1$ ,  $U = 1.0$ , a Kondo temperature  $T_K = 6.0 \times 10^{-3}$  in the presence of an external magnetic field  $h = 6.7 T_K$ . Note that NRG does not yield any information at frequencies  $\omega \ll T$ .

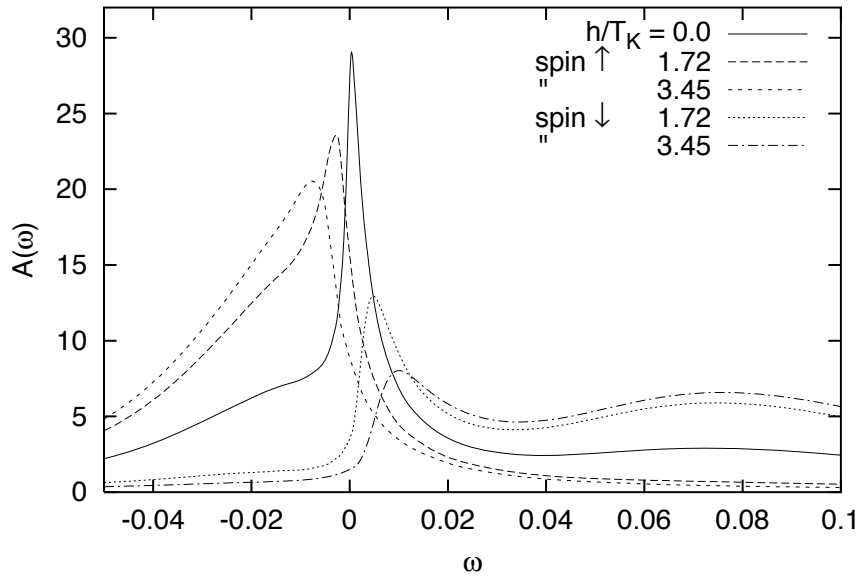


**Figure 4.7:** Spin-dependent spectral density at zero temperature for an asymmetric impurity with  $\Delta = 0.01$ ,  $U = 0.1$ ,  $\epsilon_f = -0.02$  and a Kondo temperature  $T_K = 2.9 \times 10^{-3}$ .

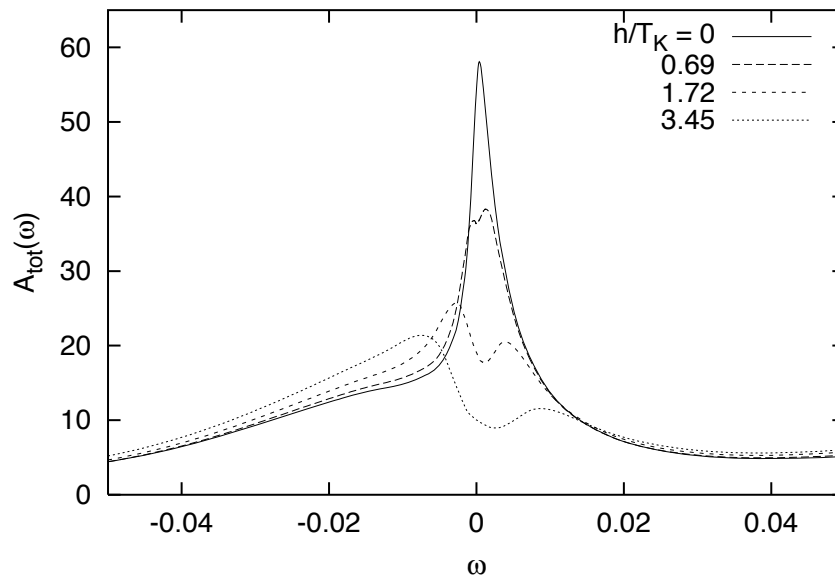


**Figure 4.8:** Total spectral density  $A_{\text{tot}} = A_{\uparrow} + A_{\downarrow}$  at zero temperature for the same parameters as in fig. 4.7. Note that upon increase of  $h$ , part of the spectral weight is shifted to the upper atomic level (not shown). The total weight is constant with high accuracy.

So far calculations have been at  $T = 0$ . Upon increase of the temperature at a finite magnetic field, we expect a reduction of the average impurity magnetization due to thermal fluctuations. As a consequence, particle excitations with polarization in the field direction should gain spectral weight. In fig. 4.6, this effect is clearly seen: At temperatures  $T \gtrsim \hbar$ , the spectral asymmetry is strongly reduced. Note that in finite temperature NRG calculations no spectral information can be obtained at frequencies  $\omega \ll T$ .

Results for an asymmetric impurity close to the mixed valence regime are shown in fig. 4.7. The almost complete shift of spectral weight to the particle (hole) sector is again observed for the two spin polarizations, which in this case are not symmetric anymore. In the total density of states (fig. 4.8), changes are less prominent. We merely observe a suppression of the quasiparticle peak and a redistribution of the corresponding weight to higher frequencies.

In order to compare our findings with previous calculations, it should be pointed out that so far only the modified perturbation theory (Takagi and Saso 1999*a*, Takagi and Saso 1999*b*) and the Quantum Monte Carlo (QMC) method (Sakai et al. 1999) have been applied to calculate the impurity spectrum in a magnetic field. The former is limited to small  $U$  and seems to overestimate the suppression of one of the atomic levels. QMC calculations have so far been done only in the mixed valence regime (and at temperatures  $T \geq T_K$ ), due to the increase in computing cost for the symmetric case. In a recent NRG calculation on the Kondo model by Costi (2000), the problems discussed here did not occur due to the absence of atomic levels. Apart from these restrictions, we find qualitative agreement with our DM–NRG results.

## 4.5 Conclusion

In this chapter we have presented a new method of calculating dynamical properties at arbitrary temperature within the numerical renormalization group. It has been demonstrated that – despite logarithmic discretization – energy scale separation is in general not valid in the case of spectral quantities. This effect is neglected in the NRG scheme used so far in the literature. Within our generalized procedure (DM–NRG), based on the reduced density matrix, we can now account for changes in the ground state occurring at energies far below the external frequency scale.

The DM–NRG introduced here has been applied to the Anderson impurity in an external magnetic field, which is of great interest in view of recent transport measurements of quantum dots. Nonperturbative  $T = 0$  studies had not been performed so far for this problem, mainly because of technical difficulties in extending NRG to systems with broken spin symmetry. Our results for the single particle spectrum are in excellent agreement with the sum rule provided by the (static) magnetization. In the total density of states we find the splitting and suppression of the quasiparticle

peak which is also observed experimentally.

Future applications will be twofold:

1) DMFT calculations for phases with long range order (antiferromagnetism, orbital ordering) require a reliable treatment of any symmetry-breaking perturbation. As outlined in the present chapter, the DM-NRG is the appropriate method in this situation.

2) With the rapid advances in nanoscale preparation techniques, more complex impurity systems including orbital degeneracy and even molecules coupled to a fermionic bath (see for example Kergueris, Bourgoïn, Palacin, Esteve, Urbina, Magoga and Joachim (1999)) will be realized. Our generalized NRG procedure provides a suitable tool for predicting and explaining spectral measurements which depend sensitively on the nature of the ground state.



# Chapter 5

## Direct application of flow equations

### 5.1 Luttinger model

#### Preliminary attempt

In this section we apply the flow–equation formalism to the Luttinger model with a linear dispersion and forward scattering. As is well known, this model can be converted into a quadratic form by bosonization and is then easily solvable. Our goal will be to diagonalize the Hamiltonian in the fermionic language and to determine which approximation of the flow corresponds to the bosonization limit.

The conduction band consists of “right” and “left” movers with a linear dispersion

$$H_0 = \sum_k k \left( : c_{1k}^\dagger c_{1k} : - : c_{2k}^\dagger c_{2k} : \right) \quad (5.1)$$

where “:” denotes normal ordering with respect to the noninteracting ground state (the filled Fermi sea). The Fermi velocity has been set to  $v_F = 1$ . Forward scattering is introduced according to

$$H_{\text{int}} = \sum_{kk'q} U_{kk'q} : c_{1k+q}^\dagger c_{1k} : : c_{2k'-q}^\dagger c_{2k'} : \quad (5.2)$$

where  $U_{kk'q=0} = 0$  is assumed and the possible momentum transfers will be limited by some UV–cutoff. We take constant couplings  $U_{kk'q} = U$ , and explicitly factorize the correlation term

$$H_{\text{int}} = U W. \quad (5.3)$$

Following an idea originally developed by MacDonald et al. (1988) and later applied by Stein (1997), we write the reduced interaction  $W$  as an infinite sum

$$W = \sum_n W_n \quad (5.4)$$

where each  $W^{(n)}$  consists of all the terms that lead to the same change in  $H_0$ , that is

$$[H_0, W_n] = n W_n. \quad (5.5)$$

Anticipating the generation of additional terms in the course of the flow, we write the total Hamiltonian as

$$H(l) = H_0 + \sum_{k=1}^{\infty} \sum_{\{\mathbf{m}\}} F^{(k)}(l, \mathbf{m}) W^{(k)}(\mathbf{m}) \quad (5.6)$$

where we have used the shortcut notation

$$W^{(k)}(\mathbf{m}) = W^{(k)}(m_1, \dots, m_k) = W_{m_1} W_{m_2} \dots W_{m_k}. \quad (5.7)$$

Initially,  $F^{(1)}(l=0, \mathbf{m}) = U$  and  $F^{(k>1)}(l=0, \mathbf{m}) = 0$ . Following the choice proposed by Wegner (1994), the generator is given by

$$\eta(l) = [H_0, H(l)] = \sum_{k=1}^{\infty} \sum_{\{\mathbf{m}\}} M^{(k)}(\mathbf{m}) F^{(k)}(l, \mathbf{m}) W^{(k)}(\mathbf{m}) \quad (5.8)$$

with the abbreviation

$$M^{(k)}(\mathbf{m}) \equiv \sum_{i=1}^k m_i. \quad (5.9)$$

The change of the Hamiltonian is obtained in the usual fashion

$$\begin{aligned} \partial_l H(l) &= [\eta(l), H(l)] \quad (5.10) \\ &= - \sum_{k=1}^{\infty} \sum_{\{\mathbf{m}\}} |M^{(k)}(\mathbf{m})|^2 F^{(k)}(l, \mathbf{m}) W^{(k)}(\mathbf{m}) \\ &\quad + \sum_{k,r=1}^{\infty} \sum_{\substack{\{\mathbf{m}_1\} \\ \{\mathbf{m}_2\}}} M(\mathbf{m}_1) F^{(k)}(l, \mathbf{m}_1) F^{(r)}(l, \mathbf{m}_2) [W^{(k)}(\mathbf{m}_1), W^{(r)}(\mathbf{m}_2)] \end{aligned}$$

where the first part leads to exponentially decaying couplings and in the second one higher and higher interactions are generated, which motivated the definition (5.6). By collecting equivalent terms, we obtain the following recursion relations for the couplings (see also Stein (1997))

$$\begin{aligned} \partial_l F^{(k)}(l, \mathbf{m}) &= -|M(\mathbf{m})|^2 F^{(k)}(l, \mathbf{m}) \quad (5.11) \\ &\quad + \sum_{n=1}^{k-1} \sum_{\substack{\{\mathbf{m}_1, \mathbf{m}_2\} \\ \mathbf{m}=(\mathbf{m}_1, \mathbf{m}_2)}} (M(\mathbf{m}_1) - M(\mathbf{m}_2)) F^{(n)}(l, \mathbf{m}_1) F^{(k-n)}(l, \mathbf{m}_2). \end{aligned}$$

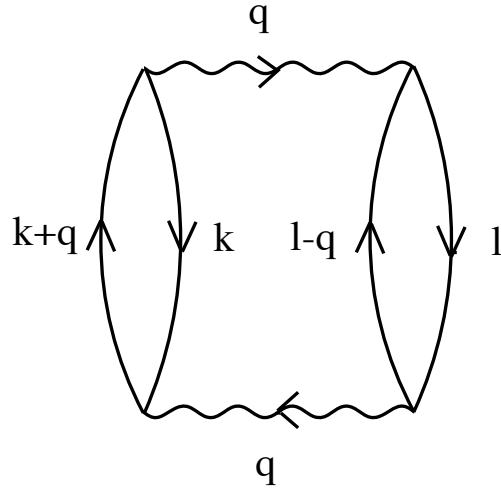


**Figure 5.1:** Second order Goldstone contribution to the ground state energy.

These can now be solved order by order. The  $k = 1$  couplings just decay exponentially

$$F^{(1)}(l, m) = e^{-m^2 l} U \quad (5.12)$$

and the second order terms can be integrated:

$$F^{(2)}(l, (m, n)) = U^2 \frac{m - n}{2mn} \left( e^{-(m^2+n^2)l} - e^{-(m+n)^2 l} \right). \quad (5.13)$$

Only the “resonant” terms survive and the effective Hamiltonian reads

$$H(l = \infty) = H_0 + U W^{(1)}(0) + U^2 \sum_{n \neq 0} \frac{1}{n} W^{(2)}(n, -n) + O(U^3). \quad (5.14)$$

We thus obtain a strictly perturbative result. Taking the expectation value of (5.14) with respect to the noninteracting groundstate leads to the ground state energy of the full system. As a consequence of the uniqueness theorem for power series (Fischer and Lieb 1992) this is equivalent to the Goldstone series (Goldstone (1957), see also Metzner and Vollhardt (1989b)). We can see that explicitly: The first term  $U \langle W^{(1)}(0) \rangle_0$  yields a Hartree contribution, which in our case vanishes due to  $U_{kk'q=0} = 0$ . The second-order term can be written as

$$\begin{aligned} \sum_{n \neq 0} \frac{U^2}{n} \langle W^{(2)}(n, -n) \rangle_0 &= \sum_{\substack{kk'q \\ k''k'''}} \frac{U^2}{2q} \langle c_{1k+q}^\dagger c_{1k} c_{2k'-q}^\dagger c_{2k'} c_{1k''-q}^\dagger c_{1k''} c_{2k'''+q}^\dagger c_{2k'''} \rangle \\ &= \sum'_{klq} \frac{U^2}{\epsilon_{1k+q} + \epsilon_{2l-q} - \epsilon_{1k} - \epsilon_{2l}} \end{aligned} \quad (5.15)$$

where dispersions  $\epsilon_{1(2)k} = \pm k$  have been introduced and the primed sum is constrained to  $k + q, l < 0$  and  $k, l - q > 0$ . This expression corresponds to the second-order Goldstone diagram in fig. 5.1.

The implementation of flow equations outlined here, although very convenient, can therefore not reproduce the nonperturbative bosonization result. We have to find another representation of the interaction terms.

## Normal-ordered version

One central element of flow equations as proposed by Wegner (1994) is the *normal ordering* of interaction terms. In the previous section, this has not been taken into account. The higher-order terms were so far written as simple products of the interaction.

In the following, we will now use the normal-ordered version of the flow equations, keeping only two-particle terms. Again the Hamiltonian is given by (5.1) and (5.2). Following Wegner's ansatz, the generator has the form

$$\eta = 2 \sum_{kk'q} q U_{kk'q} : c_{1k+q}^\dagger c_{1k} :: c_{2k'-q}^\dagger c_{2k'} : \cdot \quad (5.16)$$

For small  $U$ , the leading contribution to the flow is induced by the noninteracting part  $H_0$

$$[\eta, H_0] = -4 \sum_{kk'q} q^2 U_{kk'q} : c_{1k+q}^\dagger c_{1k} :: c_{2k'-q}^\dagger c_{2k'} : \quad (5.17)$$

yielding simply an exponential decay of the couplings. Due to the interaction part (5.2), new terms will appear. In order to simplify the notation for multiple momentum sums, we use the convention that all indices are constrained to be inside the noninteracting band. We obtain the following expression:

$$\begin{aligned} [\eta, H_{\text{int}}] &= \sum_{\substack{k_1 k_2 q \\ k p}} 2q U_{k_1, k_2, q} \left\{ \left( U_{k_1-p, k, p} c_{1k_1+q}^\dagger c_{1k_1-p} - U_{k_1+q, k, p} c_{1k_1+p+q}^\dagger c_{1k_1} \right) \right. \\ &\quad \times : c_{2k-p}^\dagger c_{2k} :: c_{2k_2-q}^\dagger c_{2k_2} : \\ &\quad + \left( U_{k, k_2+p, p} c_{2k_2-q}^\dagger c_{2k_2+p} - U_{k, k_2-q, p} c_{2k_2-q-p}^\dagger c_{2k_2} \right) \\ &\quad \left. \times : c_{1k_1+q}^\dagger c_{1k_1} :: c_{1k+p}^\dagger c_{1k} : \right\}. \quad (5.18) \end{aligned}$$

It is now necessary to transform the different terms into normal order. This is achieved by repeatedly applying the following identity:

$$\begin{aligned}
& : c_{1k_1+q}^\dagger c_{1k_1} :: c_{1k_2+p}^\dagger c_{1k_2} := & (5.19) \\
& = : c_{1k_1+q}^\dagger c_{1k_1} c_{1k_2+p}^\dagger c_{1k_2} : - \delta_{k_1+q, k_2} n_{1k_1+q} : c_{1k_2+p}^\dagger c_{1k_1} : \\
& \quad + \delta_{k_2+p, k_1} (1 - n_{1k_1}) : c_{1k_1+q}^\dagger c_{1k_2} : + \delta_{k_1+q, k_2} \delta_{k_2+p, k_1} (1 - n_{1k_1}) n_{1k_1+q}.
\end{aligned}$$

The full Hamiltonian

$$\begin{aligned}
H(l) = H_0 + \sum_k (V_{1k}(l) : c_{1k}^\dagger c_{1k} : + V_{2k}(l) : c_{2k}^\dagger c_{2k} :) & (5.20) \\
+ \sum_{k_1 k_2 q} \left( W_{1k_1 k_2 q}(l) : c_{1k_1+q}^\dagger c_{1k_1} c_{1k_2-q}^\dagger c_{1k_2} : + W_{2k_1 k_2 q}(l) : c_{2k_1+q}^\dagger c_{2k_1} c_{2k_2-q}^\dagger c_{2k_2} : \right) \\
+ \sum_{k_1 k_2 q} U_{k_1 k_2 q}(l) : c_{1k_1+q}^\dagger c_{1k_1} :: c_{2k_2-q}^\dagger c_{2k_2} : + E(l)
\end{aligned}$$

then includes a new two-particle interaction  $W$  between fermions of the same species, a one-particle component  $V$  and a shift  $E$  of the ground state energy. If normal-ordered interactions between three and more particles are neglected, a closed system of flow equations emerges:

$$\begin{aligned}
\partial_l E &= \sum_{k_1 k_2 q} 2q U_{k_1 k_2 q} \left\{ U_{k_1+q, k_2-q, -q} (n_{1k_1+q} - n_{1k_1}) (1 - n_{2k_2-q}) n_{2k_2} \right. \\
&\quad \left. + U_{k_1+q, k_2-q, -q} (n_{2k_2-q} - n_{2k_2}) (1 - n_{1k_1}) n_{1k_1+q} \right\} & (5.21)
\end{aligned}$$

$$\begin{aligned}
\partial_l V_{1k} &= \sum_{k_1 q} \left\{ 2q (1 - n_{2k_1-q}) n_{2k_1} (U_{k-q, k_1, q} U_{k, k_1-q, -q} - U_{k, k_1, q} U_{k+q, k_1-q, -q}) \right. \\
&\quad + 2q (n_{2k_1-q} - n_{2k_1}) (-n_{1k+q} U_{k, k_1, q} U_{k+q, k_1-q, -q} \\
&\quad \left. + (1 - n_{1k-q}) U_{k-q, k_1, q} U_{k, k_1-q, -q} \right\} & (5.22)
\end{aligned}$$

$$\begin{aligned}
\partial_l V_{2k} &= \sum_{k_1 q} \left\{ 2q (1 - n_{1k_1}) n_{k_1+1} (U_{k_1, k+q, q} U_{k_1+q, k, -q} - U_{k_1, k, q} U_{k_1+q, k-q, -q}) \right. \\
&\quad + 2q (n_{1k_1+q} - n_{1k_1}) (-n_{2k+q} U_{k_1, k+q, q} U_{k_1+q, k, -q} \\
&\quad \left. + (1 - n_{2k-q}) U_{k_1, k, q} U_{k_1+q, k-q, -q} \right\} & (5.23)
\end{aligned}$$

$$\partial_l W_{1k_1, k_2, q} = \sum_k 2q U_{k_1, k, q} U_{k_2, k-q, -q} (n_{2k-q} - n_{2k}) & (5.24)$$

$$\partial_l W_{2k_1, k_2, q} = \sum_k 2q U_{k, k_2, q} U_{k+q, k_1, -q} (n_{1k+q} - n_{1k}) & (5.25)$$

$$\begin{aligned}
\partial_l U_{k_1, k_2, q} = & \sum_p 2(q-p) \left\{ U_{k_1, k_2, p} U_{k_1+p, k_2-p, q-p} (1 - n_{1k_1+p} - n_{2k_2-p}) \right. \\
& + U_{k_1, k_2-q+p, p} U_{k_1+p, k_2, q-p} (n_{1k_1+p} - n_{2k_2-q+p}) \\
& + U_{k_1+q-p, k_2, p} U_{k_1, k_2-p, q-p} (n_{2k_2-p} - n_{1k_1+q-p}) \\
& - U_{k_1+q-p, k_2, p} U_{k_1, k_2-p, q-p} (n_{2k_2-p} - n_{1k_1+q-p}) \\
& \left. - U_{k_1+q-p, k_2-q+p, p} U_{k_1, k_2, q-p} (1 - n_{2k_2-q+p} - n_{1k_1+q-p}) \right\} \\
& - 4q^2 U_{k_1, k_2, q} \\
& + 2q \sum_p \left\{ U_{k_1+p, k_2, q} W_{1k_1, k_1+p+q, p} (n_{1k_1+p} - n_{1k_1+p+q}) \right. \\
& \left. + U_{k_1-p, k_2, q} W_{1k_1-p+q, k_1, p} (n_{1k_1-p} - n_{1k_1-p+q}) \right\} \\
& + 2q \sum_k U_{k, k_2, q} (W_{1k+q, k_1, -q} + W_{1k_1, k+q, q}) (n_{1k+q} - n_{1k}) \\
& + 2q \sum_p \left\{ U_{k_1, k_2+p, q} W_{2k_2, k_2+p-q, p} (n_{2k_2+p} - n_{2k_2+p-q}) \right. \\
& \left. + U_{k_1, k_2-p, q} W_{2k_2-p-q, k_2, p} (n_{2k_2-p} - n_{2k_2-p-q}) \right\} \\
& + 2q \sum_k U_{k_1, k, q} (W_{2k-q, k_2, q} + W_{2k_2, k-q, -q}) (n_{2k-q} - n_{2k}) \\
& + 2q U_{k_1, k_2, q} (V_{1k_1} - V_{1k_1+q}) \\
& + 2q U_{k_1, k_2, q} (V_{2k_2} - V_{2k_2-q}). \tag{5.26}
\end{aligned}$$

This system of coupled differential equations is solved numerically by a fourth-order Runge–Kutta algorithm (Press et al. 1995). Again we take momentum-independent initial values for the couplings which we scale as  $U_{kk'q} = U/N$  where  $N$  is the system size.

At  $l = \infty$ , only the  $V$  and  $W$  couplings remain, which commute with the non-interacting part  $H_0$ . The Hamiltonian is then block-diagonal in the degenerate subspaces of the conduction band (note that this is a special situation due to the linear dispersion: For an interaction between particles of the same species, momentum conservation is equivalent to energy conservation).

First, we examine the interaction dependence of the ground-state energy  $E$ , where the contribution of the noninteracting Fermi sea has already been subtracted. Results for a small finite system are shown in fig. 5.2. For comparison, we have also plotted the exact ground-state energy obtained by a Lanczos calculation and the  $\mathcal{O}(U^2)$  term in the Goldstone expansion. Evidently, at weak interaction the three methods show good agreement. If  $U$  is increased, the exact result displays a crossover to a linear behaviour in  $U$  (the interaction is then the dominant energy scale) not captured by the perturbative result. Flow equations, on the other hand, describe the

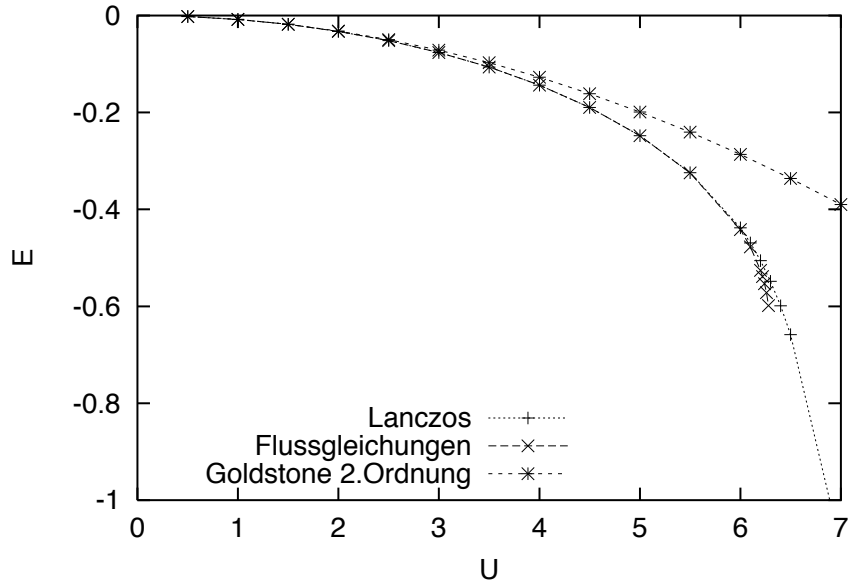


**Figure 5.2:** Ground state energy of the half-filled Luttinger model at  $N = 10$  and a momentum transfer cutoff  $N_C = 1$ .

deviations from the  $U^2$  behaviour well until, at  $U \approx 6.2$ , an instability occurs and the equations diverge. This breakdown, while unphysical for the finite system, is a precursor of *phase separation* which occurs in the thermodynamic limit of the Luttinger model as demonstrated by Mattis and Lieb (1965). Varying the momentum cutoff (fig. 5.3) leads to another instructive comparison of the different methods. Here the bosonization result for the ground state energy is also plotted

$$E_{\text{bos}} = - \sum_{n=1}^{N_C} \frac{2\pi n}{N} \left( 1 - \sqrt{1 - \left(\frac{U}{2\pi}\right)^2} \right) \quad (5.27)$$

leading to a quadratic dependence of  $E$  on the momentum transfer cutoff  $p_c = \frac{2\pi}{N} N_C$ . The instability at  $U = 2\pi$  agrees well with the observed critical  $U$  in the finite system (see above). Fig. 5.3 clearly shows that bosonization and flow equations are virtually exact for small  $N_C = 1, 2$  whereas the Goldstone result deviates slightly. If we increase the range of possible momentum transfers, the preconditions for the bosonization formalism (no excitations close to the band edge) are not valid any more, which leads to an unphysically low ground state energy. Both flow equations and perturbation theory capture the transition to a *saturation* at large  $N_C$ , although in this regime the Goldstone result is superior.

In order to calculate expectation values of an observable  $\hat{O}$ , it is necessary to

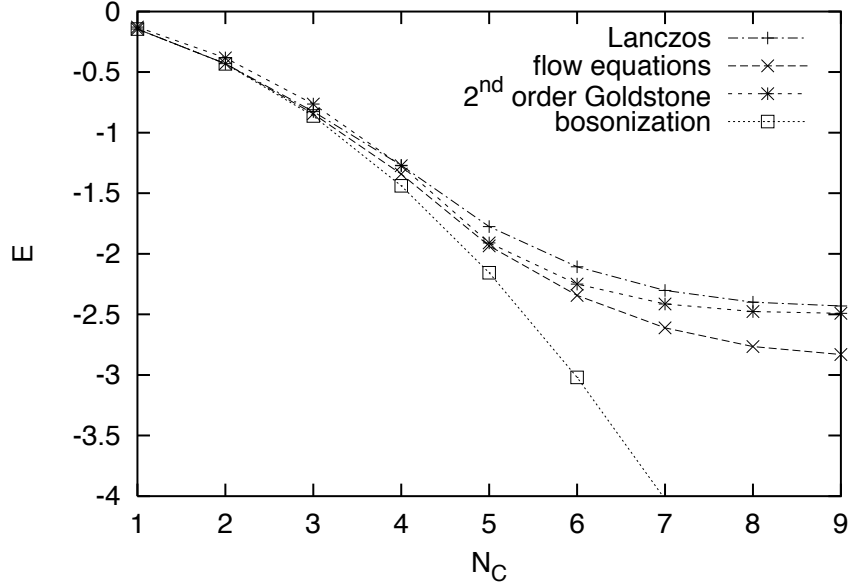


**Figure 5.3:** Ground state energy of the half filled Luttinger model at  $N = 10$  and interaction  $U = 4.0$ .

perform an additional unitary transformation

$$\partial_l \hat{O} = [\eta, \hat{O}]. \quad (5.28)$$

We are interested in the occupation-number distribution in momentum space and choose

$$\hat{O}(l=0) \equiv \hat{n}_{k_0} = c_{1k_0}^\dagger c_{1k_0}. \quad (5.29)$$

Again, the flow (5.28) will generate higher-order terms in  $\hat{O}(l)$  which need to be truncated. We make the following ansatz

$$\begin{aligned} \hat{O}(l) = & K(l) + \sum_{k_1 k_2 q} M_{k_1 k_2 q}(l) : c_{1k_1+q}^\dagger c_{1k_1} :: c_{2k_2-q}^\dagger c_{2k_2} : \\ & + \sum_{k_1 k_2 q} N_{1k_1 k_2 q}(l) : c_{1k_1+q}^\dagger c_{1k_1} c_{1k_2-q}^\dagger c_{1k_2} : \\ & + \sum_{k_1 k_2 q} N_{2k_1 k_2 q}(l) : c_{2k_1+q}^\dagger c_{2k_1} c_{2k_2-q}^\dagger c_{2k_2} : \\ & + \sum_{k_1} P_{1k_1}(l) : c_{1k_1}^\dagger c_{1k_1} : + \sum_{k_1} P_{2k_1}(l) : c_{2k_1}^\dagger c_{2k_1} : \end{aligned} \quad (5.30)$$

where initially all couplings vanish except  $P_{1k_0}(l=0) = 1$ . The constant term

determines the ground–state expectation value we are interested in:

$$\langle \Psi_0 | \hat{n}_{1k_0} | \Psi_0 \rangle = K \quad (5.31)$$

After evaluating  $[\eta, \hat{O}]$  we again convert the result into normal order and neglect terms not contained in (5.30). This leads to an additional set of flow equations:

$$\begin{aligned} \partial_l K &= \sum_{k_1 k_2 q} 2q U_{k_1 k_2 q} M_{k_1+q, k_2-q, -q} \left\{ (n_{1k_1+q} - n_{1k_1}) (1 - n_{2k_2-q}) n_{2k_2} \right. \\ &\quad \left. + (n_{2k_2-q} - n_{2k_2}) (1 - n_{1k_1}) n_{1k_1+q} \right\} \end{aligned} \quad (5.32)$$

$$\begin{aligned} \partial_l P_{1k} &= \sum_{k_1 q} 2q \left\{ (1 - n_{2k_1-q}) n_{2k_1} (U_{k-q, k_1, q} M_{k, k_1-q, -q} - U_{k, k_1, q} M_{k+q, k_1-q, -q}) \right. \\ &\quad + (n_{2k_1-q} - n_{2k_1}) (-n_{1k+q} U_{k, k_1, q} M_{k+q, k_1-q, -q} \\ &\quad \left. + (1 - n_{1k-q}) U_{k-q, k_1, q} M_{k, k_1-q, -q}) \right\} \end{aligned} \quad (5.33)$$

$$\begin{aligned} \partial_l P_{2k} &= \sum_{k_1 q} 2q \left\{ (1 - n_{1k_1}) n_{1k_1+q} (U_{k_1, k+q, q} M_{k_1+q, k, -q} - U_{k_1, k, q} M_{k_1+q, k-q, -q}) \right. \\ &\quad + (n_{1k_1+q} - n_{1k_1}) (-n_{2k+q} U_{k_1, k+q, q} M_{k_1+q, k, -q} \\ &\quad \left. + (1 - n_{2k-q}) U_{k_1, k, q} M_{k_1+q, k-q, -q}) \right\} \end{aligned} \quad (5.34)$$

$$\begin{aligned} \partial_l M_{k_1, k_2, q} &= \sum_p 2(q-p) \left\{ M_{k_1, k_2, p} U_{k_1+p, k_2-p, q-p} (1 - n_{1k_1+p} - n_{2k_2-p}) \right. \\ &\quad + M_{k_1, k_2-q+p, p} U_{k_1+p, k_2, q-p} (n_{1k_1+p} - n_{2k_2-q+p}) \\ &\quad + M_{k_1+q-p, k_2, p} U_{k_1, k_2-p, q-p} (n_{2k_2-p} - n_{1k_1+q-p}) \\ &\quad - M_{k_1+q-p, k_2-q+p, p} U_{k_1, k_2, q-p} (1 - n_{2k_2-q+p} - n_{1k_1+q-p}) \\ &\quad + 2q \left\{ \sum_p \left( U_{k_1+p, k_2, q} N_{1k_1, k_1+p+q, p} (n_{1k_1+p} - n_{1k_1+p+q}) \right. \right. \\ &\quad \left. \left. + U_{k_1-p, k_2, q} N_{1k_1-p+q, k_1, p} (n_{1k_1-p} - n_{1k_1-p+q}) \right) \right. \\ &\quad \left. + \sum_k U_{k, k_2, q} (N_{1k+q, k_1, -q} + N_{1k_1, k+q, q}) (n_{1k+q} - n_{1k}) \right\} \\ &\quad + 2q \left\{ \sum_p \left( U_{k_1, k_2+p, q} N_{2k_2, k_2+p-q, p} (n_{2k_2+p} - n_{2k_2+p-q}) \right. \right. \end{aligned}$$

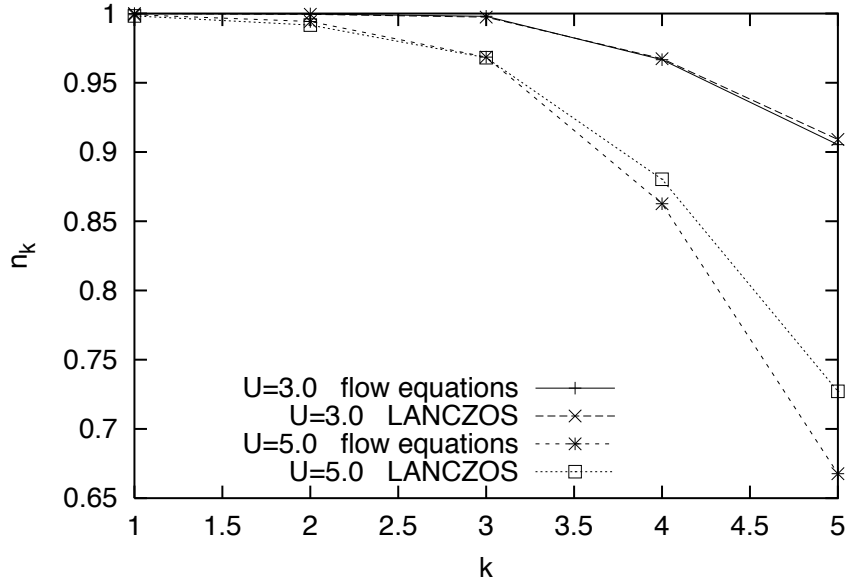


**Figure 5.4:** Occupation number  $n_k$  of the half filled Luttinger model at  $N = 10$ , a momentum transfer cutoff  $N_C = 2$  and interactions  $U = 3.0/5.0$ .

$$\begin{aligned}
& + U_{k_1, k_2-p, q} N_{2k_2-p-q, k_2, p} (n_{2k_2-p} - n_{2k_2-p-q}) \\
& + \left. \sum_k U_{k_1, k, q} (N_{2k-q, k_2, q} + N_{2k_2, k-q, -q}) (n_{2k-q} - n_{2k}) \right\} \\
& + 2q U_{k_1, k_2, q} (P_{1k_1} - P_{1k_1+q}) \\
& + 2q U_{k_1, k_2, q} (P_{2k_2} - P_{2k_2-q}) \tag{5.35}
\end{aligned}$$

$$\partial_l N_{1k_1, k_2, q} = \sum_k 2q U_{k_1, k, q} M_{k_2, k-q, -q} (n_{2k-q} - n_{2k}) \tag{5.36}$$

$$\partial_l N_{2k_1, k_2, q} = \sum_k 2q U_{k, k_2, q} M_{k+q, k_1, -q} (n_{1k+q} - n_{1k}). \tag{5.37}$$

Some results of the numerical solution are shown in fig. (5.4). For weak interactions, the agreement with the exact Lanczos data is excellent. At  $U = 5.0$ , however, the error in  $n_k$  close to the Fermi edge is already significant, although the ground state energy is still reasonably accurate. This can be understood as follows: The main approximation becomes exact only for the Hamiltonian, where the neglected many-particle terms indeed vanish in the limit of small momentum transfer cutoff. For the observable  $\hat{n}_k$  this is not the case: Even in the bosonization regime, the ansatz (5.30) is not exact. Instead one would have to use the *bosonization identity* (see chapter 6), which is, however, hard to generalize to the case of a finite bandwidth.

The  $n_k$  results are therefore strictly perturbative and cannot reflect the anomalous power law behaviour close to the Fermi edge, which is typical for a Luttinger liquid (see for example Schönhammer (1997)).

## 5.2 Wolff model

Wolff (1961) introduced the following Hamiltonian to describe a magnetic impurity in a metallic host:

$$H = \sum_{k\sigma} \epsilon_k c_{k\sigma}^\dagger c_{k\sigma} + U(n_{0\uparrow} - \frac{1}{2})(n_{0\downarrow} - \frac{1}{2}) - \frac{h}{2}(n_{0\uparrow} - n_{0\downarrow}). \quad (5.38)$$

Here  $c_{0\sigma} = \frac{1}{\sqrt{N}} \sum_k c_{k\sigma}$  denotes the local impurity orbital which – in contrast to the Anderson model (Anderson 1961) – is part of the conduction electron lattice with lattice constant  $a = 1$  and system size  $N$ . An additional magnetic field  $h$  is coupled to the impurity. Mattis (1975) has presented an “exact” solution of this model for the case of a linear dispersion

$$\epsilon_k = k \quad (-\pi < k < \pi) \quad (5.39)$$

using bosonization. Although a more detailed introduction to this technique is given in the next chapter, we already outline the main idea at this point. With the help of the *Kronig identity* (Kronig 1935) the kinetic energy is represented in the form

$$H_0 = \frac{2\pi}{N} \sum_{q>0} \rho_\sigma(q) \rho_\sigma(-q) \quad (5.40)$$

with the density operators

$$\rho_\sigma(q) = \sum_k c_{k+q\sigma}^\dagger c_{k\sigma}. \quad (5.41)$$

If band–edge effects are neglected, the  $\rho$ 's obey *bosonic* commutation relations

$$[\rho_\sigma(-q), \rho_\sigma(q')] = \delta_{q,q'} \frac{qN}{2\pi} \quad (5.42)$$

and after rescaling  $b_{q\sigma} \equiv \sqrt{\frac{2\pi}{qN}} \rho_\sigma(-q)$  the Hamiltonian can be written as a quadratic form

$$\begin{aligned} H = & \sum_{\substack{q>0 \\ \sigma}} q b_{q\sigma}^\dagger b_{q\sigma} + \frac{U}{2\pi N} \sum_{q,q'>0} (qq')^{\frac{1}{2}} (b_{q\uparrow} + b_{q\uparrow}^\dagger)(b_{q'\downarrow} + b_{q'\downarrow}^\dagger) \\ & - \frac{h}{2\sqrt{2\pi N}} \sum_{q>0} q^{\frac{1}{2}} (b_{q\uparrow} + b_{q\uparrow}^\dagger - b_{q\downarrow} - b_{q\downarrow}^\dagger). \end{aligned} \quad (5.43)$$

This expression is trivially diagonalized by separating spin and charge degrees of freedom. For interactions larger than  $U_c = \pi$ , no ground state exists any more in the spin sector. As a consequence, the local magnetic susceptibility diverges

$$\chi = -\frac{\partial^2 E_0(h)}{\partial h^2} \sim \left(1 - \frac{U}{U_c}\right)^{-1} \quad (5.44)$$

and the ground-state energy has singular derivatives with respect to  $U$ . These results were interpreted by Mattis as the formation of an unscreened local moment at a finite interaction strength. However, it was soon realized by Fogedby (1977) that the appearance of a critical coupling strength comparable to the bandwidth is an artefact of the bosonic representation. At values  $U \approx U_c$ , the neglected band-edge terms become relevant, and (5.43) is no longer valid. In fact, the impurity physics of the Wolff model is equivalent to that of an Anderson model with a non-constant hybridization strength of the order of the bandwidth, which is known to have a singlet ground state at arbitrary coupling.

In the weak coupling regime, on the other hand, bosonization is expected to perform well. Motivated by the Luttinger model results, we therefore again apply flow equations in order to take band edge effects into account. In our calculation we focus on the ground state energy which is compared to exact Lanczos results. Anticipating new terms generated by the flow, we write down the following ansatz for the Hamiltonian:

$$\begin{aligned} H(l) = & H_0 + E(l) + \sum_{kk'\sigma} V_{kk'}(l) : c_{k\sigma}^\dagger c_{k'\sigma} : \\ & + \sum_{kk'k''k'''} U_{kk'k''k'''}(l) : c_{k\uparrow}^\dagger c_{k'\uparrow} c_{k''\downarrow}^\dagger c_{k'''\downarrow} : + \sum_{kk'k''k'''\sigma} W_{kk'k''k'''}(l) : c_{k\sigma}^\dagger c_{k'\sigma} c_{k''\sigma}^\dagger c_{k'''\sigma} : \end{aligned} \quad (5.45)$$

Again normal-ordered terms involving three and more particles have been neglected. In contrast to the Luttinger case, there is no momentum conservation. As a consequence, the interaction  $W$  between particles with equal spin does not commute with the conduction band  $H_0$  and therefore yields an additional contribution to the generator. Wegner's choice leads to

$$\begin{aligned} \eta = & \sum_{k_1 k_2 \sigma} (k_1 - k_2) V_{k_1 k_2} : c_{k_1 \sigma}^\dagger c_{k_2 \sigma} : \\ & + \sum_{k_1 k_2 k_3 k_4} (k_1 - k_2 + k_3 - k_4) U_{k_1 k_2 k_3 k_4} : c_{k_1 \uparrow}^\dagger c_{k_2 \uparrow} c_{k_3 \downarrow}^\dagger c_{k_4 \downarrow} : \\ & + \sum_{k_1 k_2 k_3 k_4 \sigma} (k_1 - k_2 + k_3 - k_4) W_{k_1 k_2 k_3 k_4} : c_{k_1 \sigma}^\dagger c_{k_2 \sigma} c_{k_3 \sigma}^\dagger c_{k_4 \sigma} : . \end{aligned} \quad (5.46)$$

The resulting flow equations for the couplings have been evaluated by using *Mathematica* and are given in appendix D. They are again solved numerically by fourth-order Runge-Kutta. Some results for the ground-state energy as a function of  $U$  are

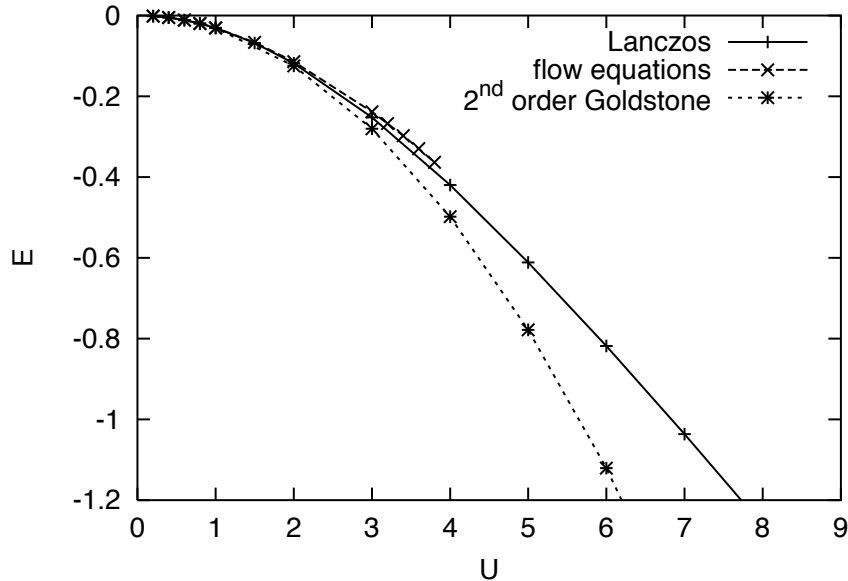


**Figure 5.5:** Ground state energy of the Wolff model with  $N=10$  conduction band orbitals: Flow equations become numerically unstable at  $U \approx 4$ .

given in fig. (5.5) and compared to the exact Lanczos and perturbative Goldstone values. For small interaction, we obtain  $E \sim U^2$  and the three methods agree. At  $U \approx 5$ , the behaviour changes to  $E \sim U$  because the interaction term then defines the dominant energy scale. This change of behaviour is not captured in perturbation theory. Flow equations, on the other hand, describe at least part of the crossover until, at  $U \approx 4$ , the system of differential equations becomes numerically unstable. This indicates that beyond a critical value of the interaction, the truncation scheme applied here (keeping only two-particle interactions after normal ordering) is not reliable any more.

## 5.3 Conclusion

In this chapter flow equations have been applied to fermionic many-particle systems in second quantization. The Tomonaga-Luttinger model with forward scattering has been studied as a “toy model” where flow equations can be compared to bosonization and exact diagonalization. A preliminary implementation without normal ordering has yielded perturbative results, essentially reproducing the Goldstone series for the ground state energy. To achieve partial summation of this series in a nonperturbative way it has been necessary to represent higher many-particle interactions in a normal-

ordered fashion. Keeping only two-particle terms then leads to the bosonization result for the ground-state energy in the limit of a small momentum transfer. Upon increase of the cutoff, flow equations correctly reproduce the saturation of the ground state energy. On the other hand, we have found that the results for the occupation number distribution are always strictly perturbative.

For the Wolff model, we have demonstrated that flow equations become exact only in the limit of vanishing coupling. In contrast to the Luttinger model, there is no additional small parameter (like the momentum-transfer cutoff) that could make bosonization work: The local Hubbard interaction is long range in momentum space and therefore creates excitations arbitrarily close to the band edges, which become important at intermediate couplings of the order of the bandwidth.

Instead of keeping higher terms in the flow equations (which is impractical), we will consider a different way of parametrizing many-particle terms in the analysis of the Kondo problem presented in the next chapter.

# Chapter 6

## Flow equation analysis of the Kondo model

### 6.1 Introduction

The Kondo model (1.1) is the most basic Hamiltonian describing the interaction of a localized moment with a sea of conduction electrons (fig. 6.1). It is relevant for systems where local charge fluctuations can occur only virtually: If the Anderson model (1.3) is projected into a sector with fixed number of particles  $n_d$  on the impurity site, an effective exchange Hamiltonian emerges as noticed first by Schrieffer and Wolff (1966). Neglecting spin-orbit coupling, the resulting exchange is  $SU(2)$ -invariant. Nevertheless it is useful to generalize the model to *anisotropic* couplings

$$H = \sum_{k\sigma} \epsilon_k c_{k\sigma}^\dagger c_{k\sigma} + \sum_{\mu\nu} J_{\parallel} c_{0\mu}^\dagger \sigma_{\mu\nu}^z c_{0\nu} S^z + \sum_{\mu\nu} \frac{J_{\perp}}{2} \left( c_{0\mu}^\dagger \sigma_{\mu\nu}^+ c_{0\nu} S^- + h.c. \right) \quad (6.1)$$

where  $c_0^\dagger = (1/\sqrt{L}) \sum_k c_k^\dagger$  represents the local conduction electron orbital. In the present chapter, we denote the system size as  $L$ . Physically, this extended Hamiltonian may be motivated by the equivalence to the dissipative two-state system (see Leggett, Chakravarty, Dorsey, Fisher, Garg and Zwerger (1987)) where the dissipation and the tunneling amplitude are indeed two independent parameters and one is usually interested in the strongly anisotropic limit. From the theoretical point of view, the independent choice of the longitudinal ( $J_{\parallel}$ ) and spin-flip ( $J_{\perp}$ ) couplings has the advantage that the phase diagram includes the exactly solvable *Toulouse limit* (Toulouse 1969): At a certain (large) value  $J_{\parallel T}$  of the longitudinal interaction, the Kondo model can be mapped onto a noninteracting resonant level model (an Anderson impurity model without spin) as long as  $J_{\perp} \ll J_{\parallel T}$  provides a small energy scale. For the following flow equation analysis of the Kondo model, the Toulouse limit is an essential ingredient: It corresponds to the fixed point of the Hamiltonian flow. In

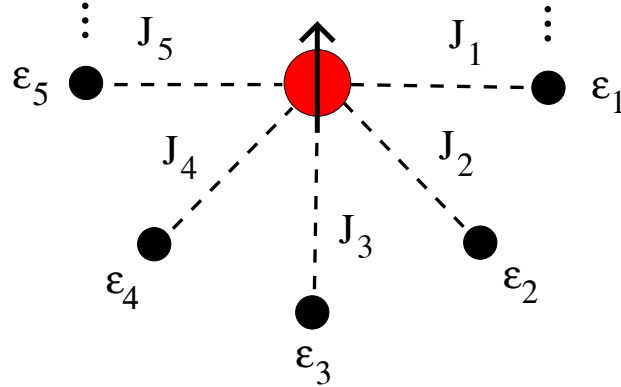


**Figure 6.1:** Local moment interacting with a conduction electron bath.

contrast to earlier scaling calculations of Anderson and Yuval (1969), Anderson et al. (1970) and Anderson (1970) one can therefore avoid a strong coupling divergence, which is the main advantage of the present approach.

## 6.2 Bosonization

In principle, flow equations could be directly applied to the Kondo Hamiltonian in the fermionic representation (6.1). But, as we have seen in the Wolff model calculation (section 5.2), this requires truncation of the flow, keeping only a finite number of the additionally generated higher-order terms. The truncation becomes only exact in the trivial limit of vanishing coupling and therefore – in the Kondo case – leads to a result that is purely perturbative in  $J$ . Unlike the Wolff model, however, the Kondo Hamiltonian has an exactly solvable point at finite coupling strength, the *Toulouse limit* mentioned already in the introduction. Our goal will be to use a representation where the flow equations close at this particular point. The simplicity of the Toulouse limit is not visible in the fermionic language: Originally, the reduction to the noninteracting resonant level model has been derived via the partition function by Toulouse (1969) and Anderson et al. (1970); it was later generalized by Wiegmann and Finkelstein (1978). The most convenient technique, however, to establish this equivalence is the *bosonization* method. In the following we introduce some of its basic concepts, following the seminal paper of Haldane (1981) and two recent reviews of von Delft and Schöller (1998) and Schönhammer (1997).

The main idea is to work with the Fourier components of the fermionic density instead of the creation and annihilation operators:

$$\rho_{\sigma}(q) \equiv \sum_k c_{\sigma k+q}^{\dagger} c_{\sigma k}. \quad (6.2)$$

Here the momenta are supposed to be discrete ( $k = 2\pi n/L$ ) and bounded ( $k_{\min} < k < k_{\max}$ ). The general commutation relations of these objects are of the form

$$[\rho_\sigma(p), \rho_\sigma(q)] = 0 \quad (6.3)$$

if  $p$  and  $q$  have equal sign and

$$[\rho_\sigma(p), \rho_\sigma(-q)] = \left( \sum_{k=k_{\max}-q+1}^{k_{\max}} - \sum_{k=k_{\min}+p-q}^{k_{\min}+p-1} \right) : c_{\sigma k}^\dagger c_{\sigma k+q-p} : - \frac{pL}{2\pi} \delta_{pq} \quad (6.4)$$

for  $p > q > 0$ . In (6.4), normal-ordered terms with momenta close to the band edge arise. They can be neglected if acting on a state which contains only particle/hole excitations close to the Fermi edge (this usually requires that either the interaction is weak or an explicit momentum transfer cutoff is built in, see also section 5.1). Keeping only the  $c$ -number in (6.4), the density modes can be considered as *bosons*. For a linear dispersion of the conduction band

$$H_0 = \sum_k k : c_{\sigma k}^\dagger c_{\sigma k} : \quad (6.5)$$

the *Kronig identity* (Kronig 1935) states that the kinetic energy can be expressed in terms of the density modes:

$$H_0 = \frac{2\pi}{L} \sum_{q>0} \rho_\sigma(q) \rho_\sigma(-q) \quad (6.6)$$

Note that the Fermi velocity has been chosen as  $v_F = 1$ . It is easy to prove that this relation remains exact even in the presence of band edges (see Schönhammer (1997)). To bosonize a general interaction term it is necessary to express the fermionic (real space) field operators in terms of the density modes. In order to do this, we define a bosonic field

$$\Phi_\sigma(x) \equiv -i \sum_{q \neq 0} \frac{e^{-iqx - a|q|/2}}{n_q} \rho_\sigma(q) \quad (6.7)$$

where  $n_q = Lq/2\pi$  is the orbital number. An ultraviolet cutoff  $a$  has been built in to regularize the momentum sum. For our purposes, it can be identified with the lattice constant of the conduction band, thus defining the bandwidth. We will set  $a = 1$  throughout his chapter. Then

$$[\Phi_\sigma(x), \partial_{x'} \Phi_\sigma(x')] = -2\pi i \delta(x - x') \quad (6.8)$$

or, put in other words,  $-\partial_x \Phi(x)$  is the momentum field canonically conjugate to  $\Phi(x)$ . Note that finite size terms  $\sim 1/L$  have been neglected here. It is easy to check that the fermionic density in real space may be written as

$$: \Psi_\sigma^\dagger(x) \Psi_\sigma(x) : = -\frac{\partial_x \Phi_\sigma(x)}{2\pi} + \mathcal{O}(1/L) \quad (6.9)$$

where

$$\Psi^\dagger(x)_\sigma = \frac{1}{L^{1/2}} \sum_k e^{-ikx} c_{\sigma k}^\dagger. \quad (6.10)$$

It was observed by von Delft and Schöller (1998) that acting with  $\Psi^\dagger(x)$  on the Fermi sea with an arbitrary number  $N$  of particles leads to a *boson coherent state*. This is the reason why the fermion creator can be written as the exponential of the Bose field:

$$\boxed{\Psi_\sigma^\dagger(x) = F_\sigma^\dagger e^{i\Phi_\sigma(x)}} \quad (6.11)$$

This equation (the *bosonization identity*) has already been simplified in that only the application to the noninteracting ground state is considered; acting on excited states would lead to an additional phase factor. The *Klein factor*  $F^\dagger$  changes the fermionic particle number by one, which cannot be achieved by the bosons.

Now we have introduced the necessary tools to bosonize the Kondo model

$$H = H_0 + H_\parallel + H_\perp \quad (6.12)$$

as first proposed by Schotte (1970) and later also applied by Schlottmann (1982), Guinea, Hakim and Muramatsu (1985) and Leggett et al. (1987). For the conduction band  $H_0$ , bosonization has already been achieved in (6.6). The longitudinal coupling is rewritten using (6.9)

$$\begin{aligned} H_\parallel &= \frac{J_\parallel}{2} S^z \left( \Psi_\uparrow^\dagger(0) \Psi_\uparrow(0) - \Psi_\downarrow^\dagger(0) \Psi_\downarrow(0) \right) \\ &\rightarrow -\frac{J_\parallel}{\sqrt{2}2\pi} \partial_x \Phi(0) S^z \end{aligned} \quad (6.13)$$

At this point the spin density operators

$$\sigma(q) \equiv \frac{1}{\sqrt{2}} (\rho_\uparrow(q) - \rho_\downarrow(q)) \quad (6.14)$$

and the corresponding bosonic field

$$\Phi(x) \equiv \frac{1}{\sqrt{2}} (\Phi_\uparrow(x) - \Phi_\downarrow(x)) \quad (6.15)$$

have been introduced. The impurity couples only to the spin degrees of freedom, therefore the charge sector of the conduction band will be omitted in the following. Using the bosonization identity (6.11), we can also rewrite the spin flip coupling:

$$\begin{aligned} H_\perp &= \frac{J_\perp}{2} \left( \Psi_\uparrow^\dagger(0) \Psi_\downarrow(0) S^- + \Psi_\downarrow^\dagger(0) \Psi_\uparrow(0) S^+ \right) \\ &\rightarrow \frac{J_\perp}{4\pi} \left( e^{i\sqrt{2}\Phi(0)} F_\uparrow^\dagger F_\downarrow S^- + e^{-i\sqrt{2}\Phi(0)} F_\downarrow^\dagger F_\uparrow S^+ \right) \end{aligned} \quad (6.16)$$

For the application of the flow equation method it is advantageous to eliminate the longitudinal term  $H_{\parallel}$  by a discrete unitary transformation

$$U = e^{i\mu S^z \Phi(0)} \quad (6.17)$$

with  $\mu$  as a free parameter. In the context of the two-channel model this is known as the Emery–Kivelson transformation (Emery and Kivelson 1992, Zarand and von Delft 2000). Notice that the conduction band is transformed according to

$$\begin{aligned} U H_0 U^\dagger &= e^{i\mu S^z \Phi(0)} \left( \frac{1}{2} \int_{-L/2}^{L/2} \frac{dx}{2\pi} : (\partial_x \Phi(x))^2 : \right) e^{-i\mu S^z \Phi(0)} \\ &= H_0 + \frac{1}{2} i \mu S^z \int \frac{dx}{2\pi} [\Phi(0), (\partial_x \Phi(x))^2] \\ &= H_0 + \mu S^z \partial_x \Phi(0) \end{aligned} \quad (6.18)$$

where a constant has been dropped. Furthermore,

$$U H_{\parallel} U^\dagger = H_{\parallel} \quad (6.19)$$

up to a constant, and

$$U H_{\perp} U^\dagger = \frac{J_{\perp}}{4\pi} \left( e^{i(\sqrt{2}-\mu)\Phi(0)} F_{\uparrow}^\dagger F_{\downarrow} S^- + e^{-i(\sqrt{2}-\mu)\Phi(0)} F_{\downarrow}^\dagger F_{\uparrow} S^+ \right). \quad (6.20)$$

With the choice

$$\mu = \frac{J_{\parallel}}{2\sqrt{\pi}} \quad (6.21)$$

we therefore arrive at the transformed Hamiltonian

$$\boxed{U H U^\dagger = H_0 + g_0 (V(\lambda_0, 0) \sigma^- + V(-\lambda_0, 0) \sigma^+)} \quad (6.22)$$

where a new notation has been introduced. First, the Klein factors have been absorbed into redefined spin operators

$$\sigma^{-(+)} = F_{\uparrow(\downarrow)}^\dagger F_{\downarrow(\uparrow)} S^{-(+)} \quad , \quad \sigma^z = S^z \quad (6.23)$$

obeying the usual commutator algebra. These new spins are coupled to generalized fermions, usually referred to as *vertex operators*:

$$V(\lambda, x) = e^{i\lambda\Phi(x)}. \quad (6.24)$$

If the *scaling dimension* takes the special value  $\lambda = 1$ , this expression reduces to the right-hand side of the bosonization identity (6.11) and – apart from the missing Klein

factor  $-$  can be interpreted as a fermionic creation operator. Similarly,  $V(-1, x)$  represents an annihilator. For general values of  $\lambda$ , the vertex operators are complicated many-body objects that have no simple equivalent in fermionic language. These properties can be summarized in a concise form by the operator product expansion (OPE)

$$\{V(\lambda, x), V(-\lambda, y)\} = \left( \frac{1}{[i(x-y) + a]^{\lambda^2}} + \frac{1}{[i(y-x) + a]^{\lambda^2}} \right) \times (1 + i\lambda(x-y)\partial_x\Phi(x) + \dots) \quad (6.25)$$

which may be derived by normal ordering (von Delft and Schöller 1998). In spite of  $a = 1$ , we have shown the cutoff explicitly at this point. Higher terms in this series are suppressed by increasing powers of the distance  $x - y$ . In particular, for  $\lambda = 1$  the right-hand side is proportional to a delta function and one obtains the usual fermionic anticommutation relations.

The parameters of the bosonized Kondo Hamiltonian are related to the initial couplings via

$$g_0 = \frac{J_{\perp}}{4\pi} \quad , \quad \lambda_0 = \sqrt{2} - \frac{J_{\parallel}}{\sqrt{2}2\pi} \quad (6.26)$$

One special case is the *decoupling point* (following the terminology of Kotliar and Si (1996)) where the scaling dimension vanishes

$$H_{T_2} = H_0 + g_0 (\sigma^- + \sigma^+) \quad (6.27)$$

and the system is trivial, exhibiting free spin precession. This limit is equivalent to the spin-boson model without dissipation. More relevant for our analysis is the *Toulouse point*, where

$$\lambda_0 = 1 \quad (6.28)$$

and the Hamiltonian can be mapped on a noninteracting resonant level model (an Anderson impurity model without spin). This situation corresponds to a large  $J_{\parallel}$  comparable to the bandwidth while the spin flip coupling  $J_{\perp}$  can still assume arbitrary values. It should be small, however, to ensure that no excitations close to the band edges are generated which would invalidate bosonization (see (6.4)). Without going into details at this moment, we just mention that the impurity physics at the Toulouse point can be calculated exactly. At low temperatures the impurity spin forms a singlet with the conduction band and the Kondo temperature is simply given by the Anderson width  $T_K \sim g_0^2$  of the resonant level.

### 6.3 Flow equations

For general parameters, (6.22) is a nontrivial many-body problem due to the vertex operators with noninteger scaling dimension  $\lambda$ . Motivated by the recent calculation

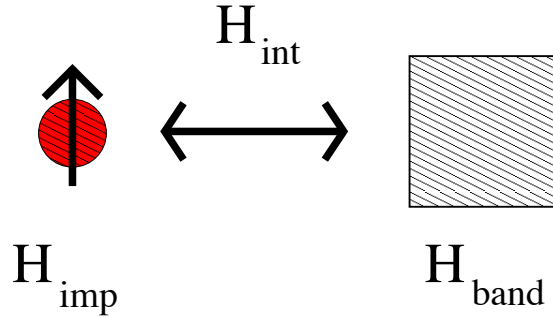


**Figure 6.2:** Quantum mechanical system (impurity) coupled to an environment (the conduction electrons) by an interaction (the Kondo coupling). By means of a unitary transformation,  $H_{\text{int}}$  is eliminated.

of Kehrein (1999) for the quantum sine–Gordon model, we now apply Wegner’s flow equation method to diagonalize the Hamiltonian. A series of infinitesimal unitary transformations

$$\partial_t H = [\eta, H] \quad (6.29)$$

is performed so that the impurity and the conduction band are gradually decoupled (see fig. 6.2). In the course of the flow, the structure of the interaction will change and new terms will appear. We therefore introduce a position dependence of the coupling

$$H_{\text{int}} = \int dx g(x) (V(\lambda, x) \sigma^- + V(-\lambda, x) \sigma^+) \quad (6.30)$$

where initially

$$g(x) \Big|_{t=0} = g_0 \delta(x) \quad (6.31)$$

In the momentum space representation we obtain

$$\begin{aligned} g(x) &= \frac{1}{\sqrt{L}} \sum_p g_p e^{-ipx} \\ V(\lambda, p) &= \frac{1}{L} \int dx e^{-ipx} V(\lambda, x) \end{aligned} \quad (6.32)$$

so that

$$H_{\text{int}} = \sum_p g_p (V(\lambda, p) \sigma^- + V(-\lambda, p) \sigma^+) . \quad (6.33)$$

Following Wegner, we define the generator as

$$\eta^{(1)} = [H_0, H_{\text{int}}] = - \sum_p p g_p (V(\lambda, p) \sigma^- + V(-\lambda, p) \sigma^+) \quad (6.34)$$

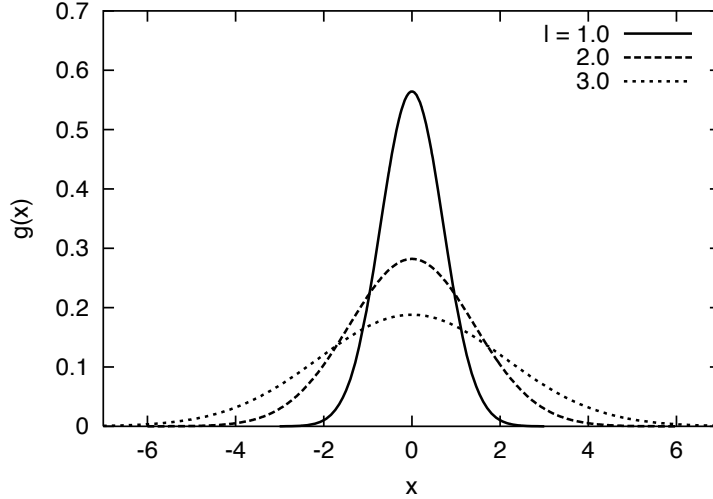


**Figure 6.3:** Diffusion of the Kondo coupling in real space. The resulting position dependence of the coupling is shown for different values of the flow parameter.

which leads to decreasing Kondo couplings. In the derivation we have used the basic commutator

$$[H_0, V(\lambda, p)] = -p V(\lambda, p). \quad (6.35)$$

Note that, by definition,  $V(\lambda, p)$  corresponds to a creator of momentum  $-p$  if  $\lambda > 0$  and to an annihilator of momentum  $p$  otherwise. The choice (6.34) gives the main contribution to the flow, although we will later introduce a second generator part  $\eta^{(2)}$  in order to keep the structure of the Hamiltonian as simple as possible. The leading behaviour is obtained by just transforming the conduction band:

$$[\eta^{(1)}, H_0] = - \sum_p p^2 g_p (V(\lambda, p) \sigma^- + V(-\lambda, p) \sigma^+). \quad (6.36)$$

It corresponds to an exponential decay of the couplings

$$\partial_l g_p = -p^2 g_p \quad (6.37)$$

or, equivalently, diffusion of  $g(x)$  in real space (see fig. 6.3). Of course, no intrinsic low energy scale appears in this decay. To capture the Kondo effect we therefore need to go beyond (6.36). For the evaluation of further terms in the flow, we employ the following generalized fermionic anticommutation relations

$$\begin{aligned} \{V(\lambda, p), V(-\lambda, -q)\} &= \delta_{pq} \frac{2\pi}{\Gamma(\lambda^2)} |p|^{\lambda^2-1} \\ \{V(\lambda, p), V(\lambda, q)\} &= 0 \end{aligned} \quad (6.38)$$

which are valid in the leading order of the OPE. Now we can take the interaction part into account, neglecting products of operators with equal scaling dimensions:

$$\begin{aligned}
[\eta^{(1)}, H_{\text{int}}] &= \tag{6.39} \\
&= \sum_{pq} (-p g_p) g_q [V(\lambda, p) \sigma^- + V(-\lambda, p) \sigma^+, V(\lambda, q) \sigma^- + V(-\lambda, q) \sigma^+] \\
&= - \sum_{pq} (p - q) g_p g_q \left( \frac{1}{2} [V(\lambda, p), V(-\lambda, q)] - \sigma^z \{V(\lambda, p), V(-\lambda, q)\} \right).
\end{aligned}$$

The first term is a potential scattering contribution, which will (in parts) remain finite in the limit  $l \rightarrow \infty$  and lead to impurity effects. The second term has a new structure, describing the coupling of the impurity to *two* band fermions. Within our approximation scheme – the operator product expansion – it can, however, be simplified. This is most easily seen by switching to the real space representation

$$\begin{aligned}
H_{\text{new}}^{(1)} &= \sum_{pq} (p - q) g_p g_q \{V(\lambda, p), V(-\lambda, q)\} \sigma^z \\
&= i \iint dx dy [(\partial_x - \partial_y) g(x) g(y)] \{V(\lambda, x), V(-\lambda, y)\} \sigma^z \tag{6.40}
\end{aligned}$$

and remembering that we can evaluate the anticommutator of two vertex operators by the OPE (6.25). Due to the antisymmetric integration measure in (6.40), the leading term drops out and we are left with the subdominant contribution

$$H_{\text{new}}^{(1)} = \int dx f(x) \sigma^z \partial_x \Phi(x) \tag{6.41}$$

where the coupling function  $f$  is determined by

$$\begin{aligned}
\partial_l f(x) &= -\lambda \int dy [(\partial_x - \partial_y) g(x) g(y)] (x - y) \\
&\times \left( \frac{1}{[i(x - y) + 1]^{\lambda^2}} + \frac{1}{[i(y - x) + 1]^{\lambda^2}} \right). \tag{6.42}
\end{aligned}$$

We notice that – apart from the position dependence – the new term  $H_{\text{new}}^{(1)}$  is equivalent to the longitudinal exchange in the original Hamiltonian. In order to eliminate it, we apply a two-step procedure:

- First,  $H_{\text{new}}^{(1)}$  is generated infinitesimally by integrating the flow from  $l$  to  $l + dl$ .
- Next, we perform an infinitesimal Emery–Kivelson transformation

$$U = \exp \left\{ i \int dx r(x) \Phi(x) \sigma^z \right\} \tag{6.43}$$

like in the initial setup of the Hamiltonian.

The transformation  $U$  leaves  $H_{\text{new}}^{(1)}$  invariant in the leading order. The conduction band is modified according to

$$U H_0 U^\dagger = H_0 + \sigma^z \int dx r(x) \partial_x \Phi(x) \quad (6.44)$$

so that with the choice

$$\partial_l r(x) = -\partial_l f(x) \quad (6.45)$$

the new term (6.41) is compensated. Again, the unitary transformation leads to a change in the scaling dimension. Assuming that  $g(x)$  and therefore also  $f(x)$  is localized, we can extract the leading effect in a *short-distance expansion*

$$\begin{aligned} UV(\lambda, y)U^\dagger &= V(\lambda, y) \sigma^- + i \int dx r(x) [\Phi(x) \sigma^z, V(\lambda, y) \sigma^-] + O(r^2) \\ &\approx V(\lambda, y) \sigma^- + \left( i \int dx r(x) \right) \Phi(y) V(\lambda, y) (-\sigma^-) \\ &= V(\lambda, y) \sigma^- + i d\lambda \Phi(y) V(\lambda, y) \sigma^- \\ &= \sigma^- V(\lambda + d\lambda, y) \end{aligned} \quad (6.46)$$

where

$$d\lambda = dl \int dx \partial_l f(x) \quad (6.47)$$

has been defined. No renormalization of the coupling occurs so far. We have to take into account, though, that the assumption of localization is only valid on the length scale

$$d_{\text{eff}} = \sqrt{l} \quad (6.48)$$

because the more rapidly varying modes  $g_p$  have already been integrated out. We therefore separate the bosonic field into a “fast” and a “slow” part

$$V(\lambda, x) = e^{i\lambda\Phi_{\text{slow}}(x)} e^{i\lambda\Phi_{\text{fast}}(x)} \quad (6.49)$$

where

$$\begin{aligned} \Phi_{\text{slow}}(x) &= -i \sum_{|k| < \frac{1}{\sqrt{l}}} \frac{e^{-ikx - |k|/2}}{n_k} \sigma(k) \\ &\approx -i \sum_{k \neq 0} \frac{e^{-ikx - \sqrt{l}k/2}}{n_k} \sigma(k) \end{aligned} \quad (6.50)$$

is obtained by summing up only the slow modes and  $\Phi_{\text{fast}}$  contains the rest. In particular, upon normal ordering of the vertex operators, the two fields give different

contributions:

$$\begin{aligned} : e^{i\lambda\Phi_{\text{slow}}} : &= \left( \frac{L}{2\pi\sqrt{l}} \right)^{\lambda^2/2} e^{i\lambda\Phi_{\text{slow}}} \\ : e^{i\lambda\Phi_{\text{fast}}} : &= \sqrt{l}^{\lambda^2/2} e^{i\lambda\Phi_{\text{fast}}}. \end{aligned} \quad (6.51)$$

Now the important point is that in (6.46) only the scaling dimension corresponding to  $\Phi_{\text{slow}}$  is modified:

$$U \sigma^- V(\lambda, y) U^\dagger = \sigma^- e^{i(\lambda+d\lambda)\Phi_{\text{slow}}} e^{i\lambda\Phi_{\text{fast}}}. \quad (6.52)$$

To avoid an explicit  $k$ -dependence of the scaling dimension, we approximate this expression by a vertex operator with one single scaling dimension, but with a renormalization factor  $\beta$  chosen in such a way that the vacuum expectation values are equal:

$$\langle e^{i(\lambda+d\lambda)\Phi_{\text{slow}}} e^{i\lambda\Phi_{\text{fast}}} \rangle = \langle \beta e^{i(\lambda+d\lambda)\Phi} \rangle. \quad (6.53)$$

From the normal ordering contributions (6.51) one easily obtains

$$\beta = \sqrt{l}^{\lambda d\lambda} \quad (6.54)$$

and the coupling constant is therefore replaced by a *running coupling*

$$g \rightarrow g \sqrt{l}^{\lambda d\lambda}. \quad (6.55)$$

To proceed further we have to evaluate the flow of  $\lambda$ . First we define

$$q_\lambda(x) = [ix + 1]^{-\lambda^2} + [-ix + 1]^{-\lambda^2}. \quad (6.56)$$

From (6.47) and the definition (6.42) we obtain

$$\begin{aligned} \partial_l \lambda^2 &= -2\lambda^2 \iint dx dy [(\partial_x - \partial_y) g(x) g(y)] (x - y) q_\lambda(x - y) \\ &= \frac{8\pi\lambda^2(1 - \lambda^2)}{\Gamma(\lambda^2)} \sum_p g_p g_{-p} |p|^{\lambda^2-1}. \end{aligned} \quad (6.57)$$

Let us now consider the second new interaction generated by the flow (6.39), the *potential scattering term*:

$$\partial_l H_{\text{new}}^{(2)} = -\frac{1}{2} \sum_{pq} (p - q) g_p g_q (V(\lambda, p) V(-\lambda, q) + V(-\lambda, p) V(\lambda, q)). \quad (6.58)$$

For a generic value of the scaling dimension, the Vertex operators are nontrivial interaction terms, although (6.35) suggests a single particle interpretation. Motivated by the generalized anticommutation relations (6.38) we define *normalized Vertex operators* in the following way

$$\boxed{C_p^\dagger = \alpha_p^{-1} V(\lambda, -p) \quad , \quad C_p = \alpha_p^{-1} V(-\lambda, p)} \quad (6.59)$$

where

$$\alpha_p^2 = \frac{2\pi}{\Gamma(\lambda^2)} |p|^{\lambda^2-1}. \quad (6.60)$$

In the leading order of the OPE, the new operators behave like fermions

$$\{C_p^\dagger, C_q\} = \delta_{pq} \quad , \quad \{C_p^\dagger, C_q^\dagger\} = \{C_p, C_q\} = 0 \quad (6.61)$$

In this representation, the potential scattering term has the form

$$H_{\text{new}}^{(2)} = \sum_{pq} s_{pq} (C_p^\dagger C_q - C_p C_q^\dagger) \quad (6.62)$$

and its flow-induced change is given by

$$\partial_t H_{\text{new}}^{(2)} = \frac{1}{2} \sum_{pq} (p+q) g_p g_q \alpha_p \alpha_q (C_p^\dagger C_q - C_p C_q^\dagger). \quad (6.63)$$

It is convenient – although by no means essential – to suppress the generation of non-diagonal terms with  $p \neq q$ . In particular, this reduces the number of coupled differential equations to be solved and thus simplifies the numerical evaluation. Therefore we introduce a second generator part

$$\eta^{(2)} = \sum_{pq} \eta_{pq}^{(2)} (C_p^\dagger C_q - C_q C_p^\dagger) \quad (6.64)$$

with real and antisymmetric coefficients

$$\eta_{pq}^{(2)} = -\eta_{qp}^{(2)} \quad (6.65)$$

which will be chosen in such a way that only diagonal terms in (6.63) survive. To calculate the full flow,  $\eta^{(2)}$  has to be commuted with every term in the Hamiltonian. Several new contributions arise:

$$[\eta^{(2)}, H_0] = - \sum_{pq} \eta_{pq}^{(2)} (p-q) (C_p^\dagger C_q + C_q^\dagger C_p) \quad (6.66)$$

$$[\eta^{(2)}, H_{\text{int}}] = 2 \sum_{pq} \frac{\alpha_q}{\alpha_p} \eta_{pq}^{(2)} g_q (V(\lambda, p) \sigma^- + V(-\lambda, p) \sigma^+). \quad (6.67)$$

In deriving the last identity, the following symmetry property has been used:

$$\eta_{-p-q}^{(2)} = \eta_{pq}^{(2)}. \quad (6.68)$$

Note that the Kondo interaction is still written in terms of the *unnormalized* vertex operators – this ensures that we can keep track of the flow of the scaling dimension, which is essential for the calculation presented here.

Finally, we have to consider the effect of the potential scattering term (6.62) on the flow. We first calculate the commutator with the main generator part

$$\begin{aligned} [\eta^{(1)}, H_{\text{new}}^{(2)}] &= - \sum_p p g_p \sum_{qr} s_{qr} [V(\lambda, p) \sigma^- + V(-\lambda, p) \sigma^+, C_q^\dagger C_r - C_q C_r^\dagger] \\ &= - \sum_{pq} 2p \left( \frac{\alpha_p}{\alpha_q} \right) g_p s_{pq} (V(\lambda, q) \sigma^- + V(-\lambda, q) \sigma^+). \end{aligned} \quad (6.69)$$

which contributes to the Kondo coupling flow. Notice that the  $\alpha$ -dependent prefactor does not arise once the offdiagonal potential scattering has been eliminated. Furthermore,

$$[\eta^{(2)}, H_{\text{new}}^{(2)}] = \sum_{pq} 2 \eta_{pq}^{(2)} (C_p^\dagger C_q + C_q^\dagger C_p) (s_{qq} - s_{pp}) \quad (6.70)$$

where another symmetry property

$$\eta_{pq}^{(2)} = -\eta_{qp}^{(2)} \quad (6.71)$$

has been used. Using (6.70), (6.63) and (6.66), we can now give a definition for  $\eta^{(2)}$  that ensures the elimination of offdiagonal potential scattering terms:

$$\eta_{pq}^{(2)} = \frac{1}{2} \frac{(p+q) g_p g_q}{p-q+2(s_{pp}-s_{qq})} \alpha_p \alpha_q. \quad (6.72)$$

What has been achieved up to now? Within our approximation (truncation of the OPE after the first nonvanishing order) we have obtained the following closed system of flow equations:

$$\begin{aligned} \partial_t g_p &= -p^2 g_p + g \ln \sqrt{l} \lambda \partial_t \lambda + 2 \sum_q \frac{\alpha_q}{\alpha_p} \eta_{pq}^{(2)} g_q - 2p g_p s_{pp} \\ \partial_t \lambda^2 &= \frac{8\pi \lambda^2 (1-\lambda^2)}{\Gamma(\lambda^2)} \sum_p g_p g_{-p} |p|^{\lambda^2-1} \\ \partial_t s_{pp} &= p g_p^2 \alpha_p^2 \end{aligned} \quad (6.73)$$

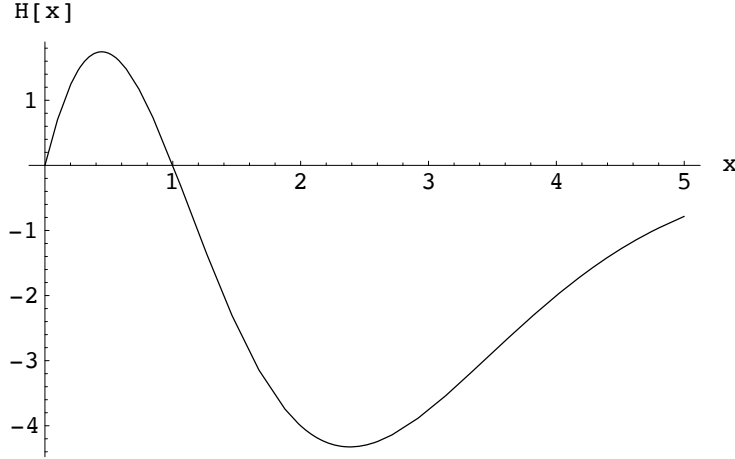


**Figure 6.4:** Beta function of the flow.

for an extended Hamiltonian including potential scattering

$$H(l) = H_0 + \sum_p g_p (V(\lambda, p) \sigma^- + V(-\lambda, p) \sigma^+) + 2 \sum_p s_{pp} C_p^\dagger C_p \quad (6.74)$$

It is now straightforward to discretize the momentum  $k$  and solve the flow equations numerically. A complete analytical solution of (6.73) is difficult due to the momentum dependence of the couplings. However, not too close to the strong coupling fixed point one may assume that potential scattering is irrelevant and that the main  $p$  dependence in the couplings is given by the exponential decay (6.37). In the next section we show that an analytical evaluation is then possible which already illustrates the main features of the flow and furthermore yields the Kondo temperature.

## 6.4 Approximate evaluation

To get a qualitative understanding of the physics contained in (6.73) we neglect potential scattering and approximate the coupling flow as

$$\partial_l g_p = -p^2 g_p + g_p \ln \sqrt{l} \lambda \partial_l \lambda. \quad (6.75)$$

The remaining momentum dependence – the exponential decay – is trivially taken into account by defining a *running coupling* via

$$g_p(l) = e^{-p^2 l} \tilde{g}(l). \quad (6.76)$$

One can then perform the momentum sum for  $\partial_l \lambda^2$  and arrives at a set of two coupled differential equations

$$\partial_l \tilde{g}(l) = \frac{1}{4} \tilde{g} \ln(l) \partial_l \lambda^2 \quad (6.77)$$

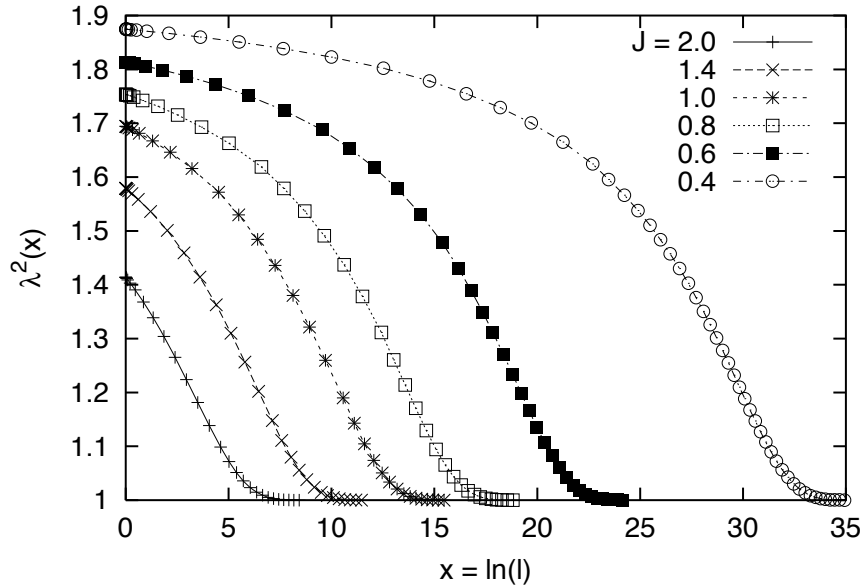


**Figure 6.5:** Flow of the scaling dimension towards the Toulouse point. We consider the symmetric antiferromagnetic Hamiltonian with  $J_{\perp} = J_{\parallel} = J$ .

$$\partial_l \lambda^2 = L H(\lambda^2) l^{-\lambda^2/2} \tilde{g}^2(l) \quad (6.78)$$

where a *beta function*

$$H(\lambda^2) \equiv \frac{2^{2-\lambda^2/2} \lambda^2 (1 - \lambda^2) \Gamma\left(\frac{\lambda^2}{2}\right)}{\Gamma(\lambda^2)} \quad (6.79)$$

has been defined which is plotted in fig. 6.4. Remarkably, it has a zero at  $\lambda^2 = 1$  corresponding to a stable fixed point, which is precisely the Toulouse limit discussed previously. In the course of the flow, the transformed Hamiltonian will therefore always approach this exactly solvable point. In fig. 6.5, the flow of the scaling dimension is plotted for several initial parameters. Defining a logarithmic measure for the flow parameter

$$x \equiv \ln l \quad (6.80)$$

the running coupling can be formally integrated:

$$\tilde{g}(x) = \tilde{g}_0 \exp \left\{ \frac{1}{4} \lambda^2(x) x - \frac{1}{4} \int_0^x dx' \lambda^2(x') \right\}. \quad (6.81)$$

For weak antiferromagnetic couplings, the scaling dimension is always decreasing (see fig. 6.5) and therefore  $\tilde{g}$  will be renormalized to a smaller value. The renormalization stops when  $\lambda^2$  has reached its fixed point value. Examples for the behaviour of the

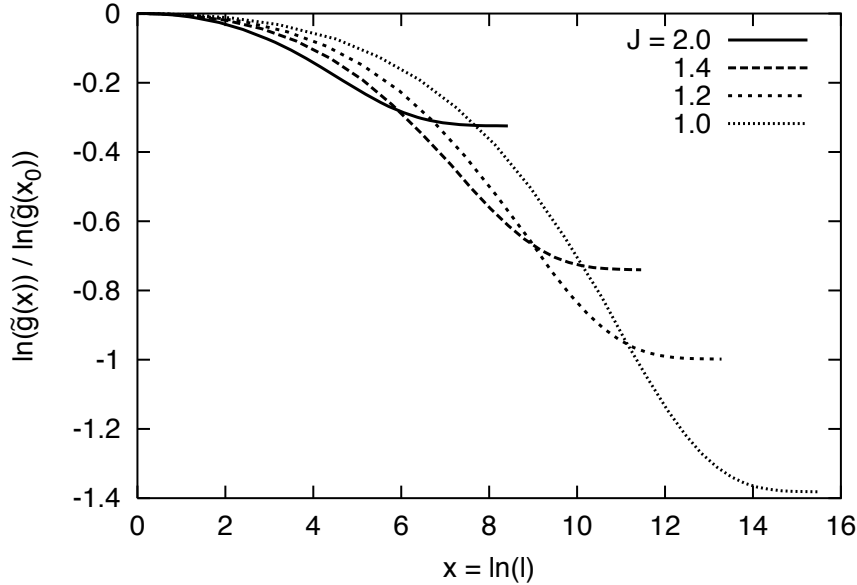


**Figure 6.6:** Renormalization of the running coupling constant in the symmetric case  $J_{\perp} = J_{\parallel} = J$ . The initial value  $x_0$  of the logarithmic flow parameter is determined by the bandwidth and set equal to unity in the present calculation.

running coupling are shown in fig. 6.6. A very instructive reformulation of (6.77) and (6.78) is possible by introducing new coupling functions

$$v(x) \equiv \sqrt{L} \tilde{g}_0 \exp \left\{ \frac{1}{2} x - \frac{1}{4} \int_0^x dx' \lambda^2(x') \right\} \quad (6.82)$$

$$u(x) \equiv \frac{1}{2} \left( 1 - \frac{\lambda^2(x)}{2} \right) \quad (6.83)$$

with initial values  $v(0) = J_{\perp}/4\pi$  and  $u(0) = J_{\parallel}/4\pi + \mathcal{O}(J_{\parallel}^2)$ . The flow equations then take the form

$$\begin{aligned} \partial_x u(x) &= -\frac{1}{4} H(\lambda^2(x)) v^2(x) \xrightarrow{\lambda^2 \rightarrow 2} v^2(x) \\ \partial_x v(x) &= u(x) v(x). \end{aligned} \quad (6.84)$$

In the limit of small coupling  $J$  and as long as  $\lambda^2 \rightarrow 2$ , they are equivalent to the scaling equations derived by Anderson (1970). We thus recover the well-known Kosterlitz–Thouless phase diagram (fig. 6.7). But obviously, deviations arise as soon as  $\lambda^2$  starts to flow. The most important advantage of the flow equation solution is that the *strong coupling divergence* typical of scaling approaches *does not occur here*. The effective Hamiltonian derived in the limit  $l \rightarrow \infty$  (in the simplified treatment this is a Toulouse model) has finite renormalized parameters (see fig. 6.6).

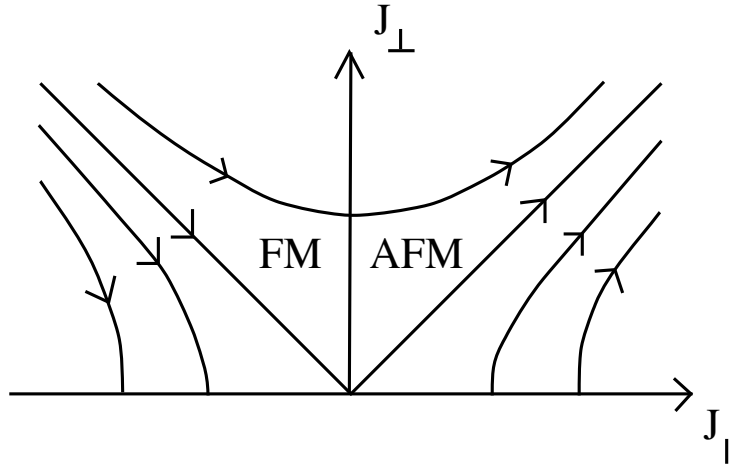


Figure 6.7: Phase diagram of the Kondo model.

## 6.5 Kondo scale

From the approximate solution in the preceding chapter we can already extract the characteristic low energy scale of the problem, the Kondo temperature. To do this, we note that the  $l \rightarrow \infty$  fixed point of the flow is the Toulouse Hamiltonian equivalent to a noninteracting resonant level model. For the latter, the low energy scale is simply given by the *Anderson width* of the resonant level and therefore

$$T_K \sim \tilde{g}(\infty)^2. \quad (6.85)$$

One only needs to insert the value for the renormalized coupling which can be determined by solving (6.84) with *Mathematica*. Two cases are of particular interest:

- variation of  $J_{\perp}$  at constant  $J_{\parallel}$ , corresponding to a fixed dissipation strength  $\alpha = (1 - J_{\parallel}/4\pi)^2$  in the ohmic spin boson model. In the limit  $J_{\perp} \rightarrow 0$  we obtain the power law

$$T_K \sim J^{\frac{1}{1-\alpha}} \quad (6.86)$$

consistent with scaling results for the renormalized tunneling amplitude (Leggett et al. 1987).

- the *symmetric* Kondo model  $J_{\perp} = J_{\parallel} = J$ . For small coupling, the low energy scale is given by

$$T_K \sim J^{\tau} \exp\left\{-\frac{2\pi}{J}\right\} \quad (6.87)$$

with an exponent  $\tau \approx 0.30$ . While the leading exponential dependence is consistent with NRG and scaling results (Wilson 1975), the prefactor deviates

from the expected  $\tau = 1/2$ . Possible reasons for this discrepancy are either the neglected higher-order OPE terms, or the different cutoff schemes in the fermionic and bosonized models. A similar deviation occurs in the flow equation solution for the quantum sine-Gordon model; note however that in this case the correction is much smaller (Kehrein 1999).

## 6.6 Calculation of observables

So far our objective has been diagonalization of the Hamiltonian, leading to thermodynamic properties like the Kondo scale. Very often, however, one is also interested in calculating expectation values and correlation functions of an *observable*  $\hat{O}$  (an additional hermitean operator which need not commute with  $H$ ). In fact, the screening of the local moment due to the Kondo effect is best seen in the dynamical spin-spin correlation function of the impurity. As it is very difficult to obtain zero temperature dynamical properties of correlated systems by other methods, we will now discuss in detail how this can be achieved with flow equations.

The idea is to evaluate general matrix elements  $\langle m | \hat{O} | n \rangle$  in the representation where  $H(l)$  is diagonal, i.e. at  $l = \infty$ . In order to do this, one needs to perform on  $\hat{O}$  the same sequence of unitary transformations as on the Hamiltonian. An additional set of flow equations is therefore defined by

$$\partial_l \hat{O} = [\eta, \hat{O}]. \quad (6.88)$$

Like equation (6.29) for the Hamiltonian, this cannot be solved exactly and truncations are necessary. Once more our criterion to assess the importance of interaction terms will be the OPE; the resulting approximations again become exact at the Toulouse point. This is in contrast to the Luttinger model calculation presented in section 5.1 where only the Hamiltonian flow closes in the bosonization limit. In the following, we focus on the  $z$ -component of the local spin

$$\hat{O} \equiv \sigma^z. \quad (6.89)$$

Instead of directly calculating the transformation of  $\sigma^z$ , it is convenient to use the representation

$$\sigma^z = \frac{1}{2} [\sigma^+, \sigma^-] \quad (6.90)$$

and consider  $\sigma^+(l)$ . For the additional terms generated by the flow we make the following *ansatz*

$$\sigma^+(l) = h(l) \sigma^+ + \sigma^z \sum_p a_p C_p^\dagger. \quad (6.91)$$

Each of the two generator parts then gives a contribution to the flow:

$$\begin{aligned}
[\eta^{(1)}, \sigma^+(l)] &= - \sum_p p g_p h(l) [V(\lambda, p) \sigma^- + V(-\lambda, p) \sigma^+, \sigma^+] \\
&\quad - \sum_{pq} p g_p a_q [V(\lambda, p) \sigma^- + V(-\lambda, p) \sigma^+, C_q^\dagger \sigma^z] \\
&= -2 \sum_p p g_p \alpha_p h(l) C_p^\dagger \sigma^z + \frac{1}{2} \sum_p p g_p a_p \alpha_p \sigma^+ \tag{6.92}
\end{aligned}$$

$$\begin{aligned}
[\eta^{(2)}, \sigma^+(l)] &= \sum_{pqr} \eta_{pq}^{(2)} a_r [C_p^\dagger C_q - C_q C_p^\dagger, \sigma^z C_r^\dagger] \\
&= 2 \sigma^z \sum_{pq} \eta_{pq}^{(2)} a_q C_p^\dagger \tag{6.93}
\end{aligned}$$

In deriving these identities, we have again used the fermionic anticommutation relations (6.61) of the  $C$ 's which are valid in the leading order of the OPE. The flow equations for the observable can now be written in closed form:

$$\begin{aligned}
\partial_l h(l) &= \frac{1}{2} \sum_p p \alpha_p a_p g_p \\
\partial_l a_p &= -2 p g_p \alpha_p h(l) + 2 \sum_q \eta_{pq}^{(2)} a_q
\end{aligned}$$

(6.94)

In general, they have to be evaluated numerically because no simple approximation of the momentum dependence is possible. However, multiplying the second equation by  $a_p$ , summing over  $p$  and using the antisymmetry  $\eta_{pq}^{(2)} = -\eta_{qp}^{(2)}$ , the following sum rule is easily established (Wegner 1999)

$$1 = h^2 + \frac{1}{4} \sum_p a_p^2 \tag{6.95}$$

which is equivalent to the normalization of the spectral function (see below). From the numerical solution shown in fig. 6.8 one can also see that the observable decays completely in the thermodynamic limit, i.e.  $\lim_{l \rightarrow \infty} h(l) = 0$ . This is a necessary condition for Kondo screening, because in the final Hamiltonian  $H(\infty)$  the impurity is decoupled from the bath. If  $\hat{O}(l = \infty)$  still contained part of the local moment, the impurity susceptibility would diverge. Similar observations have been made for dissipative quantum systems by Kehrein and Mielke (1997).

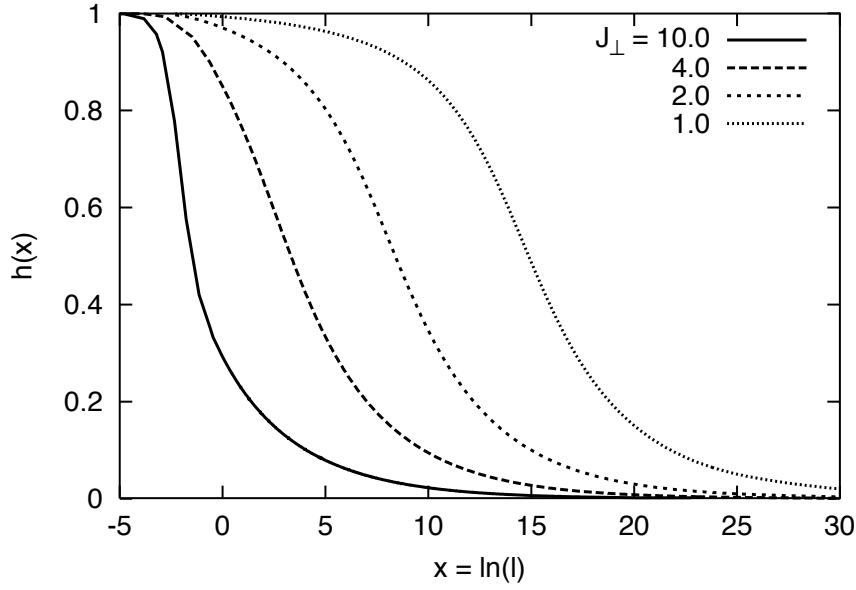


**Figure 6.8:** Decay of the observable in the course of the flow. The longitudinal coupling is chosen as  $J_{\parallel} = 1.0$ .

## 6.7 Dynamical susceptibility

After solving the flow of  $\sigma^+(l)$  we now calculate the zero temperature dynamical susceptibility as the response of the system to a local magnetic field:

$$\chi(t) = i \theta(t) \langle [\sigma^z(t), \sigma^z(0)] \rangle. \quad (6.96)$$

Here  $\langle \rangle$  denotes a ground state expectation value. Inserting a complete set of eigenstates, the imaginary part is given by

$$\chi''(\omega) = \pi \sum_m |\langle 0 | \sigma^z | m \rangle|^2 (\delta(\omega - E_m + E_0) - \delta(\omega + E_m - E_0)). \quad (6.97)$$

This expression is easily analyzed because the final Hamiltonian is diagonal

$$H(l = \infty) = H_0 + \mathcal{O}(1/N) \quad (6.98)$$

where the corrections to the dispersion can be omitted if one is only interested in the leading  $\mathcal{O}(1)$  term of the susceptibility. Using relation (6.90), we write the observable as

$$\sigma^z(l) = h^2 \sigma^z - \frac{\hbar}{2} \sum_p a_p (C_p^\dagger \sigma^- + C_p \sigma^+) + \frac{1}{8} \sum_{pq} a_p a_q (C_p^\dagger C_q - C_q C_p^\dagger). \quad (6.99)$$

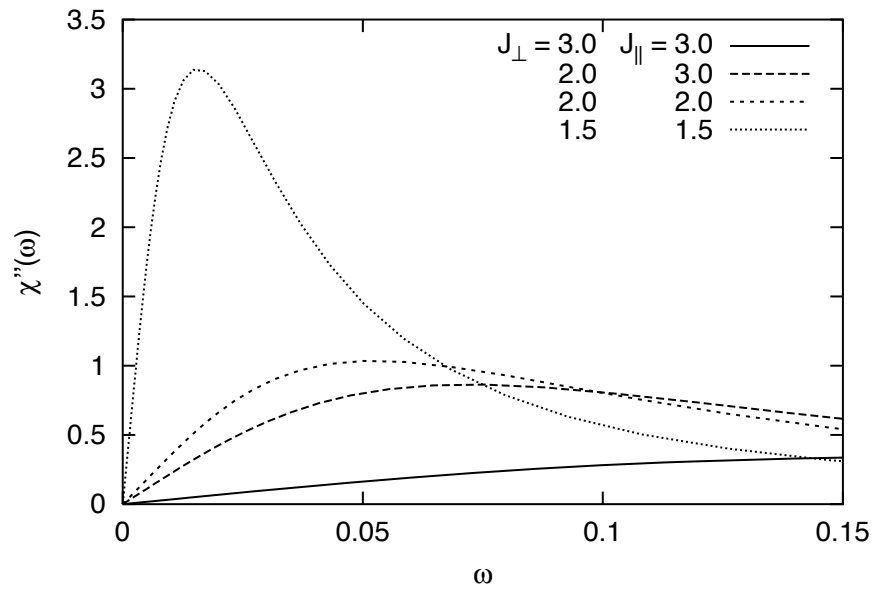


**Figure 6.9:** *Imaginary part of the dynamical impurity susceptibility.*

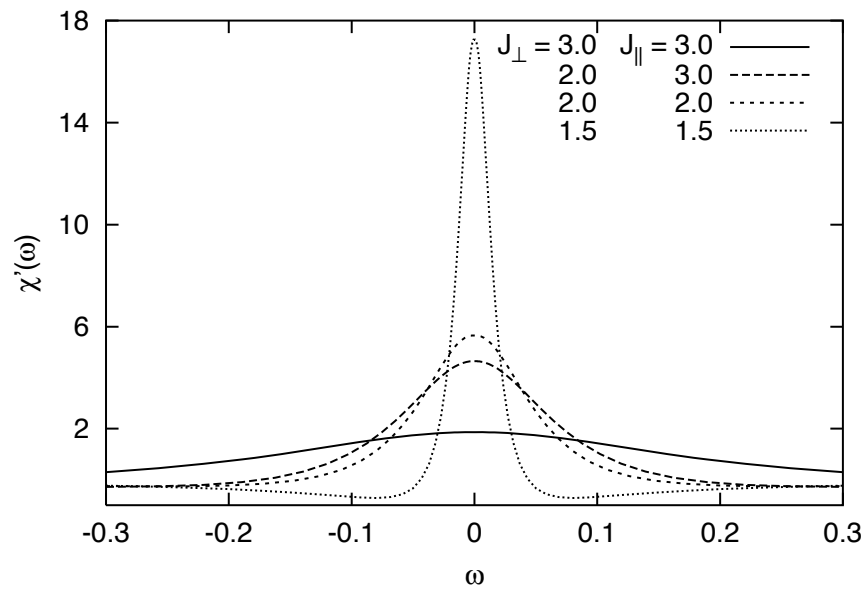


**Figure 6.10:** *Real part obtained by Kramers–Kronig transformation.*

In the thermodynamic limit, only the last term, which is of the potential scattering type, will survive for  $l \rightarrow \infty$ . In the following, we use the generalized fermionic anti-commutation relations (6.61) in order to evaluate matrix elements of (6.99) between noninteracting eigenstates. As the ground state of  $H_0$  is doubly degenerate due to the free impurity, we choose

$$|GS\rangle = |\uparrow 0\rangle \quad (6.100)$$

where the 0 indicates the Fermi sea of the conduction electrons. Then

$$\langle \uparrow 0 | h^2 \sigma^z | \uparrow 0 \rangle = \frac{h^2}{2} \quad (6.101)$$

and

$$\langle 0 \uparrow | \frac{h}{2} \sigma^+ a_p C_p | \downarrow p \rangle = \frac{h}{2} a_p \quad (6.102)$$

give the contributions of the first two terms in (6.99). The remaining quadratic part can still be simplified:

$$\frac{1}{8} \sum_{pq} a_p a_q (C_p^\dagger C_q - C_q C_p^\dagger) = \frac{1}{4} \sum_{p \neq q} a_p a_q C_p^\dagger C_q + \frac{1}{8} \sum_p a_p^2 (2 C_p^\dagger C_p - 1). \quad (6.103)$$

Note that the ground state expectation value of the diagonal part vanishes at half filling

$$\langle 0 | \sum_p a_p^2 (2 C_p^\dagger C_p - 1) | 0 \rangle = 0 \quad (6.104)$$

and moreover

$$\langle 0 | C_p^\dagger C_q | \bar{p}q \rangle = 1 \quad (p < 0, q > 0). \quad (6.105)$$

In the last equation,  $\bar{p}$  denotes a hole and similarly  $q$  a particle excitation. The spectral function can now be calculated

$$\begin{aligned} \chi''(\omega) &= \frac{\pi}{4} h^2 \sum_{p>0} a_p^2 (\delta(\omega - \epsilon_p) - \delta(\omega + \epsilon_p)) \\ &\quad + \frac{\pi}{16} \sum_{p,q>0} a_p^2 a_q^2 (\delta(\omega - \epsilon_p - \epsilon_q) - \delta(\omega + \epsilon_p + \epsilon_q)) \end{aligned} \quad (6.106)$$

where the  $\epsilon_p$  are simply the one-particle energies of the conduction band.

Results are shown in fig. 6.9. The curves display a broad maximum at an energy of the order of the Kondo scale and a power law decay

$$\chi''(\omega) \sim \omega^{-(3-2\alpha)} \quad (6.107)$$

at high frequencies, consistent with results obtained for the ohmic spin-boson model (see for example (Costi and Kieffer 1996) and (Costi 1998)). Here, the dissipation

parameter is given by  $\alpha = (1 - J_{\parallel}/4\pi)^2$  as before. Note that the antiferromagnetic weak coupling limit of the Kondo model corresponds to the case of strong dissipation  $\alpha \rightarrow 1^-$ . At low frequencies one finds  $\chi''(\omega) \sim \omega$ , where the corresponding slope scales as  $T_K^{-2}$  with a prefactor of order one<sup>1</sup>. From the fact that we are dealing with an impurity of spin 1/2 one easily derives the normalization condition

$$\int_0^{\infty} d\omega \chi''(\omega) = \frac{\pi}{4} \quad (6.108)$$

which is equivalent to the sum rule (6.95).

In the weak coupling limit  $J_{\perp} \rightarrow 0$  one obtains a *universal scaling form* of  $\chi''(\omega)$ , which only depends on the longitudinal coupling  $J_{\parallel}$  as shown in fig. 6.11. Note that with increasing dissipation  $\alpha$  (decreasing  $J_{\parallel}$ ) more and more spectral weight is contained in the high-frequency tail.

Performing a Kramers–Kronig transformation, the real part of the susceptibility can be calculated as

$$\chi'(\omega) = \mathcal{P} \int_{-\infty}^{\infty} \frac{d\omega'}{\pi} \frac{\chi''(\omega')}{\omega' - \omega} \quad (6.109)$$

(see fig. 6.10). The resonance width is again determined by the Kondo temperature. From the peak value at zero frequency we determine the *static* susceptibility in response to a local field:

$$\chi_0 = \chi'(\omega = 0). \quad (6.110)$$

Due to the Kramers–Kronig transformation it contains spectral information on all energy scales. Results for different values of  $J_{\parallel}$  are shown in fig. 6.12. In the limit of small coupling  $J_{\perp}$  one again obtains a power-law behaviour well known from the ohmic spin boson model (Costi and Zarand 1999)

$$\chi_0 \sim J_{\perp}^{-\frac{1}{1-\alpha}}. \quad (6.111)$$

---

<sup>1</sup>This prefactor is not obtained correctly in the present approach. However, this discrepancy occurs on an energy scale  $\ll \omega_0$  and cannot be resolved in fig. 6.11. The deviation is due to the approximations made here and will be improved in future publications.

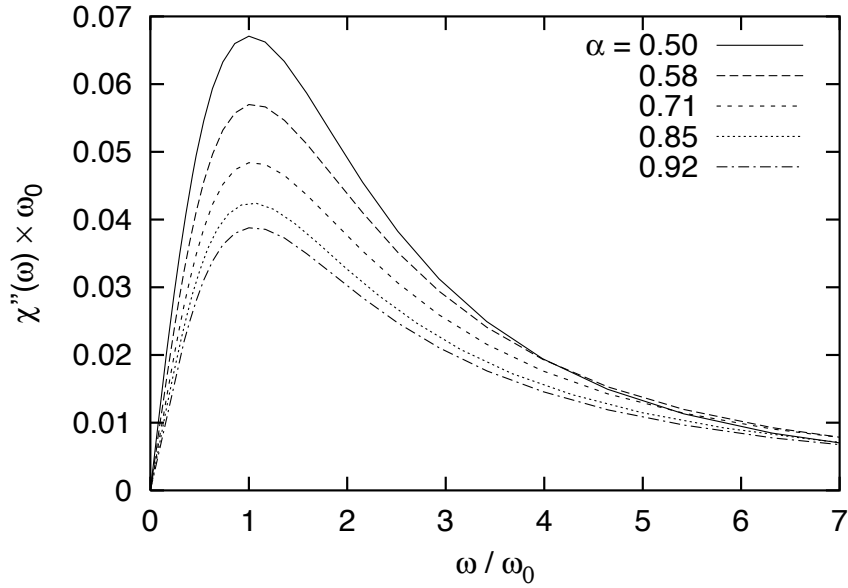


**Figure 6.11:** Universal scaling forms of the dynamical impurity susceptibility for different dissipation strengths  $\alpha = (1 - J_{\parallel}/4\pi)^2$  in the limit of small coupling  $J_{\perp}$ :  $\omega_0$  is defined by the maximum of the curves. One finds  $\omega_0 \sim T_K$ .

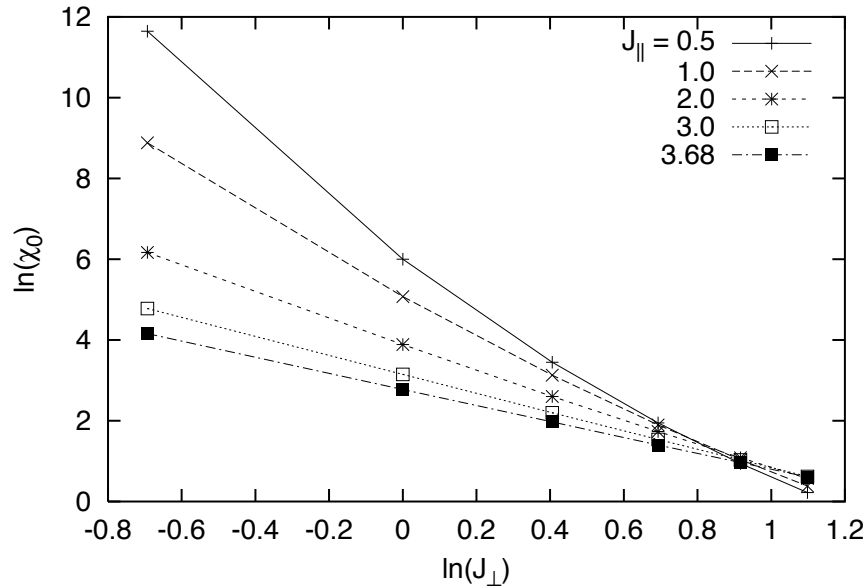


**Figure 6.12:** Local static susceptibility of the Kondo model as obtained from (6.110).

## 6.8 Conclusion

In this chapter we have outlined the application of Wegner's flow equations to the anisotropic Kondo problem. Using bosonization, the Hamiltonian has been written in terms of vertex operators with a scaling dimension that changes in the course of the flow. Higher interaction terms are thus taken into account in a concise notation. This represents the main progress compared to earlier applications of the method which were formulated directly in the fermionic language. In contrast to traditional scaling approaches, flow equations close exactly at the Toulouse point which has finite couplings and a nontrivial strong coupling behaviour. No divergence of the renormalized couplings is encountered.

We are thus able to give an *analytic* description of the crossover from weak to strong coupling by considering the flow of the scaling dimension. To leading order, the correct low energy scale is obtained, while the subdominant term is only approximate. Higher terms in the OPE would have to be considered for a more precise estimate.

Furthermore, the equilibrium dynamics of the impurity has been determined at zero temperature by evaluating the flow equations for an observable. As an example, we have calculated the local dynamical susceptibility, which is shown to be in agreement with results known from the spin-boson model.

Problems are so far encountered in the calculation of the impurity density of states. Here the new potential scattering terms give the leading contribution (in contrast to the dynamical susceptibility), which turns out to be singular at low energy. It may be necessary to take into account subleading terms of the OPE in order to remove this deficiency.

Possible future developments include the extension of the flow equation procedure to finite temperatures. In this case the operator product expansion has to be modified to account for the smeared Fermi distribution of the conduction electrons. More general Hamiltonians like the two channel Kondo model or an impurity in a Luttinger liquid will also be accessible by the method.



# Summary

In this thesis we have discussed the physics of small but strongly correlated quantum systems which are coupled to a metallic environment. At the same time our goal has been the development and improvement of nonperturbative techniques that can extract information from the many-particle Hamiltonians used to model quantum impurity systems. The idea of the *renormalization group* has proved to be very fruitful in that respect: Both NRG and flow equations are based on the elimination of degrees of freedom and the construction of effective Hamiltonians. In NRG this is achieved by actually reducing the size of the Hilbert space, while the flow equation approach aims at rotating away coupling terms by successive unitary transformations.

Different regimes of applicability have been established for both techniques. Wilson's NRG provides a reliable tool for studying systems containing largely differing energy scales. With the DM-NRG presented here, dynamical properties can be extracted accurately also in the presence of arbitrary symmetry breaking. Flow equations, on the other hand, yield comprehensive analytic information about the crossover between the high and low temperature regimes of many-particle systems. They are, however, so far limited to models where bosonization permits efficient bookkeeping of the interaction terms.

Characteristics of the two methods have been illustrated in the analysis of several extended versions of the Anderson and Kondo Hamiltonians:

## Narrow-band Anderson model

Motivated by controversial DMFT results on the Mott metal-insulator transition, we have studied the limit of an extremely narrow hybridization function where the bandwidth is the smallest energy scale in the problem. Using equations of motion, we have established that close to the Fermi edge the total single-particle density of states is always *reduced* by the impurity, because the large hybridization shifts spectral weight into resonances outside the band. At weak coupling, this transfer of weight has also been observed in the negative impurity susceptibility, while for a large Coulomb interaction it has been found that higher many-particle excitations again lead to a positive susceptibility. In addition, the impurity level spectral function has

been calculated, exhibiting characteristic side peaks outside the conduction band. We have demonstrated that due to these resonances the skeleton expansion breaks down at an intermediate energy scale. Consequences for the Mott scenario have been pointed out, as well as open questions with respect to the derivation of the DMFT equations based on self-consistent perturbation theory.

## Magnetic impurity in a correlated band

In order to model realistic impurity systems with interacting conduction electrons, we have considered the Anderson–Hubbard Hamiltonian in the limit of infinite coordination number. It has been demonstrated that in this case the model can be reduced to an effective two-site problem with an effective noninteracting bath. Based on a previous DMFT study of the pure Hubbard model, we have calculated single particle spectra and the dynamical impurity susceptibility in a nonperturbative fashion using NRG. A strong enhancement of the Kondo scale due to band correlations has been found, but at the same time an analysis of the flow diagram revealed that the system remains a local Fermi liquid as long as the host is metallic. In particular, we have demonstrated that in the limit of small hybridization the Kondo temperature always vanishes exponentially, in contrast to results obtained previously. Furthermore, it has been shown that noninteger filling of the conduction band reduces the effective band correlations and their impact on impurity physics. We expect that the doping dependence of the Kondo scale will be seen in future ESR measurements on rare earth impurities in a strongly correlated host.

## Generalized NRG for dynamical properties

Analyzing the Anderson impurity in an external magnetic field, we have found a serious defect in the NRG technique used so far to calculate spectral properties. In particular, it has become clear that for dynamical properties the principle of energy scale separation is not generally valid: Small external fields or a temperature comparable to the Kondo scale can strongly influence spectral features at high frequency. This has been demonstrated explicitly for the spin resolved spectral density, where the procedure previously used strongly underestimates the asymmetry of the atomic levels. To solve the problem, we have developed a new formalism – the DM–NRG – which is based on the reduced density matrix of the *correct* ground state. Accurate spectra in agreement with the static magnetization have thus been obtained. The new method, representing the true generalization of Wilson’s original thermodynamic calculation, provides a unifying framework to calculate dynamical quantities at any temperature. It will be essential for future DMFT calculations in phases with long-range order, and also for studies of more general impurity systems including orbital degeneracy.

## Direct application of flow equations

In a first attempt to diagonalize many-particle Hamiltonians using Wegner's flow equations, we have applied the technique directly to fermionic systems in second quantization. The Luttinger model with forward scattering has served as a toy model where calculations can be tested against bosonization and exact diagonalization. It has been found that normal ordering of the interaction terms is essential to obtain nonperturbative results. Truncating the flow and retaining only two-particle contributions yields an interpolation scheme between the bosonization limit and the regime dominated by band edges. For the Wolff model, we have demonstrated that flow equations close only in the weak coupling limit, due to the absence of an additional control parameter like the momentum transfer cutoff.

## Flow equation analysis of the Kondo model

Motivated by the studies of the Luttinger and Wolff Hamiltonians, the anisotropic Kondo model has been analyzed in a different representation where the conduction band is described by a set of bosonic spin density excitations. It has been shown that in this way new terms generated by the unitary transformations can be parameterized efficiently by using Vertex operators, while the truncation of higher interactions is controlled by the operator product expansion. We have been able to characterize the crossover between the weak and strong coupling limits by the flow of a single real number, the scaling dimension. A nontrivial stable fixed of the formalism has been established (the Toulouse limit) where the flow equations close exactly and no higher terms are generated. Performing similar unitary transformations on a local observable – the impurity spin – we have also calculated the dynamical susceptibility at zero temperature. Problems have so far been encountered in determining the impurity specific heat, where higher order terms of the operator product expansion may become important. In conclusion, the formalism presented here has the advantage of yielding analytic information about highly complex many-particle phenomena. At present, bosonization of the conduction electrons and the existence of a Toulouse-type fixed point are necessary preconditions for the application of the method. Important future extensions include the generalization of flow equations to finite temperatures and the application to more complex systems like the two-channel Kondo model.



# Appendix A

## Details of the mapping on a linear chain

In chapter 1 we have outlined how the Anderson Hamiltonian can be transformed into a semi-infinite chain with a logarithmic structure of the conduction band. Here we give details for some of the missing steps. First we define the maximally localized conduction band orbital  $d_{0\sigma}$ , following Bulla (1994). Using the expansion (1.7), we write

$$\begin{aligned} \int_{-1}^1 d\epsilon \sqrt{\Delta(\epsilon)} c_{\epsilon\sigma} &= \\ &= \sum_{np} \left[ a_{np\sigma} \int_{\Lambda^{-(n+1)}}^{\Lambda^{-n}} d\epsilon \sqrt{\Delta(\epsilon)} \frac{e^{i\omega_n p \epsilon}}{\sqrt{v_n}} + b_{np\sigma} \int_{-\Lambda^{-n}}^{-\Lambda^{-(n+1)}} d\epsilon \sqrt{\Delta(\epsilon)} \frac{e^{-i\omega_n p \epsilon}}{\sqrt{v_n}} \right]. \end{aligned} \quad (\text{A.1})$$

Assuming that the hybridization function  $\Delta$  is sufficiently smooth, it is easy to see that in the continuum limit  $\Lambda \rightarrow 1$  the  $p \neq 0$  contributions vanish. This is a consequence of the Riemann–Lebesgue lemma known from classical analysis which states that for any sufficiently regular function  $f$  the integral  $\int d\epsilon f(\epsilon) \exp(i\omega\epsilon)$  vanishes in the high frequency limit  $\omega \rightarrow \infty$ . Keeping only the  $p = 0$  terms is therefore equivalent to approximating  $\Delta$  by a step function (see fig. 1.3), which becomes exact as the width of the steps approaches zero for  $\Lambda \rightarrow 1$ . The maximally localized state then takes the form

$$d_{0\sigma} \equiv \frac{1}{\sqrt{\xi_0}} \int_{-1}^1 d\epsilon \sqrt{\Delta(\epsilon)} c_{\epsilon\sigma} = \frac{1}{\sqrt{\xi_0}} \sum_n (\gamma_n^+ a_{n0\sigma} + \gamma_n^- b_{n0\sigma}) \quad (\text{A.2})$$

with the coefficients

$$\gamma_n^+ = \frac{1}{\sqrt{v_n}} \int_{\Lambda^{-(n+1)}}^{\Lambda^{-n}} d\epsilon \sqrt{\Delta(\epsilon)} \quad (\text{A.3})$$

$$\gamma_n^- = \frac{1}{\sqrt{v_n}} \int_{-\Lambda^{-n}}^{-\Lambda^{-(n+1)}} d\epsilon \sqrt{\Delta(\epsilon)} \quad (\text{A.4})$$

and the normalization

$$\xi_0 = \sum_n \left( \gamma_n^{+2} + \gamma_n^{-2} \right). \quad (\text{A.5})$$

Next, we derive the transformation of the conduction band

$$H_0 = \sum_{n=0}^{\infty} \Lambda^{-n} \left( a_n^\dagger a_n - b_n^\dagger b_n \right) \quad (\text{A.6})$$

into a linear chain form

$$H_0 = \sum_{n=0}^{\infty} \left[ \epsilon_n \left( d_n^\dagger d_{n+1} + h.c. \right) + \delta_n d_n^\dagger d_n \right]. \quad (\text{A.7})$$

The spin index  $\sigma$  has been dropped as the two spin orientations decouple. To simplify notation, we have also omitted the constant prefactor  $(1 + \Lambda^{-1})/2$ . The new single-particle operators are given by the following ansatz:

$$d_n^\dagger = \sum_m \left( u_{nm} a_m^\dagger + v_{nm} b_m^\dagger \right). \quad (\text{A.8})$$

The coefficients are determined recursively using the tridiagonalization procedure developed by Lanczos (1950), equivalent to Gram–Schmidt orthogonalization. Starting from an initial one-particle state  $|\Psi_0\rangle$ , a new single-particle basis is constructed according to

$$\epsilon_n |\Psi_{n+1}\rangle = H_0 |\Psi_n\rangle - |\Psi_n\rangle \overbrace{\langle \Psi_n | H_0 | \Psi_n \rangle}^{\delta_n} - |\Psi_{n-1}\rangle \overbrace{\langle \Psi_{n-1} | H_0 | \Psi_n \rangle}^{\epsilon_{n-1}} \quad (\text{A.9})$$

and the  $d_n$  are defined via

$$|\Psi_n\rangle = d_n^\dagger |0\rangle \quad (\text{A.10})$$

We choose  $|\Psi_0\rangle$  to be the *maximally localized* state:

$$|\Psi_0\rangle = d_0^\dagger |0\rangle \quad (\text{A.11})$$

where  $|0\rangle$  denotes the Fock vacuum. The initial conditions for the recursive procedure are therefore given by

$$u_{0m} = \frac{\gamma_m^+}{\sqrt{\xi_0}} \quad , \quad v_{0m} = \frac{\gamma_m^-}{\sqrt{\xi_0}} \quad (\text{A.12})$$

Inserting the definition (A.10) into (A.9) yields

$$\epsilon_{n-1} = \sum_m \Lambda^{-m} (u_{(n-1)m} u_{nm} - v_{(n-1)m} v_{nm}) \quad (\text{A.13})$$

as a consequence of hermiticity. Furthermore

$$\delta_n = \sum_m \Lambda^{-m} (u_{nm}^2 - v_{nm}^2). \quad (\text{A.14})$$

Notice that for a symmetric hybridization  $\Delta(\epsilon) = \Delta(-\epsilon)$  the coefficients  $u$  and  $v$  are equal and the on-site energies  $\delta_n$  vanish. Finally,

$$\begin{aligned} \epsilon_n^2 = \sum_m \left[ (\Lambda^{-m} u_{nm} - \epsilon_{n-1} u_{(n-1)m} - \delta_n u_{nm})^2 \right. \\ \left. + (-\Lambda^{-m} v_{nm} - \epsilon_{n-1} v_{(n-1)m} - \delta_n v_{nm})^2 \right] \end{aligned} \quad (\text{A.15})$$

and the new creation operator  $d_{(n+1)}$  is defined by the coefficients

$$u_{(n+1)m} = \frac{1}{\epsilon_n} (\Lambda^{-m} u_{nm} - \epsilon_{n-1} u_{(n-1)m} - \delta_n u_{nm}) \quad (\text{A.16})$$

$$v_{(n+1)m} = \frac{1}{\epsilon_n} (-\Lambda^{-m} v_{nm} - \epsilon_{n-1} v_{(n-1)m} - \delta_n v_{nm}). \quad (\text{A.17})$$

This concludes the set of recursion relations. Due to the exponentially decaying band energies, the above equations have to be evaluated using arbitrary precision arithmetics for chain lengths  $N \gtrsim 40$ .



## Appendix B

# Iterative diagonalization with rotational symmetry

In this appendix we give details of the iterative diagonalization of the truncated Hamiltonians (1.12), see also Krishna-murthy et al. (1980). Let  $|l, N\rangle$  denote the eigenstates of  $H_N$ , with  $l = 0$  corresponding to the ground state. Suppose one knows all the energy levels  $E(l, N)$  and matrix elements  $\langle l, N | d_{n\sigma}^\dagger | l', N' \rangle$ . A new basis that spans the Hilbert space of  $H_{N+1}$  is then provided by the following states:

$$\begin{aligned}
 |l, N; 0\rangle &\equiv |l, N\rangle \\
 |l, N; \uparrow\rangle &\equiv d_{(N+1)\uparrow}^\dagger |l, N\rangle \\
 |l, N; \downarrow\rangle &\equiv d_{(N+1)\downarrow}^\dagger |l, N\rangle \\
 |l, N; \uparrow\downarrow\rangle &\equiv d_{(N+1)\uparrow}^\dagger d_{(N+1)\downarrow}^\dagger |l, N\rangle.
 \end{aligned}
 \tag{B.1}$$

The matrix elements of  $H_{N+1}$  can be written down in this basis

$$\begin{aligned}
 \langle l', N; i' | H_{N+1} | l, N; i \rangle &= \Lambda^{1/2} E(l, N) \delta_{ii'} \delta_{ll'} + \sum_{\sigma} \Lambda^{N/2} \epsilon_N \times \\
 &\times \left( \langle l', N | d_{N\sigma}^\dagger | l, N \rangle \langle i' | d_{(N+1)\sigma} | i \rangle + \langle i' | d_{(N+1)\sigma}^\dagger | i \rangle \langle l', N | d_{N\sigma} | l, N \rangle \right)
 \end{aligned}
 \tag{B.2}$$

and are completely determined by the knowledge of  $H_N$  (with  $i, i' \in \{0, \uparrow, \downarrow, \uparrow\downarrow\}$ ). Diagonalization yields the new eigenvalues  $E(l, N+1)$  and matrix elements of  $d_{(N+1)\sigma}^\dagger$  and in this way the procedure can be iterated.

So far no use has been made of the spin (1.16) and charge (1.15) conservation. For actual calculations the resulting block diagonal structure of the Hamiltonian can be taken into account in order to reduce the size of the matrices to be diagonalized. Here we consider the case where all three components of the total spin  $\mathbf{S}$  are good quantum numbers (which is not true anymore if a magnetic field is applied, see chapter 4). We

can then construct a simultaneous eigenbasis of the operators  $H$ ,  $Q$ ,  $S^2$  and  $S^z$ . Due to

$$[H, S^\pm] = 0 \quad (\text{B.3})$$

states differing only in  $S^z$  are degenerate and can be represented by a single "multiplet" state. Wilson (1975) realised that the diagonalization can be formulated in terms of the multiplet states only, thus eliminating the degeneracy. This is achieved by applying the *Wigner–Eckart theorem* (see for example Sakurai (1994))

$$\begin{aligned} \langle Q', S', S^{z'}, r' | T_q^{(k)} | Q, S, S^z, r \rangle &= \quad (\text{B.4}) \\ &= \underbrace{\langle Q', S', r' || T^{(k)} || Q, S, R \rangle}_{\text{reduced matrix element}} \underbrace{\langle S, k, S^z, q | S, k, S', S^{z'} \rangle}_{\text{Clebsch--Gordan}}. \end{aligned}$$

In this expression,  $T_q^{(k)}$  is the  $q$ -component of a spherical tensor of rank  $k$  defined by the following commutation relations:

$$[S^z, T_q^{(k)}] = q T_q^{(k)} \quad (\text{B.5})$$

$$[S^\pm, T_q^{(k)}] = \sqrt{(k \mp q)(k \pm q + 1)} T_{q\pm 1}^{(k)} \quad (\text{B.6})$$

In particular, for the creation operator  $d_\sigma^\dagger$  we have  $k = 1/2$  and  $q = \pm 1/2$ . Instead of working directly with (B.1) it is more convenient to form linear combinations that are again eigenstates of the total spin:

$$\begin{aligned} |Q, S, S^z, r; 1\rangle_{N+1} &\equiv |Q + 1, S, S^z, r; 0\rangle_N \quad (\text{B.7}) \\ |Q, S, S^z, r; 2\rangle_{N+1} &\equiv \sqrt{\frac{S + S^z}{2S}} |Q, S - \frac{1}{2}, S^z - \frac{1}{2}, r; \uparrow\rangle_N \\ &\quad + \sqrt{\frac{S - S^z}{2S}} |Q, S - \frac{1}{2}, S^z + \frac{1}{2}, r; \downarrow\rangle_N \\ |Q, S, S^z, r; 3\rangle_{N+1} &\equiv -\sqrt{\frac{S - S^z + 1}{2S + 2}} |Q, S + \frac{1}{2}, S^z - \frac{1}{2}, r; \uparrow\rangle_N \\ &\quad + \sqrt{\frac{S + S^z + 1}{2S + 2}} |Q, S + \frac{1}{2}, S^z + \frac{1}{2}, r; \downarrow\rangle \\ |Q, S, S^z, r; 4\rangle_{N+1} &\equiv |Q - 1, S, S^z, r; \uparrow\downarrow\rangle_N \end{aligned}$$

It turns out that knowledge of the reduced matrix elements  $\langle ||d_N^\dagger|| \rangle$  is sufficient to write down the Hamiltonian matrix for the new hopping term  $\overline{\Delta H} = \sum_\sigma (d_{N\sigma}^\dagger d_{(N+1)\sigma} + h.c.)$  because

$$\langle Q, S, r'; 1 | \overline{\Delta H} | Q, S, r; 2 \rangle_{N+1} = \langle Q + 1, S, r' | d_N^\dagger | Q, S - \frac{1}{2}, r \rangle_N \quad (\text{B.8})$$

$$\begin{aligned}
\langle Q, S, r'; 1 | \overline{\Delta H} | Q, S, r; 3 \rangle_{N+1} &= \langle Q + 1, S, r' | d_N^\dagger | Q, S + \frac{1}{2}, r \rangle_N \\
\langle Q, S, r'; 2 | \overline{\Delta H} | Q, S, r; 4 \rangle_{N+1} &= \sqrt{\frac{2S}{2S+1}} \langle Q, S - \frac{1}{2}, r' | d_N^\dagger | Q - 1, S, r \rangle_N \\
\langle Q, S, r'; 3 | \overline{\Delta H} | Q, S, r; 4 \rangle_{N+1} &= -\sqrt{\frac{2S+2}{2S+1}} \langle Q, S + \frac{1}{2}, r' | d_N^\dagger | Q - 1, S, r \rangle_N
\end{aligned}$$

Inserting this result into the recursion relation (B.2), one can diagonalize  $H_{N+1}$  and thus obtains the new eigenenergies  $E_{N+1}(Q, S, \omega)$  and eigenstates

$$| Q, S, \omega \rangle_{N+1} = \sum_{i,r} U_{QS}(\omega; ri) | Q, S, r; i \rangle_{N+1} \quad (\text{B.9})$$

where  $U$  is an orthogonal matrix. In the final step, the new reduced matrix elements  $\langle Q, S, \omega | f_{N+1}^\dagger | Q', S', \omega' \rangle$  are directly obtained using (B.9) and the definition (B.7).



# Appendix C

## Calculation of $\rho(\omega)$ and $\chi(\omega)$

In this section we outline the calculation of dynamical quantities within the NRG formalism presented in appendix B, which has been applied to the Anderson impurity in a correlated band (see chapter 3). In particular, rotational invariance is taken into account by writing both the single-particle spectrum and the dynamical susceptibility in terms of reduced matrix elements. For simplicity, we focus on the case of even chain length  $N$  where the ground state is a singlet ( $S_g = 0$ ) and nondegenerate.

### Single-particle spectrum

From the eigenstates in iteration step  $N$  and the matrix elements of the impurity fermion  $f_\sigma^\dagger$  the spectral density on the frequency scale  $\omega \sim \Lambda^{-N/2}$  is obtained:<sup>1</sup>

$$\begin{aligned}\rho_N^+(\omega) &= \sum_a |\langle a | f_\sigma^\dagger | g \rangle_N|^2 \delta(\omega - (E_{aN} - E_{gN})) \\ \rho_N^-(\omega) &= \sum_a |\langle g | f_\sigma^\dagger | a \rangle_N|^2 \delta(\omega - (E_{gN} - E_{aN})).\end{aligned}\quad (\text{C.1})$$

The ground state  $|g\rangle$  and the excitations  $|a\rangle$  can be characterized by their quantum numbers

$$\begin{aligned}|g\rangle_N &= |Q_g, S_g = 0, S_g^z = 0, r_g\rangle_N \\ |a\rangle_N &= |Q, S, S^z, r\rangle_N\end{aligned}\quad (\text{C.2})$$

where the additional indices  $r, r_g$  count states within a sector of fixed charge and spin. As shown in the previous section,  $T^{(1/2)} = (f_\uparrow^\dagger, f_\downarrow^\dagger)$  is a spherical tensor of

---

<sup>1</sup>Here we consider only the isotropic case where  $\sigma = \uparrow, \downarrow$  are equivalent. If this symmetry is broken (for example by an external magnetic field) one has to apply the DM-NRG approach introduced in chapter 4, which however cannot be formulated in terms of reduced matrix elements.

rank 1/2. By using the Wigner–Eckart theorem (B.4) we can therefore eliminate the  $S^z$  degeneracy and obtain

$$\begin{aligned}\rho_N^+(\omega) &= \sum_r \left| \langle Q_g + 1, S_g + 1/2, r || f^\dagger || Q_g, S_g, r_g \rangle_N \right|^2 \\ &\quad \times \delta(\omega - (E_N(Q_g + 1, S_g + 1/2, r) - E_{gN})) \\ \rho_N^-(\omega) &= \frac{1}{2} \sum_r \left| \langle Q_g, S_g, r_g || f^\dagger || Q_g - 1, S_g + 1/2, r \rangle_N \right|^2 \\ &\quad \times \delta(\omega - (E_{gN} - E_N(Q_g - 1, S_g + 1/2, r))).\end{aligned}\quad (\text{C.3})$$

The reduced matrix elements of the impurity fermion are calculated recursively in two steps:

- After diagonalization, the new eigenstates are unitarily related to the previous basis by the transformation (B.9). One can therefore write

$$\begin{aligned}\langle Q, S, w || f^\dagger || Q', S', w' \rangle_N &= \\ &= \sum_{rr'} \sum_{pp'=1}^4 U_{QS}(w, rp) U_{Q'S'}(w', r'p') \langle Q, S, r, p || f^\dagger || Q', S', r', p' \rangle_N\end{aligned}\quad (\text{C.4})$$

with the  $p = 1, \dots, 4$  states defined in equation (B.7).

- The following recursion relations hold for the non-vanishing matrix elements:

$$\begin{aligned}\langle Q, S, r, 1 || f^\dagger || Q - 1, S \pm 1/2, r', 1 \rangle_N &= \\ &= \langle Q + 1, S, r || f^\dagger || Q, S \pm 1/2, r' \rangle_{N-1}\end{aligned}$$

$$\begin{aligned}\langle Q, S, r, 2 || f^\dagger || Q - 1, S + 1/2, r', 2 \rangle_N &= \\ &= -\frac{2\sqrt{S(S+1)}}{2S+1} \langle Q, S - 1/2, r || f^\dagger || Q - 1, S, r' \rangle_{N-1}\end{aligned}$$

$$\begin{aligned}\langle Q, S, r, 2 || f^\dagger || Q - 1, S - 1/2, r', 2 \rangle_N &= \\ &= -\langle Q, S - 1/2, r || f^\dagger || Q - 1, S - 1, r' \rangle_{N-1}\end{aligned}$$

$$\begin{aligned}\langle Q, S, r, 3 || f^\dagger || Q - 1, S + 1/2, r', 3 \rangle_N &= \\ &= -\langle Q, S + 1/2, r || f^\dagger || Q - 1, S + 1, r' \rangle_{N-1}\end{aligned}$$

$$\begin{aligned}\langle Q, S, r, 3 || f^\dagger || Q - 1, S - 1/2, r', 3 \rangle_N &= \\ &= -\frac{2\sqrt{S(S+1)}}{2S+1} \langle Q, S + 1/2, r || f^\dagger || Q - 1, S, r' \rangle_{N-1}\end{aligned}$$

$$\begin{aligned} \langle Q, S, r, 2 || f^\dagger || Q - 1, S - 1/2, r', 3 \rangle_N &= \\ &= -\frac{1}{2S+1} \langle Q, S - 1/2, r || f^\dagger || Q - 1, S, r' \rangle_{N-1} \end{aligned}$$

$$\begin{aligned} \langle Q, S, r, 3 || f^\dagger || Q - 1, S + 1/2, r', 2 \rangle_N &= \\ &= \frac{1}{2S+1} \langle Q, S + 1/2, r || f^\dagger || Q - 1, S, r' \rangle_{N-1} \end{aligned}$$

$$\begin{aligned} \langle Q, S, r, 4 || f^\dagger || Q - 1, S \pm 1/2, r', 4 \rangle_N &= \\ &= \langle Q - 1, S, r || f^\dagger || Q - 2, S \pm 1/2, r' \rangle_{N-1}. \end{aligned}$$

Inserting the resulting matrix elements into equation (C.3) then yields a set of peaks at positions determined by the excitation energies. These have to be broadened in order to get a continuous spectrum. It has been found by Sakai et al. (1989) and Costi et al. (1994) that a logarithmic Gaussian yields the best results:

$$\delta(\omega - \omega_n) \longrightarrow \frac{e^{-b_n^2/4}}{b_n \omega_n \sqrt{\pi}} \exp \left[ -\frac{(\ln \omega - \ln \omega_n)^2}{b_n^2} \right]. \quad (\text{C.5})$$

This type of broadening is also used for other dynamical quantities like the susceptibility. Most spectra in this thesis have been obtained by using a broadening factor  $b = 0.5$ .

## Dynamical susceptibility

Within the NRG formalism we calculate the imaginary part of the dynamical susceptibility on the frequency scale  $\omega \sim \Lambda^{-N/2}$  according to

$$\chi_N''(\omega) = \pi \sum_a |\langle a | \sigma^z | g \rangle_N|^2 (\delta(\omega - E_{aN} + E_{gN}) - \delta(\omega + E_{aN} - E_{gN})) \quad (\text{C.6})$$

using the same notation as before. As for the single particle spectrum, we can eliminate the dependence on  $S^z$  by applying the Wigner-Eckart theorem. It is easily verified that the following components of the impurity spin form a spherical tensor of rank 1:

$$T_q^{(1)} = \begin{pmatrix} -\frac{1}{\sqrt{2}} \sigma^+ \\ \sigma^z \\ \frac{1}{\sqrt{2}} \sigma^- \end{pmatrix}. \quad (\text{C.7})$$

The expression (C.6) then simplifies to

$$\begin{aligned} \chi''_N(\omega) &= \pi \sum_r |\langle Q_g, S_g + 1, r \parallel \sigma \parallel Q_g, S_g = 0, r_g \rangle_N|^2 \\ &\times (\delta(\omega - E_N(Q_g, S_g + 1, r) + E_{gN}) - \delta(\omega + E_N(Q_g, S_g + 1, r) - E_{gN})) \end{aligned} \quad (\text{C.8})$$

where the summation is now restricted to the excitations in the  $Q = Q_g, S = S_g + 1$  sector. The reduced matrix elements are again obtained in two steps:

- After diagonalization, a unitary transformation analogous to (C.4) has to be performed:

$$\begin{aligned} \langle Q, S, w \parallel \sigma \parallel Q', S', w' \rangle_N &= \\ &= \sum_{rr'} \sum_{pp'=1}^4 U_{QS}(w, rp) U_{Q'S'}(w', r'p') \langle Q, S, r, p \parallel \sigma \parallel Q', S', r', p' \rangle_N \end{aligned} \quad (\text{C.9})$$

- The following recursion relations hold:

$$\begin{aligned} \langle Q, S, r, 1 \parallel \sigma \parallel Q, S', s, 1 \rangle_N &= \\ &= \langle Q + 1, S, r \parallel \sigma \parallel Q + 1, S', s \rangle_{N-1} \end{aligned}$$

$$\begin{aligned} \langle Q, S, r, 2 \parallel \sigma \parallel Q, S - 1, s, 2 \rangle_N &= \\ &= \langle Q, S - \frac{1}{2}, r \parallel \sigma \parallel Q, S - \frac{3}{2}, s \rangle_{N-1} \end{aligned}$$

$$\begin{aligned} \langle Q, S, r, 2 \parallel \sigma \parallel Q, S, s, 2 \rangle_N &= \\ &= \sqrt{\frac{(S+1)(2S-1)}{S(2S+1)}} \langle Q, S - \frac{1}{2}, r \parallel \sigma \parallel Q, S - \frac{1}{2}, s \rangle_{N-1} \end{aligned}$$

$$\begin{aligned} \langle Q, S, r, 2 \parallel \sigma \parallel Q, S + 1, s, 2 \rangle_N &= \\ &= \sqrt{\frac{S(2S+3)}{(S+1)(2S+1)}} \langle Q, S - \frac{1}{2}, r \parallel \sigma \parallel Q, S + \frac{1}{2}, s \rangle_{N-1} \end{aligned}$$

$$\begin{aligned} \langle Q, S, r, 3 \parallel \sigma \parallel Q, S - 1, s, 3 \rangle_N &= \\ &= \sqrt{\frac{(S+1)(2S-1)}{S(2S+1)}} \langle Q, S + \frac{1}{2}, r \parallel \sigma \parallel Q, S - \frac{1}{2}, s \rangle_{N-1} \end{aligned}$$

$$\begin{aligned} \langle Q, S, r, 3 \parallel \sigma \parallel Q, S, s, 3 \rangle_N &= \\ &= \sqrt{\frac{S(2S+3)}{(S+1)(2S+1)}} \langle Q, S + \frac{1}{2}, r \parallel \sigma \parallel Q, S + \frac{1}{2}, s \rangle_{N-1} \end{aligned}$$

$$\begin{aligned} \langle Q, S, r, 3 \parallel \sigma \parallel Q, S + 1, s, 3 \rangle_N &= \\ &= \langle Q, S + \frac{1}{2}, r \parallel \sigma \parallel Q, S + \frac{3}{2}, s \rangle_{N-1} \end{aligned}$$

$$\begin{aligned} \langle Q, S, r, 2 \parallel \sigma \parallel Q, S - 1, s, 3 \rangle_N &= \\ &= \frac{1}{\sqrt{S(2S+1)}} \langle Q, S - \frac{1}{2}, r \parallel \sigma \parallel Q, S - \frac{1}{2}, s \rangle_{N-1} \end{aligned}$$

$$\begin{aligned} \langle Q, S, r, 2 \parallel \sigma \parallel Q, S, s, 3 \rangle_N &= \\ &= \frac{1}{\sqrt{(S+1)(2S+1)}} \langle Q, S - \frac{1}{2}, r \parallel \sigma \parallel Q, S + \frac{1}{2}, s \rangle_{N-1} \end{aligned}$$

$$\begin{aligned} \langle Q, S, r, 3 \parallel \sigma \parallel Q, S, s, 2 \rangle_N &= \\ &= -\frac{1}{\sqrt{S(2S+1)}} \langle Q, S + \frac{1}{2}, r \parallel \sigma \parallel Q, S - \frac{1}{2}, s \rangle_{N-1} \end{aligned}$$

$$\begin{aligned} \langle Q, S, r, 3 \parallel \sigma \parallel Q, S + 1, s, 2 \rangle_N &= \\ &= -\frac{1}{\sqrt{(S+1)(2S+1)}} \langle Q, S + \frac{1}{2}, r \parallel \sigma \parallel Q, S + \frac{1}{2}, s \rangle_{N-1} \end{aligned}$$

$$\begin{aligned} \langle Q, S, r, 4 \parallel \sigma \parallel Q, S', s, 4 \rangle_N &= \\ &= \langle Q - 1, S, r \parallel \sigma \parallel Q - 1, S', s \rangle_{N-1} \end{aligned}$$

All matrix elements not shown are zero.



# Appendix D

## Details of the Wolff model flow

In this appendix we present the full differential equations for the flow of the couplings in (5.45). The relevant commutators were evaluated using the symbolic engine of *Mathematica*.

$$\begin{aligned}
\partial_l E(l) = & \sum_{q_1 q_2} 2(q_1 - q_2)(n_{q_1} - n_{q_2})V_{q_1 q_2}^2 \\
& + \sum_{q_1 q_2 q_3 q_4} \left[ (q_1 - q_2)(-2n_{q_1} + n_{q_2})n_{q_3}(-1 + n_{q_4})U_{q_1 q_2 q_4 q_3} U_{q_2 q_1 q_3 q_4} \right. \\
& - 2(q_1 - q_2)n_{q_1}(-1 + n_{q_2})(n_{q_3} - n_{q_4})U_{q_1 q_2 q_3 q_4} U_{q_2 q_1 q_4 q_3} \\
& \left. + (q_1 - q_4)n_{q_2}(-1 + n_{q_3})n_{q_4}U_{q_1 q_4 q_3 q_2} U_{q_2 q_3 q_4 q_1} \right] \\
& + \sum_{q_1 q_2 q_3} \left[ 2(q_1 - q_3)n_{q_2}V_{q_1 q_3}((-1 + n_{q_3})W_{q_1 q_2 q_2 q_3} - n_{q_3}W_{q_2 q_1 q_3 q_2}) \right. \\
& \left. + 2(q_1 - q_2)(-1 + n_{q_1} + n_{q_2})n_{q_3}V_{q_1 q_2}W_{q_2 q_3 q_3 q_1} \right] \\
& + \sum_{q_1 q_2 q_3 q_4} \left[ -4(q_1 - q_2 + q_3 - q_4)n_{q_1}(-1 + n_{q_2})(n_{q_3} - n_{q_4})W_{q_1 q_2 q_3 q_4} W_{q_2 q_1 q_4 q_3} \right. \\
& + 2n_{q_3}(-1 + n_{q_4})(-(q_1 - q_2 - q_3 + q_4)(2n_{q_1} - n_{q_2})W_{q_1 q_2 q_4 q_3} W_{q_2 q_1 q_3 q_4}) \\
& + (q_2 - q_4)(-1 + 2n_{q_1})W_{q_1 q_2 q_4 q_1} W_{q_2 q_3 q_3 q_4} \\
& + 2(q_1 - q_2 + q_3 - q_4)(n_{q_1}(n_{q_2}(1 + n_{q_3} - 2n_{q_4}) + (1 + n_{q_3})(-1 + n_{q_4}))W_{q_1 q_2 q_3 q_4} \\
& + n_{q_2}(-1 + n_{q_3})n_{q_4}(-W_{q_1 q_2 q_3 q_4} + W_{q_1 q_4 q_3 q_2}))W_{q_2 q_3 q_4 q_1} \\
& + 2(q_1 - q_2 - q_3 + q_4)(-1 + n_{q_2})(n_{q_1} - n_{q_3})(-1 + n_{q_4})W_{q_1 q_2 q_4 q_3} W_{q_2 q_4 q_3 q_1} \\
& + 2(-q_1 - q_2 + q_3 + q_4)n_{q_2}(-1 + n_{q_3})(-1 + n_{q_4})W_{q_1 q_4 q_2 q_3} W_{q_3 q_1 q_4 q_2} \\
& + n_{q_4}(-2(q_2 - q_3)n_{q_1}(-1 + n_{q_2} + n_{q_3})W_{q_1 q_2 q_3 q_4} W_{q_2 q_4 q_4 q_3} \\
& + n_{q_3}(-2(q_1 - q_4)(-1 + n_{q_2})W_{q_1 q_2 q_2 q_4} W_{q_3 q_1 q_4 q_3} \\
& \left. + 2(-q_2 + q_4)n_{q_1}W_{q_1 q_4 q_2 q_1} W_{q_3 q_2 q_4 q_3}) \right]
\end{aligned}$$

$$+2(q_1 - q_3)(-1 + n_{q_2})(-1 + n_{q_1} + n_{q_3})W_{q_1q_2q_2q_3}W_{q_3q_4q_4q_1}] \quad (D.1)$$

$$\begin{aligned}
\partial_l V_{p_1 p_2}(l) &= -(p_1 - p_2)^2 V_{p_1 p_2} \\
&+ \sum_{q_1} \left[ (p_1 + p_2 - 2q_1) V_{p_1 q_1} V_{p_2 q_1} \right] \\
&+ \sum_{q_1 q_2} \left[ (p_1 - p_2 + q_1 - q_2)(n_{q_1} - n_{q_2}) V_{q_1 q_2} U_{p_1 p_2 q_1 q_2} \right] \\
&+ \sum_{q_1 q_2} \left[ (q_1 - q_2)(n_{q_1} - n_{q_2}) V_{q_1 q_2} U_{p_1 p_2 q_2 q_1} \right] \\
&+ \sum_{q_1 q_2 q_3} \left[ (n_{q_2}((p_2 - q_1)n_{q_1} - (p_1 - q_1)(-1 + n_{q_3})) + (-p_2 + q_1)n_{q_1}n_{q_3}) \times \right. \\
&U_{p_1 q_1 q_3 q_2} U_{q_1 p_2 q_2 q_3} + ((p_1 - q_1)(-1 + n_{q_1})n_{q_3} + n_{q_2}(p_1 + p_2 - 2q_1 + (-p_1 + q_1)n_{q_1} \\
&+ (-p_2 + q_1)n_{q_3}))U_{p_1 q_1 q_2 q_3} U_{q_1 p_2 q_3 q_2} + (q_1 - q_2)(-(n_{q_1}n_{q_3}) \\
&+ n_{q_2}(-1 + n_{q_1} + n_{q_3}))U_{p_1 q_3 q_2 q_1} U_{q_1 q_2 q_3 p_2} \\
&\left. + (q_1 - q_2)(n_{q_2}n_{q_3} - n_{q_1}(-1 + n_{q_2} + n_{q_3}))U_{p_1 q_3 q_1 q_2} U_{q_2 q_1 q_3 p_2} \right] \\
&- \sum_{q_1 q_2} \left[ (q_1 - q_2) V_{q_1 q_2} (W_{p_1 q_1 q_2 p_2} + n_{q_1}(-2W_{p_1 p_2 q_2 q_1} + W_{p_1 q_1 q_2 p_2})) \right. \\
&\left. + n_{q_2}(2W_{p_1 p_2 q_2 q_1} - 2W_{p_1 q_1 q_2 p_2} - W_{p_1 q_2 q_1 p_2}) + W_{p_1 q_2 q_1 p_2} \right] \\
&+ \sum_{q_1 q_2 q_3} \left[ n_{q_2}(-((p_1 - p_2 - q_1 + q_3)(-1 + n_{q_3})U_{p_1 p_2 q_3 q_1} W_{q_1 q_2 q_2 q_3}) \right. \\
&+ (-p_1 + p_2 - q_1 + q_3)n_{q_3}U_{p_1 p_2 q_1 q_3} W_{q_2 q_1 q_3 q_2}) \\
&\left. + (p_1 - p_2 + q_1 - q_2)(-1 + n_{q_1} + n_{q_2})n_{q_3}U_{p_1 p_2 q_1 q_2} W_{q_2 q_3 q_3 q_1} \right] \\
&+ \sum_{q_1 q_2} \left[ (n_{q_1} - n_{q_2}) V_{q_1 q_2} (2(p_1 - p_2 + q_1 - q_2)W_{p_1 p_2 q_1 q_2} \right. \\
&\left. + (p_1 - p_2 - q_1 + q_2)W_{p_1 q_1 q_2 p_2} + (-p_1 + p_2 - q_1 + q_2)W_{p_1 q_2 q_1 p_2}) \right] \\
&+ \sum_{q_1 q_2 q_3} \left[ (-q_2 + q_3)n_{q_1}(n_{q_2}U_{p_1 p_2 q_2 q_3} W_{q_1 q_2 q_3 q_1} + n_{q_3}U_{p_1 p_2 q_3 q_2} W_{q_1 q_3 q_2 q_1}) \right] \\
&+ \sum_{q_1 q_2 q_3} \left[ -2(p_1 - q_1 + q_2 - q_3)(-1 + n_{q_1})(n_{q_2} - n_{q_3})W_{p_1 q_1 q_2 q_3} W_{q_1 p_2 q_3 q_2} \right. \\
&+ (q_1 - q_3)(-1 + n_{q_1})(-1 + n_{q_2})W_{p_1 q_1 q_3 p_2} W_{q_1 q_2 q_2 q_3} \\
&+ (p_1 - q_1 + q_2 - q_3)(n_{q_1}(1 + n_{q_2} - 2n_{q_3}) + (1 + n_{q_2})(-1 + n_{q_3}))W_{p_1 q_1 q_2 q_3} W_{q_1 q_2 q_3 p_2} \\
&\left. - (p_2 - q_1 + q_2 - q_3)W_{p_1 q_3 q_2 q_1} ((n_{q_1} - n_{q_2})(-1 + n_{q_3})W_{q_1 p_2 q_3 q_2} \right.
\end{aligned}$$

$$\begin{aligned}
& +(-2n_{q_1}n_{q_3} + n_{q_2}(-1 + 2n_{q_1} + n_{q_3}))W_{q_1q_2q_3p_2}) \\
& - (p_2 - q_1 + q_2 - q_3)W_{p_1q_1q_2q_3}(2n_{q_2}(-1 + n_{q_3})W_{q_1p_2q_3q_2} \\
& + (-((-1 + 2n_{q_2})(-1 + n_{q_3})) + n_{q_1}(1 - 2n_{q_2} + n_{q_3}))W_{q_1q_2q_3p_2}) \\
& + (q_2 - q_3)(1 - n_{q_3} + n_{q_1}(-1 + n_{q_2} + n_{q_3}))W_{p_1q_3q_2p_2}W_{q_1q_2q_3q_1} \\
& + (p_1 - q_1 - q_2 + q_3)(-1 + n_{q_1} + n_{q_2})(-1 + n_{q_3})W_{p_1q_1q_3q_2}W_{q_1q_3q_2p_2} \\
& - (p_2 - q_1 - q_2 + q_3)W_{p_1q_2q_3q_1}(n_{q_1}(1 + n_{q_2} - 2n_{q_3})W_{q_1p_2q_2q_3} \\
& + (-1 + n_{q_2})n_{q_3}(-W_{q_1p_2q_2q_3} + W_{q_1q_3q_2p_2})) \\
& + n_{q_1}(2(p_2 - q_1 - q_2 + q_3)(n_{q_2} - n_{q_3})W_{p_1q_1q_3q_2}W_{q_1p_2q_2q_3} \\
& + 2(-q_2 + q_3)n_{q_2}W_{p_1p_2q_2q_3}W_{q_1q_2q_3q_1} \\
& + (q_2 - q_3)n_{q_3}(-2W_{p_1p_2q_3q_2} + W_{p_1q_2q_3p_2})W_{q_1q_3q_2q_1}) \\
& + (p_1 + q_1 - q_2 - q_3)(n_{q_2}n_{q_3}W_{p_1q_2q_1q_3} + (2n_{q_1}(-1 + n_{q_2}) \\
& + (1 + n_{q_1} - 2n_{q_2})n_{q_3})W_{p_1q_3q_1q_2})W_{q_2p_2q_3q_1} \\
& + (-p_2 - q_1 + q_2 + q_3)(-1 + n_{q_2})(-1 + n_{q_3})W_{p_1q_2q_1q_3}W_{q_2q_1q_3p_2} \\
& + (p_1 + q_1 - q_2 - q_3)(n_{q_2}n_{q_3} - 2n_{q_1}(-1 + n_{q_2} + n_{q_3}))W_{p_1q_3q_1q_2}W_{q_2q_1q_3p_2} \\
& + n_{q_2}((-1 + n_{q_3})(-(p_1 - q_1 - q_2 + q_3)(2W_{p_1q_1q_3q_2} - W_{p_1q_2q_3q_1})W_{q_1p_2q_2q_3}) \\
& - 2(p_1 - p_2 - q_1 + q_3)W_{p_1p_2q_3q_1}W_{q_1q_2q_2q_3}) \\
& - 2(p_1 - p_2 + q_1 - q_3)n_{q_3}W_{p_1p_2q_1q_3}W_{q_2q_1q_3q_2}) \\
& + 2(p_1 - p_2 + q_1 - q_2)(-1 + n_{q_1} + n_{q_2})n_{q_3}W_{p_1p_2q_1q_2}W_{q_2q_3q_3q_1} \Big] \tag{D.2}
\end{aligned}$$

$$\begin{aligned}
\partial_l U_{p_1p_2p_3p_4}(l) & = -(p_1 - p_2 + p_3 - p_4)^2 U_{p_1p_2p_3p_4} \\
& + \sum_{q_1} \left[ (p_1 - p_2 + p_3 - q_1)V_{p_4q_1}U_{p_1p_2p_3q_1} + (-p_1 + p_2 + p_4 - q_1)V_{p_3q_1}U_{p_1p_2q_1p_4} \right. \\
& + (p_1 + p_3 - p_4 - q_1)V_{p_2q_1}U_{p_1q_1p_3p_4} + (p_2 - p_3 + p_4 - q_1)V_{p_1q_1}U_{p_3p_4q_1p_2} \Big] \\
& + \sum_{q_1} \left[ (p_4 - q_1)V_{p_4q_1}U_{p_1p_2p_3q_1} + (p_3 - q_1)V_{p_3q_1}U_{p_1p_2q_1p_4} \right. \\
& + (p_2 - q_1)V_{p_2q_1}U_{p_1q_1p_3p_4} + (p_1 - q_1)V_{p_1q_1}U_{p_3p_4q_1p_2} \Big] \\
& + \sum_{q_1q_2} \left[ (p_3 + p_4 - 2q_1)(n_{q_1} - n_{q_2})U_{p_1q_2q_1p_4}U_{p_3q_1q_2p_2} \right. \\
& + (p_1 + p_2 - 2q_1)(n_{q_1} - n_{q_2})U_{p_1q_1q_2p_4}U_{p_3q_2q_1p_2} \\
& - (p_1 + p_2 - 2q_1)(-1 + n_{q_1} + n_{q_2})U_{p_1q_1p_3q_2}U_{q_1p_2q_2p_4} \\
& - (p_3 + p_4 - 2q_1)(-1 + n_{q_1} + n_{q_2})U_{p_1q_2p_3q_1}U_{q_1p_4q_2p_2} \Big] \\
& + \sum_{q_1q_2} \left[ -((p_3 - p_4 + q_1 - q_2)U_{p_3p_4q_1q_2}(-2(n_{q_1} - n_{q_2})W_{p_1p_2q_2q_1} \right.
\end{aligned}$$

$$\begin{aligned}
& + (1 + n_{q_1} - 2n_{q_2})W_{p_1q_1q_2p_2}) - (p_3 - p_4 - q_1 + q_2)(-1 + n_{q_2})U_{p_3p_4q_2q_1}W_{p_1q_2q_1p_2} \\
& - (p_1 - p_2 + q_1 - q_2)U_{p_1p_2q_1q_2}(-2(n_{q_1} - n_{q_2})W_{p_3p_4q_2q_1} + (1 + n_{q_1} - 2n_{q_2})W_{p_3q_1q_2p_4}) \\
& - (p_1 - p_2 - q_1 + q_2)(-1 + n_{q_2})U_{p_1p_2q_2q_1}W_{p_3q_2q_1p_4} \Big] \\
& + \sum_{q_1q_2} \left[ (n_{q_1} - n_{q_2})((p_1 - p_2 - q_1 + q_2)U_{p_3p_4q_1q_2}W_{p_1q_1q_2p_2} \right. \\
& + (p_1 - p_2 + q_1 - q_2)U_{p_3p_4q_2q_1}(2W_{p_1p_2q_1q_2} - W_{p_1q_2q_1p_2}) \\
& + (p_3 - p_4 - q_1 + q_2)U_{p_1p_2q_1q_2}W_{p_3q_1q_2p_4} \\
& \left. + (p_3 - p_4 + q_1 - q_2)U_{p_1p_2q_2q_1}(2W_{p_3p_4q_1q_2} - W_{p_3q_2q_1p_4}) \right] \tag{D.3}
\end{aligned}$$

$$\begin{aligned}
\partial_l W_{p_1p_2p_3p_4}(l) & = -(p_1 - p_2 + p_3 - p_4)^2 W_{p_1p_2p_3p_4} \\
& + \sum_{q_1q_2} \left[ (n_{q_1} - n_{q_2})((q_1 - q_2)U_{p_1p_2q_2q_1}U_{p_3p_4q_1q_2} + (p_1 - p_2)U_{p_1p_2q_1q_2}U_{p_3p_4q_2q_1}) \right] \\
& + \sum_{q_1} \left[ (p_4 - q_1)V_{p_4q_1}W_{p_1p_2p_3q_1} + (p_3 - q_1)V_{p_3q_1}W_{p_1p_2q_1p_4} \right. \\
& \left. + (p_2 - q_1)V_{p_2q_1}W_{p_1q_1p_3p_4} + (p_1 - q_1)V_{p_1q_1}W_{p_3p_4q_1p_2} \right] \\
& + \sum_{q_1} \left[ (p_1 - p_2 + p_3 - q_1)V_{p_4q_1}W_{p_1p_2p_3q_1} + (-p_1 + p_2 + p_4 - q_1)V_{p_3q_1}W_{p_1p_2q_1p_4} \right. \\
& \left. + (p_1 + p_3 - p_4 - q_1)V_{p_2q_1}W_{p_1q_1p_3p_4} + (p_2 - p_3 + p_4 - q_1)V_{p_1q_1}W_{p_3p_4q_1p_2} \right] \\
& + \sum_{q_1q_2} \left[ -((p_1 - p_2 + q_1 - q_2)(2(-n_{q_1} + n_{q_2})W_{p_1p_2q_1q_2} + n_{q_1}W_{p_1q_2q_1p_2})W_{p_3p_4q_2q_1}) \right. \\
& + (-1 + n_{q_1})((p_1 - q_2)W_{p_1q_1q_1q_2}W_{p_3p_2q_2p_4} \\
& + (p_1 - p_2 - q_1 + q_2)W_{p_1q_1q_2p_2}W_{p_3p_4q_1q_2} + (p_3 - q_2)W_{p_1p_2q_2p_4}W_{p_3q_1q_1q_2}) \\
& - (p_3 - p_4 - q_1 + q_2)(-1 + n_{q_2})W_{p_1q_2q_1p_2}(W_{p_3p_4q_2q_1} - W_{p_3q_1q_2p_4}) \\
& - (p_3 - p_4 - q_1 + q_2)(-1 + n_{q_2})W_{p_1p_2q_1q_2}W_{p_3q_1q_2p_4} \\
& - (p_1 - p_2 + q_1 - q_2)((1 + n_{q_1} - 2n_{q_2})W_{p_1p_2q_1q_2} - n_{q_1}W_{p_1q_2q_1p_2})W_{p_3q_1q_2p_4} \\
& - (p_1 - p_4 - q_1 + q_2)(n_{q_1} - n_{q_2})W_{p_1q_1q_2p_4}(W_{p_3p_2q_1q_2} - W_{p_3q_2q_1p_2}) \\
& + (-p_2 + p_3 + q_1 - q_2)(n_{q_1} - n_{q_2})(W_{p_1p_4q_2q_1} - W_{p_1q_1q_2p_4})W_{p_3q_2q_1p_2} \\
& + (p_1 - p_2 - q_1 + q_2)(-((-1 + n_{q_2})W_{p_1p_2q_2q_1}) - (-1 + n_{q_1})W_{p_1q_1q_2p_2})W_{p_3q_2q_1p_4} \\
& - (p_3 - p_4 + q_1 - q_2)W_{p_1q_1q_2p_2}((1 + n_{q_1} - 2n_{q_2})W_{p_3p_4q_1q_2} + n_{q_2}W_{p_3q_2q_1p_4}) \\
& + (p_3 - p_4 + q_1 - q_2)W_{p_1p_2q_2q_1}(2(n_{q_1} - n_{q_2})W_{p_3p_4q_1q_2} + n_{q_2}W_{p_3q_2q_1p_4}) \\
& - (p_1 + p_3 - q_1 - q_2)(-1 + n_{q_1} + n_{q_2})W_{p_1q_1p_3q_2}W_{q_1p_2q_2p_4} \\
& + (p_2 + p_4 - q_1 - q_2)(-1 + n_{q_1} + n_{q_2})W_{p_1q_2p_3q_1}W_{q_1p_2q_2p_4} \\
& + (-1 + n_{q_1} + n_{q_2})W_{p_1q_1p_3q_2}((-p_2 - p_4 + q_1 + q_2)W_{q_1p_2q_2p_4}
\end{aligned}$$

$$\begin{aligned}
& + (p_1 + p_3 - q_1 - q_2)W_{q_1 p_4 q_2 p_2} + n_{q_1}((p_1 - q_2)W_{p_1 q_1 q_1 q_2} W_{p_3 p_4 q_2 p_2} \\
& + (p_3 - q_2)W_{p_1 p_4 q_2 p_2} W_{p_3 q_1 q_1 q_2} + (p_2 - q_2)W_{p_1 p_4 p_3 q_2} W_{q_1 p_2 q_2 q_1} \\
& + (p_4 - q_2)W_{p_1 p_2 p_3 q_2} W_{q_1 p_4 q_2 q_1}) + (p_2 - q_1)(-1 + n_{q_2})W_{p_1 q_1 p_3 p_4} W_{q_1 q_2 q_2 p_2} \\
& + (p_4 - q_1)(-1 + n_{q_2})W_{p_1 q_1 p_3 p_2} W_{q_1 q_2 q_2 p_4} \Big] \tag{D.4}
\end{aligned}$$

In the numerical implementation, the last equation has to be symmetrized explicitly:

$$W_{q_1 q_2 q_3 q_4} \rightarrow \frac{1}{2}(W_{q_1 q_2 q_3 q_4} + W_{q_3 q_4 q_1 q_2}) \tag{D.5}$$



# Bibliography

- Abrikosov, A., 1965, *Physics* **2**, 5.
- Anderson, P., 1961, *Phys. Rev.* **124**, 41.
- Anderson, P., 1970, *J. Phys. C* **3**, 2436.
- Anderson, P., and G. Yuval, 1969, *Phys. Rev. Lett.* **23**, 89.
- Anderson, P., G. Yuval, and D. Hamann, 1970, *Phys. Rev. B* **1**, 4464.
- Andrei, N., 1980, *Phys. Rev. Lett.* **45**, 379.
- Baberschke, K., and E. Tsang, 1980, *Phys. Rev. Lett.* **45**, 1512.
- Bickers, N., D. Cox, and J. Wilkins, 1987, *Phys. Rev. B* **36**, 2036.
- Bloch, F., 1928, *Z. Phys.* **52**, 555.
- Bobroff, J., W. MacFarlane, H. Alloul, P. Mendels, N. Blanchard, G. Collin, and J.-F. Marucco, 1999, *Phys. Rev. Lett.* **83**, 4381.
- Born, M., and R. Oppenheimer, 1927, *Ann. Physik* **84**, 457.
- Brugger, T., T. Schreiner, G. Roth, P. Adelman, and G. Czjzek, 1993, *Phys. Rev. Lett.* **71**, 2481.
- Bulla, R., 1994, Ph.D. Thesis, Universität Regensburg.
- Bulla, R., 1999, *Phys. Rev. Lett.* **83**, 136.
- Bulla, R., 2000, unpublished.
- Bulla, R., A. Hewson, and T. Pruschke, 1998, *J. Phys. Condens. Matter* **10**, 8365.
- Bulla, R., T. Costi, and D. Vollhardt, 2000, unpublished.
- Costi, T., 1998, *Phys. Rev. Lett.* **80**, 1038.

- Costi, T., 2000, Phys. Rev. Lett. **85**, 1504.
- Costi, T., A. Hewson, and V. Zlatić, 1994, J. Phys. Condens. Matter **6**, 2519.
- Costi, T., and C. Kieffer, 1996, Phys. Rev. Lett. **76**, 1683.
- Costi, T., and G. Zarand, 1999, Phys. Rev. B **59**, 12398.
- Davidovich, B., and V. Zevin, 1998, Phys. Rev. B **57**, 7773.
- de Haas, W., J. de Boer, and G. van den Berg, 1934, Physica **1**, 1115.
- Drew, H., and R. Doezema, 1972, Phys. Rev. Lett. **28**, 1581.
- Duffy, D., and A. Moreo, 1997, Phys. Rev. B **55**, 676.
- Egger, R., and A. Komnik, 1998, Phys. Rev. B **57**, 10620.
- Emery, V., and S. Kivelson, 1992, Phys. Rev. B **46**, 10812.
- Feynman, R., 1972, *Statistical Mechanics* (Addison-Wesley, New York).
- Fischer, W., and E. Lieb, 1992, *Funktionentheorie* (Vieweg, Braunschweig).
- Fogedby, H., 1977, J. Phys. C **10**, 2869.
- Fröjdh, P., and A. Johannesson, 1995, Phys. Rev. Lett. **75**, 300.
- Frota, H., and L. Oliveira, 1986, Phys. Rev. B **43**, 7871.
- Fulde, P., 1995, *Electron correlations in molecules and solids*, Vol. 100 of *Springer series in solid-state sciences* (Springer, Berlin).
- Fulde, P., V. Zevin, and G. Zwicknagl, 1993, Z. Phys. B **92**, 133.
- Furusaki, A., and N. Nagaosa, 1994, Phys. Rev. Lett. **72**, 892.
- Gebhard, F., 1997, *The Mott metal-insulator transition* (Springer, Berlin).
- Georges, A., and G. Kotliar, 2000, Phys. Rev. Lett. **84**, 3500.
- Georges, A., G. Kotliar, W. Krauth, and M. Rozenberg, 1996, Rev. Mod. Phys. **68**, 13.
- Glazek, S., and K. Wilson, 1994, Phys. Rev. D **49**, 4214.
- Goldhaber-Gordon, D., H. Shtrikman, D. Mahalu, D. Abusch-Magder, U. Meirav, and M. Kastner, 1998, Nature **391**, 156.

- Goldstone, J., 1957, Proc. R. Soc. London, Ser. A **293**, 267.
- Guinea, F., V. Hakim, and A. Muramatsu, 1985, Phys. Rev. B **32**, 4410.
- Gutzwiller, M., 1963, Phys. Rev. Lett. **10**, 159.
- Haldane, F., 1981, J. Phys. C **14**, 2585.
- Hallberg, K., and C. Balseiro, 1995, Phys. Rev. B **52**, 374.
- Hasegawa, Y., and P. Avouris, 1993, Phys. Rev. Lett. **71**, 1071.
- Henggeler, W., T. Chattopadhyay, P. Thalmeier, P. Vorderwisch, and A. Furrer, 1996, Europhys. Lett. **34**, 537.
- Hewson, A., 1993, *The Kondo Problem to Heavy Fermions*, Vol. 2 of *Cambridge Studies in Magnetism* (Cambridge University Press, Cambridge).
- Hofstetter, W., 2000, Phys. Rev. Lett. **85**, 1508.
- Hofstetter, W., and D. Vollhardt, 1998, Ann. Physik **7**, 48.
- Hofstetter, W., and S. Kehrein, 1999, Phys. Rev. B **59**, R12732.
- Hofstetter, W., R. Bulla, and D. Vollhardt, 2000, Phys. Rev. Lett. **84**, 4417.
- Hubbard, J., 1963, Proc. Roy. Soc. London A **276**, 238.
- Ising, E., 1925, Z. Phys. **31**, 253.
- Itai, K., and P. Fazekas, 1996, Phys. Rev. B **54**, 752.
- Julien, M.-H., T. Fehér, M. Horvatić, C. Berthier, O. Bakharev, P. Ségransan, G. Collin, and J.-F. Marucco, 2000, Phys. Rev. Lett. **84**, 3422.
- Kadanoff, L., 1966, Physics **2**, 263.
- Kanamori, J., 1963, Prog. Theor. Phys. **30**, 275.
- Kane, C., and M. Fisher, 1992, Phys. Rev. B **46**, 15233.
- Kang, K., and B. Min, 1996, Phys. Rev. B **54**, 1645.
- Kehrein, S., 1998, Phys. Rev. Lett. **81**, 3912.
- Kehrein, S., 1999, Phys. Rev. Lett. **83**, 4914.
- Kehrein, S., and A. Mielke, 1996, Ann. Phys. **252**, 1.

- Kehrein, S., and A. Mielke, 1997, *Ann. Physik* **6**, 90.
- Keiter, H., and T. Leuders, 2000, *Europhys. Lett.* **49**, 801.
- Kergueris, C., J.-P. Bourgoïn, S. Palacin, D. Esteve, C. Urbina, M. Magoga, and C. Joachim, 1999, *Phys. Rev. B* **59**, 12505.
- Khaliullin, G., and P. Fulde, 1995, *Phys. Rev. B* **52**, 9514.
- Knetter, C., and G. Uhrig, 2000, *Eur. Phys. J. B* **13**, 209.
- Kondo, J., 1964, *Prog. Theor. Phys.* **32**, 37.
- Kotliar, G., and Q. Si, 1996, *Phys. Rev. B* **53**, 12373.
- Krishna-murthy, H., J. Wilkins, and K. Wilson, 1980, *Phys. Rev. B* **21**, 1003.
- Kronig, R., 1935, *Physica* **2**, 968.
- Krug von Nidda, H.-A., 1997, Ph.D. Thesis, Technische Universität Darmstadt.
- Laloux, L., A. Georges, and W. Krauth, 1994, *Phys. Rev. B* **50**, 3092.
- Lanczos, C., 1950, *J. Res. Natl. Bur. Stand.* **45**, 255.
- Lange, E., 1998, *Mod. Phys. Lett. B* **12**, 915.
- Langreth, D., 1966, *Phys. Rev.* **150**, 516.
- Lee, D., and J. Toner, 1992, *Phys. Rev. Lett.* **69**, 3378.
- Leggett, A., S. Chakravarty, A. Dorsey, M. Fisher, A. Garg, and W. Zwerger, 1987, *Rev. Mod. Phys.* **59**, 1.
- Lesage, F., H. Saleur, and S. Skorik, 1996, *Phys. Rev. Lett.* **76**, 3388.
- Li, J., W.-D. Schneider, R. Berndt, and B. Delley, 1998, *Phys. Rev. Lett.* **80**, 2893.
- Lin, C., A. Wallash, J. Crow, T. Mihalisin, and P. Schlottmann, 1987, *Phys. Rev. Lett.* **58**, 1232.
- Logan, D., and P. Nozières, 1998, *Phil. Trans. R. Soc. London A* **356**, 249.
- Luttinger, J., 1961, *Phys. Rev.* **121**, 942.
- MacDonald, A., S. Girvin, and D. Yoshioka, 1988, *Phys. Rev. B* **37**, 9753.

- Maiser, E., W. Mexner, R. Schäfer, T. Schreiner, P. Adelman, G. Czjzek, J. Peng, and R. Greene, 1997, *Phys. Rev. B* **56**, 12961.
- Mattis, D., 1975, *Ann. Phys.* **89**, 45.
- Mattis, D., and E. Lieb, 1965, *J. Math. Phys.* **6**, 304.
- Metzner, W., and D. Vollhardt, 1989*a*, *Phys. Rev. Lett.* **62**, 324.
- Metzner, W., and D. Vollhardt, 1989*b*, *Phys. Rev. B* **39**, 4462.
- Moeller, G., Q. Si, G. Kotliar, M. Rozenberg, and D. Fisher, 1995, *Phys. Rev. Lett.* **74**, 2082.
- Müller-Hartmann, E., 1989, *Z. Phys. B* **74**, 507.
- Murani, A., 1987, *Phys. Rev. B* **36**, 5705.
- Murani, A., and J. Tholence, 1977, *Sol. St. Comm.* **22**, 25.
- Myers, H., L. Walldén, and A. Karlsson, 1968, *Phil. Mag.* **18**, 725.
- Nagaosa, N., Y. Hatsugai, and M. Imada, 1989, *J. Phys. Soc. Jpn.* **58**, 978.
- Negele, J., and H. Orland, 1987, *Quantum Many-Particle Systems* (Addison-Wesley, New York).
- Noack, R., and F. Gebhard, 1999, *Phys. Rev. Lett.* **82**, 1915.
- Phillips, P., and N. Sandler, 1996, *Phys. Rev. B* **53**, R468.
- Press, W., S. Teukolsky, W. Vetterling, and B. Flannery, 1995, *Numerical Recipes in C* (Cambridge University Press, Cambridge).
- Sachdev, S., C. Buragohain, and M. Vojta, 1999, *Science* **286**, 2479.
- Sakai, O., S. Suzuki, W. Izumida, and A. Oguri, 1999, *J. Phys. Soc. Jpn.* **68**, 1640.
- Sakai, O., Y. Shimizu, and T. Kasuya, 1989, *J. Phys. Soc. Jpn.* **58**, 3666.
- Sakurai, J., 1994, *Modern Quantum Mechanics* (Addison-Wesley, New York).
- Scheuer, H., M. Loewenhaupt, and M. Schmatz, 1977, *Physica B* **86-88**, 842.
- Schiller, A., and K. Ingersent, 1995, *Phys. Rev. B* **51**, 4676.
- Schiller, A., and K. Ingersent, 1997, *Europhys. Lett.* **39**, 645.

- Schlipf, J., 1998, Ph.D. Thesis, Universität Augsburg.
- Schlipf, J., M. Jarrell, P. van Dongen, N. Blümer, S. Kehrein, T. Pruschke, and D. Vollhardt, 1999, Phys. Rev. Lett. **82**, 4890.
- Schlottmann, P., 1982, Phys. Rev. B **25**, 4815.
- Schönhammer, K., 1997, preprint cond-mat/9710330.
- Schork, T., 1996, Phys. Rev. B **53**, 5626.
- Schork, T., and P. Fulde, 1994, Phys. Rev. B **50**, 1345.
- Schork, T., and S. Blawid, 1997, Phys. Rev. B **56**, 6559.
- Schotte, K., 1970, Z. Phys. **230**, 99.
- Schrieffer, J., and P. Wolff, 1966, Phys. Rev. **149**, 491.
- Shiba, H., 1975, Prog. Theor. Phys. **54**, 967.
- Stein, J., 1997, J. Stat. Phys. **88**, 487.
- Takagi, O., and T. Saso, 1999*a*, J. Phys. Soc. Jpn. **68**, 1997.
- Takagi, O., and T. Saso, 1999*b*, J. Phys. Soc. Jpn. **68**, 2894.
- Takahashi, M., 1977, J. Phys. C **10**, 1289.
- Takayama, R., and O. Sakai, 1998, J. Phys. Soc. Jpn. **67**, 1844.
- Tornow, S., V. Zevin, and G. Zwicknagl, 1996, Ann. Physik **5**, 501.
- Tornow, S., V. Zevin, and G. Zwicknagl, 1997, preprint cond-mat/9701137.
- Toulouse, G., 1969, C. R. Acad. Sci. Paris **268**, 1200.
- Vollhardt, D., 1993, in *Correlated Electron Systems*, edited by V. Emery (World Scientific, Singapore ), p. 57.
- von Delft, J., and H. Schöller, 1998, Ann. Physik **7**, 225.
- Wang, X., 1998, Mod. Phys. Lett. B **12**, 667.
- Wegner, F., 1994, Ann. Physik **3**, 77.
- Wegner, F., 1999, private communication.

- White, S., 1992, Phys. Rev. Lett. **69**, 2863.
- Wiegmann, P., 1980, Sov. Phys. JETP Lett. **31**, 392.
- Wiegmann, P., 1981, Phys. Lett. A **31**, 163.
- Wiegmann, P., and A. Finkelstein, 1978, Sov. Phys. JETP **48**, 102.
- Wilson, K., 1965, Phys. Rev. **140**, 445.
- Wilson, K., 1971, Phys. Rev. B **4**, 3174.
- Wilson, K., 1975, Rev. Mod. Phys. **47**, 773.
- Wolff, P., 1961, Phys. Rev. **124**, 1030.
- Yamada, K., 1975, Prog. Theor. Phys. **54**, 316.
- Yoshimori, A., and A. Zawadowski, 1982, J. Phys. C: Solid State Phys. **15**, 5241.
- Yunoki, S., Y. Mizuno, and S. Maekawa, 1996, Physica C **263**, 90.
- Zarand, G., and J. von Delft, 2000, Phys. Rev. B **61**, 6918.
- Zener, C., 1951, Phys. Rev. **81**, 761.
- Zevin, V., 2000, private communication.
- Zhang, X., M. Rozenberg, and G. Kotliar, 1993, Phys. Rev. Lett. **70**, 1666.



# Publications

Parts of this thesis were published in the following articles:

W. Hofstetter and S. Kehrein, “Symmetric Anderson impurity model with a narrow band”, Phys. Rev. B **59**, R12732 (1999).

W. Hofstetter, R. Bulla, and D. Vollhardt, “Anderson impurity in a correlated band”, Phys. Rev. Lett. **84**, 4417 (2000).

W. Hofstetter, “Generalized Numerical Renormalization Group for Dynamical Quantities”, Phys. Rev. Lett. **85**, 1508 (2000).

W. Hofstetter and S. Kehrein, “Flow equation analysis of the anisotropic Kondo model”, cond-mat/0008242.



---

# Curriculum vitae

Name Walter Hofstetter  
Date of birth 18 July 1972  
Place of birth München  
Nationality German

## Education

09/78 – 07/82 Primary school in Kirchseeon  
09/82 – 07/91 Grammar school in Grafing  
07/91 Abitur

## Studies

11/91 – 05/97 Study of physics at LMU München  
10/94 – 08/95 Visiting student at Balliol College, Oxford  
02/96 – 02/97 Diploma thesis supervised by  
Prof. W. Zwerger, LMU München (subject:  
“Statistical mechanics of the single–electron box”)  
05/97 Diploma in physics (with honours)  
since 05/97 PhD studies supervised by Prof. D. Vollhardt,  
Universität Augsburg  
04/99 Research stay at Harvard University

## Scholarships

10/91 – 03/97 Studienstiftung des Deutschen Volkes  
07/91 – 05/97 Stiftung Maximilianeum  
10/91 – 05/97 Bayerisches Begabtenstipendium  
11/98 – 03/00 PhD scholarship, Studienstiftung des Deutschen Volkes

## Employment

since 05/97 Research assistant, Chair of Theoretical Physics III,  
Universität Augsburg



# Acknowledgements

Writing down this thesis has been a unique chance to summarize the results of my work within the last three years. At this point I would like to express my gratitude to all those persons who have supported me during this time:

In the first place, I wish to thank Prof. Dr. D. Vollhardt who gave me the opportunity to work in his group und who made this PhD thesis possible. Numerous helpful discussions as well as many valuable suggestions have provided the guidelines for my research and have lead to the present focus of my studies. Thanks to his support, I was able to attend several international workshops and conferences and also to visit Harvard University for a research stay in April 1999.

Prof. Dr. T. Kopp kindly agreed to co-report on this thesis.

I am also indebted to Dr. Stefan Kehrein from whom I learned a great deal about impurity physics in general and the flow equation method in particular. His hospitality made my visit to Harvard a unique experience.

With Dr. Ralf Bulla I have had a fruitful collaboration since he joined our group. He has also provided helpful suggestions for the final version of this thesis.

Dr. Ulrich Schollwöck helped me to clarify the physics of the Wolff model by making available his DMRG program.

I am also grateful to Dr. Hiroshi Kontani for the interest he has taken in my work.

By sharing his expert knowledge of NRG and bosonization, Dr. Theo Costi has improved my understanding of these techniques.

Last, but not least, thanks are due to Philipp Brune, Dr. Jan Schlipf, Nils Blümer, Dr. Karsten Held, Prof. Dr. Peter van Dongen, Dr. Marcus Kollar, Dr. Sabine Tornow, Igor Nekrasov, Prof. Dr. Gia Japaridze and all other members of our group for many helpful discussions and for the open and friendly atmosphere.

This work has been supported by a PhD scholarship of the Studienstiftung des deutschen Volkes.